Selective Catalytic Reduction of NO_x by ammonia: Unraveling the reaction mechanism through ab initio simulations

Tom Van Den Heede

Supervisor: Prof. dr. ir. Karen Hemelsoet
Counsellors: ir. Kristof De Wispelaere, dr. ir. Jeroen Van der Mynsbrugge

Master's dissertation submitted in order to obtain the academic degree of
Master of Science in Chemical Engineering

Department of Applied Physics
Chairman: Prof. dr. ir. Christophe Leys
Faculty of Engineering and Architecture
Academic year 2013-2014

UNIVERSITEIT GENT

Center for
Molecular Modeling

This work has been performed at the Center for Molecular Modeling

Preface

The realisation of this dissertation would not have been possible without the help of many people. First of all, I would like to thank my supervisor Karen Hemelsoet, for allowing me to work on this exciting topic at the Center for Molecular Modeling and for her time and patience, helping with any problems encountered along the way. I would also like to express my gratitude towards Kristof De Wispelaere and Jeroen Van der Mynsbrugge, who were always available for guidance and providing fresh ideas. Their eye for detail was simply indispensible. Furthermore, I would like to thank all other CMM members for an all-round great atmosphere. It was an honour being part of the team and even being able to present our own poster at the NCCC-conference.

Of course this preface would not be complete without mentioning my fellow students, whom I thank for the many lunch breaks filled with laughter. In particular I would like to thank Pieter Cnudde and Thomas Deconinck, who also did their dissertation at the CMM. Not only was it comforting to know that there were other people waiting patiently for the job queue to disappear, their companionship really made these last couple of months a wonderful experience.

Last but not least, I thank my family. Even though they did not fully understand what I was working on, I always felt an immense support and was provided with everything I needed in order to successfully deliver this dissertation. For all the times I forgot to mention this: Thank you!

Permission for usage

The author gives permission to make this master dissertation available for consultation and to copy parts of this master dissertation for personal use. In the case of any other use, the limitations of the copyright have to be respected, in particular with regard to the obligation to state expressly the source when quoting results from this master dissertation.

Tom Van Den Heede
Ghent, June 2nd 2014

Selectieve Katalytische Reductie van NO_x door ammoniak: Ontrafeling van het reactiemechanisme via ab initio simulaties

Tom Van Den Heede

Supervisor: Prof. dr. ir. Karen Hemelsoet
Begeleiders: ir. Kristof De Wispelaere, dr. ir. Jeroen Van der Mynsbrugge

Masterproef ingediend tot het behalen van de academische graad van
Master in de ingenieurswetenschappen: Chemische technologie
Master of Science in Chemical Engineering

Vakgroep Toegepaste fysica
Voorzitter: Prof. dr. ir. Christophe Leys
Faculteit ingenieurswetenschappen

Academiejaar 2013-2014

Overzicht

Met het oog op toenemende restricties op NO_x emissies in de nabije toekomst, wordt veel onderzoek verricht omtrent de Selectieve Katalytische Reductie van NO_x met ammoniak als reduceermiddel. Verschillende katalytische systemen werden reeds onderzocht als nabehandeling voor uitlaatgassen van dieselmotoren. Experimenten toonden aan dat Cu-SSZ-13, een zeoliet met chabasiettopologie, een geschikte keuze is vanwege zijn activiteit, selectiviteit en stabiliteit. Het voornaamste actieve centrum, een geïsoleerd Cu^{2+}-ion, bevindt zich hierbij in de nabijheid van de ring van de d6r subeenheid. Om een verband te kunnen leggen tussen structuur en activiteit, worden dichtheidsfunctionaaltheorie berekeningen uitgevoerd op zowel periodieke eenheidscellen als eindige clusters. De focus ligt hierbij op de adsorptie van NO en mogelijke interactie van deze geadsorbeerde molecule met water. In het bijzonder wordt de mobiliteit van het Cu-ion onderzocht aan de hand van Moleculaire Dynamica berekeningen.

Trefwoorden

Selectieve Katalytische Reductie (SCR), deNO_x, dichtheidsfunctionaaltheorie (DFT), heterogene katalyse, adsorptie, Moleculaire Dynamica (MD)

Selectieve Katalytische Reductie van NO_x door ammoniak: Ontrafeling van het reactiemechanisme via ab initio simulaties

Tom Van Den Heede

Supervisor: Prof. dr. ir. Karen Hemelsoet
Begeleiders: ir. Kristof De Wispelaere, dr. ir. Jeroen Van der Mynsbrugge

***Abstract*: Met het oog op toenemende restricties op NO_x emissies, wordt veel onderzoek verricht omtrent de Selectieve Katalytische Reductie van NO_x met ammoniak als reduceer-middel (NH_3-SCR deNOx). Eerdere studies hebben aangetoond dat Cu-SSZ-13, een zeoliet met chabasiettopologie, een geschikte katalysator is voor de nabehandeling van uitlaatgassen van dieselmotoren. Het voornaamste actieve centrum, een geïsoleerd Cu^{2+}-ion, bevindt zich hierbij in de nabijheid van de ring van de d6r subeenheid. In deze thesis worden ab initio berekeningen uitgevoerd op zowel periodieke eenheidscellen als eindige clusters. De focus ligt op de adsorptie van NO en mogelijke interactie van deze geadsorbeerde molecule met water. In het bijzonder wordt de mobiliteit van het Cu-ion onderzocht aan de hand van Moleculaire Dynamica berekeningen.**

***Trefwoorden:* Selectieve Katalytische Reductie (SCR), deNO_x, dichtheidsfunctionaaltheorie (DFT), heterogene katalyse, adsorptie, Moleculaire Dynamica (MD)**

I. Inleiding

Door de aanwezigheid van stikstofcomponenten in brandstoffen, komt dagelijks een grote hoeveelheid stikstofoxides (NO_x) terecht in de atmosfeer. NO_x wordt onder atmosferische condities geconverteerd in secundaire producten die schadelijk zijn voor het milieu. Zo worden ondermeer zure regen en fotochemische smog veroorzaakt door deze emissies. Bijgevolg wordt de regelgeving omtrent NO_x emissies steeds strenger en verhoogt de nood aan geavanceerde reductietechnologieën. Aangezien NO_x vooral afkomstig is van dieselmotoren in mobiele toepassingen, dient deze technologie bovendien zeer robuust te zijn.

Een veelgebruikte technologie is de Selectieve Katalytische Reductie van NO_x met ammoniak als reduceermiddel.[1] Hierbij wordt het schadelijke NO_x omgezet in stikstof en water. Dit katalytisch systeem wordt bij zware voertuigen geïnstalleerd nabij de roetfilter (*Diesel Particulate Filter* of DPF in Figuur 1).[2] Deze deNO_x technologie wordt reeds in de praktijk toegepast, maar desondanks staat het gedetailleerde reactiemechanisme nog steeds ter discussie.[1] Om een intelligent katalysatorontwerp mogelijk te maken is de kennis van dit mechanisme echter van cruciaal belang.

Eerdere studies hebben aangetoond dat metaal-uitgewisselde zeolieten een uitstekende activiteit en selectiviteit bieden. Afhankelijk van het geselecteerde metaal en topologie worden geïsoleerde ionen, dimeren of metaaloxide clusters geobserveerd als katalytische centra.[1][2]

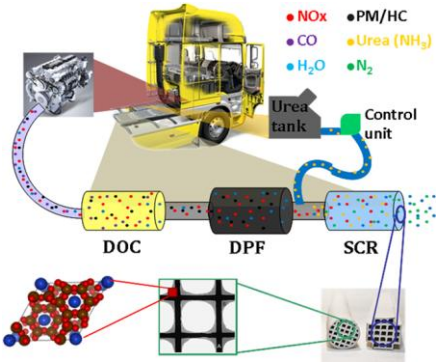

Figuur 1: Installatie van een urea-tank in zware voertuigen. Decompositie van een waterige urea-oplossing produceert geleidelijk ammoniak dat wordt verbruikt in de SCR sectie van de dieseluitlaat nabehandeling.[2]

Recent is de focus verschoven naar zeolieten met nauwere kanaalopeningen, aangezien deze gekenmerkt worden door een superieure thermische stabiliteit. Deze eigenschap is belangrijk door de nabijheid van de roetfilter, die temperaturen boven 600 K bereikt tijdens het oxidatieproces. Zowel experimentele [1][3][4] als theoretische [5][6][7] onderzoeken vestigen de aandacht op het gebruik van Cu-SSZ-13 als katalysator voor de deNO_x reactie. Cu-SSZ-13 beschikt over een chabasiettopologie die is opgebouwd uit chabasietkooien omringd door dubbele 6-ring (d6r) subeenheden. Het katalytisch centrum, voornamelijk geïsoleerde Cu-ionen, wordt geacht te verblijven nabij de top van de d6r eenheid.[8]

II. Doelstellingen

In deze thesis wordt de focus voornamelijk gelegd op de adsorptie van NO op Cu-SSZ-13 en navolgend op de interactie met additionele watermoleculen. Dit komt overeen met de eerste stappen van het reactiepad dat wordt voorgesteld door Kwak et al. zoals te zien is in Figuur 2.[3] Bijzondere aandacht gaat naar de geometrie van de geoptimaliseerde structuur, de multipliciteit van het adsorptiecomplex, de NO stretch frequenties en de ladingsverdeling. Vervolgens worden watermoleculen toegevoegd en de interactie tussen deze moleculen en het adsorptiecomplex wordt grondig onderzocht. De coördinatie en mobiliteit van het Cu-ion wordt bestudeerd aan de hand van ab initio Moleculaire Dynamica simulaties. Alle resultaten worden bekomen met quantum-chemische methoden en worden waar mogelijk gelinkt met experimentele resultaten.

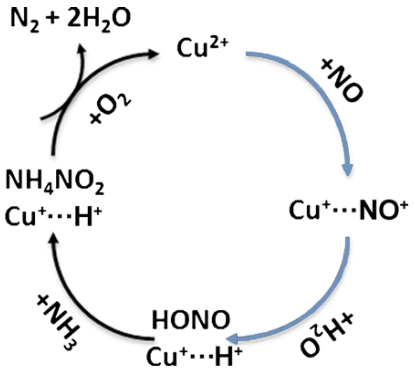

Figuur 2: NH_3-SCR reactiepad voorgesteld door Kwak et al. [3]

III. Methodologie

Om het NH_3-SCR mechanisme te bestuderen werden voornamelijk dichtheidsfunctionaaltheorie (DFT) berekeningen uitgevoerd. Het merendeel bestaat uit periodieke berekeningen op een 36T-eenheidscel zoals voorgesteld in Figuur 3, waar de geoptimaliseerde geometrie van de NO-adsorptie terug te vinden is. Hiervoor werd het CP2K softwarepakket [9] gebruikt in combinatie met een Gaussische vlakke golf basisset. Er werd geopteerd voor GGA-benaderde PBE functionalen met D3-dispersiecorrecties. Verder werd voor alle atomen behalve Cu een GTH-PBE pseudo-potentiaal geselecteerd. Cu werd daarentegen beschreven door een GTH-BLYP pseudo-potentiaal vermits de PBE pseduo-potentiaal niet voorzien is van parameters voor het Cu-atoom.

Vermits periodieke berekeningen vaak gepaard gaan met lange rekentijden werden ook eindige clusters gebruikt, dikwijls in combinatie met een ONIOM-schema. Het hoog theoretisch niveau bestaat uit PBE0 hybride functionalen, gebruik makend van een DGDZVP basis set. Het laag theoretisch niveau wordt beschreven aan de hand van het UFF krachtveld. De resultaten van deze eindige clusters voldoen echter niet aan de verwachtingen, vanwege een gebrek aan stabiliteit van de d6r eenheden en het onvermogen om de ladingsverdeling correct te beschrijven. Zo wordt bij het gebruik van een grote 54T-cluster een Cu^+-ion vastgesteld, in plaats van een Cu^{2+}-ion, ten gevolge van eindige cluster effecten. Verdere analyse van het Cu-NO adsorptiecomplex is bijgevolg gericht op periodieke berekeningen. Om de resultaten te valideren werden frequenties van het NO geadsorbeerde complex bepaald aan de hand van een analyse van de normale modes.

Voorts werden ab initio Moleculaire Dynamica (MD) berekeningen uitgevoerd om de interactie tussen het geadsorbeerde NO en watermoleculen te bestuderen. Het potentiële energie-oppervlak werd hierbij gesampled met een NVT ensemble, gebruik makend van de Nosé-Hoover thermostaat en een tijdstap van 1 fs. Het gebruikte theoretisch niveau was analoog zoals bij de statische berekeningen met periodieke randvoorwaarden. Temperaturen van 300 K en 600 K werden hierbij onderzocht.

IV. Resultaten

De periodieke geometrie-optimalisatie van de initiële adsorptie, voorgesteld in Figuur 2, toont aan dat het Cu-ion wordt geëxtraheerd uit de bovenste ring van de d6r subeenheid en zich verplaatst naar het centrum van de chabasietkooi. De geoptimaliseerde geometrie, weergegeven in Figuur 3, vertoont uitstekende overeenkomsten met zowel experimentele resultaten [3] als met voorgaande theoretische studies.[5] De berekende NO bindingslengte is 1.15 Å, en de Cu-N-O hoek bedraagt ongeveer 142° voor de energetisch bevoordeelde singlet toestand. Voor deze toestand wordt een adsorptie-energie van 126 kJ/mol berekend en de NO molecule is loodrecht gericht ten opzichte van het vlak van de dubbele 6-ring. Bovenstaande resultaten zijn bovendien vrij onafhankelijk van de initiële configuratie. Een tweede validatie van de resultaten wordt geleverd door de frequenties van de bekomen geometrie. De berekende karakteristieke NO stretch frequentie van de op Cu geadsorbeerde molecule is gelijk aan 1952 cm^{-1} en vertoont dus opnieuw een zeer goede overeenkomst met de 1948 cm^{-1} die werden bekomen aan de hand van experimentele IR metingen.[2]

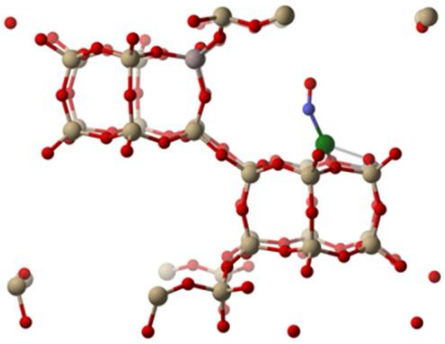

Figuur 3: Geoptimaliseerde geometrie van NO geadsorbeerd op Cu-SSZ-13. De rhombohedrische eenheidscel wordt hierbij voorgesteld gebruik makend van volgende kleurencode: rood:O beige:Si violet:Al groen:Cu blauw:N.

Met het oog op de vorming van HONO als volgend intermediair (zie Figuur 2) werd eveneens de reactie van het geadsorbeerde NO met water gemodelleerd. Hierbij werden voornamelijk dynamische berekeningen op periodieke systemen gebruikt om de positionering van maximaal 4 watermoleculen te volgen in functie van de tijd. Opnieuw wordt hierbij veel aandacht besteed aan de locatie van het Cu-ion. Uit de analyse blijkt dat de toevoeging van de eerste twee watermoleculen een sterke invloed hebben op het bekomen adsorptiecomplex. De invloed van de derde en vierde watermolecule is veel geringer, wat er op wijst dat deze niet direct interageren met Cu. De coördinatieschil van Cu bevat dus hoofdzakelijk NO, 2 watermoleculen en 1 à 2 zuurstofatomen van het zeolietrooster zoals weergegeven in Figuur 4. De data tonen aan dat de additie van watermoleculen resulteert in een langere Cu-N afstand in vergelijking met de statische optimalisatie zonder H_2O.

De dynamische simulaties laten toe om een beeld te krijgen van de meest voorkomende configuraties. Voor elk aantal watermoleculen werd een snapshot geselecteerd dat vervolgens werd geoptimaliseerd. Hierbij is het belangrijk te vermelden dat er geen garanties zijn dat de geselecteerde snapshot representatief is voor de realistische situatie. De totale simulatietijd – maximum 10 ps – is dan ook te beperkt om definitieve besluiten te trekken. Desalniettemin werd een thermodynamische analyse op deze geoptimaliseerde structuren uitgevoerd om een idee te krijgen van de trend van de enthalpische en entropische contributies.

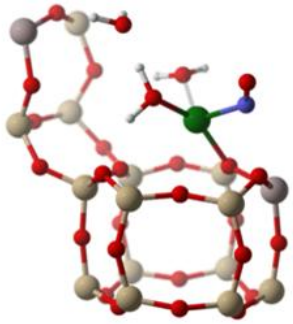

Figuur 4: Gedetailleerde snapshot van de periodieke MD simulatie met 3 additionele water moleculen, waarbij de aanwezigheid van 2 water moleculen in de coördinatieschil van Cu worden weergegeven.

De resultaten van deze thermodynamische analyse bevestigen dat de eerste twee water moleculen sterker binden aan het Cu, wat zich vertaalt in een sterk negatieve enthalpie-verandering. Elke H_2O toevoeging gaat gepaard met een daling van de entropie. In het bijzonder voor de tweede water molecule waarvan de positie volledig bepaald wordt door het zeolietrooster en de positie van de eerste watermolecule. De invoering van extra watermoleculen vermindert de interactie tussen het zeolietrooster en het Cu-ion, dat zich begeeft in de richting van de chabasietkooi. Dit heeft dus als gevolg dat de mobiliteit van het Cu-atoom toeneemt. Deze mobiliteit kan visueel voorgesteld worden door de Cu-positie uit te zetten voor elke 100 tijdstappen. Een voorbeeld van dergelijke plot wordt weergegeven in Figuur 5, die de resultaten van een dynamische simulatie zonder water bevat, bij een temperatuur van 600 K. Zelfs in afwezigheid van water is bij 600 K reeds een significante mobiliteit waar te nemen. De verplaatsing van het koper is echter geconcentreerd in één bevoordeelde richting, i.h.b. naar een negatief geladen zuurstofatoom van het zeolietrooster naast een aluminiumsubstitutie. De toevoeging van water heeft hoofdzakelijk tot gevolg dat afwijkingen van deze richting veel sneller mogelijk zijn, doordat de watermoleculen, het Cu-ion in andere richtingen aantrekt. Dit vertaalt zich in een verdeling over een groter oppervlak.

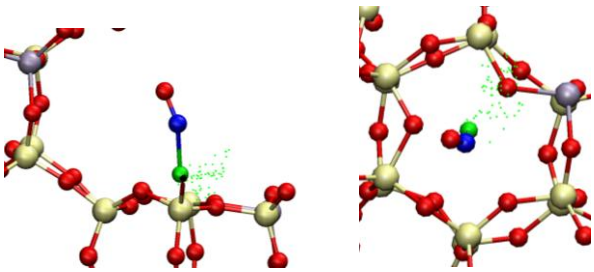

Figuur 5: Visualisatie van de Cu-mobiliteit in afwezigheid van water bij een temperatuur van 600 K. In totaal worden 83 punten uitgezet vermits de simulatie 8227 tijdstappen heeft doorlopen.

De analyse van de Cu-mobiliteit is in overeenkomst met de analyse van de coördinatiegetallen. In Figuur 6 worden de desbetreffende resultaten weergegeven voor de MD simulaties bij 300 K. Met toenemend aantal watermoleculen daalt de coördinatie van Cu met het zeolietrooster (CN zeol), wat een grotere Cu-mobiliteit met zich meebrengt. De lage waarden die gerapporteerd worden voor de coördinatie van Cu met NO (CN NO), tonen aan dat voor de berekening van de coördinatiegetallen een te lage drempelwaarde werd gebruikt. In werkelijkheid ligt CN NO dan ook dichter bij 1. Analoog zal CN water eerder een waarde 2 benaderen, i.e. de verzadigde coördinatie van Cu bevat 2 watermoleculen.

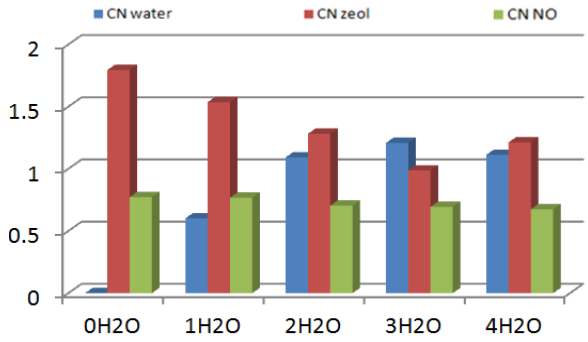

Figuur 6: Coördinatie van Cu met water, zuurstofatomen van het zeoliet en NO voor de MD simulaties met toenemend aantal water-moleculen bij een temperatuur van 300 K.

Deze analyses tonen aan dat Moleculaire Dynamica simulaties een krachtig middel zijn om een complex katalytisch proces te onderzoeken. Ze zijn in staat om inzicht te verschaffen op de moleculaire schaal, wat moeilijk te verkrijgen is via experimentele technieken.

V. Conclusies

Om de NH_3-SCR deNO_x technologie op punt te stellen, is kennis over het gedetailleerd reactiemechanisme vereist. Enkel dan is het mogelijk om een doordachte katalysator te ontwerpen die erin slaagt de NO_x emissies te reduceren conform de wetgeving. Het SCR-mechanisme op Cu-SSZ-13 werd daarom onderzocht met behulp van DFT berekeningen, waarbij de focus ligt bij de adsorptie van NO en de invloed van additionele watermoleculen. Periodieke berekeningen toonden aan dat de geoptimaliseerde structuur van het adsorptiecomplex in grote mate overeenkomt met beschikbare experimentele en computationele data. De NO molecule is loodrecht gericht op het vlak van de d6r subeenheid en het Cu begeeft zich tijdens de NO adsorptie naar de chabasietkooi. Berekeningen met een kleiner clustermodel slaagden er niet in om deze resultaten te reproduceren, door het optreden van eindige cluster effecten. Periodieke ab initio MD simulaties werden gebruikt om de invloed van watermoleculen op het adsportiecomplex te onderzoeken. Een Cu-coördinatieschil bestaande uit NO, twee watermoleculen en 1 à 2 zuurstof-atomen werd vastgesteld. Het toevoegen van extra water-moleculen leidt tot een toename van de Cu-mobiliteit.

Dankbetuigiing

De computationele middelen (Stevin Supercomputer Infrastructuur) en diensten gebruikt in dit werk werden voorzien door het VSC (Vlaams Supercomputer Centrum), gefinancierd door de Universiteit Gent, de Hercules Stichting en de Vlaamse Overheid – departement EWI. Prof. B. M. Weckhuysen (Universiteit Utrecht) en Dr. A. M. Beale (University College London) worden ook erkend voor het verstrekken van experimentele gegevens met betrekking tot dit onderzoek.

REFERENTIES

[1] Brandenberger, S.; Kroecher, O.; Tissler, A.; Althoff, R., The State of the Art in Selective Catalytic Reduction of NOx by Ammonia Using Metal-Exchanged Zeolite Catalysts. *Catalysis Reviews-Science and Engineering* **2008,** 50, (4), 492-531.

[2] Deka, U.; Lezcano-Gonzalez, I.; Weckhuysen, B. M.; Beale, A. M., Local Environment and Nature of Cu Active Sites in Zeolite-Based Catalysts for the Selective Catalytic Reduction of NOx. **2013**.

[3] Kwak, J. H.; Lee, J. H.; Burton, S. D.; Lipton, A. S.; Peden, C. H. F., A Common Intermediate for N2 Formation in Enzymes and Zeolites: Side-On Cu–Nitrosyl Complexes. *Angewandte Chemie International* **2013,** 52, (38), 9985-9989.

[4] Gao, F. H. K., Ja. Szanyi, Janos. H.F.Peden, Charles., Current Understanding of Cu-Exchanged Chabazite Molecular Sieves for Use as Commercial Diesel Engine DeNOx Catalysts - Springer. *Top Catal* **2013,** 56, *1441-1459*.

[5] Goeltl, F.; Hafner, J., Structure and properties of metal-exchanged zeolites studied using gradient-corrected and hybrid functionals. III. Energetics and vibrational spectroscopy of adsorbates. *Journal of Chemical Physics* **2012,** 136, (6), 061503.

[6] Goeltl, F.; Bulo, R. E.; Hafner, J.; Sautet, P., What Makes Copper-Exchanged SSZ-13 Zeolite Efficient at Cleaning Car Exhaust Gases? *Journal of Physical Chemistry Letters* **2013,** 4, (14), 2244-2249.

[7] Lezcano-Gonzalez, I.; Deka, U.; Van Yperen-De Deyne, A.; Hemelsoet, K.; Waroquier, M.; Van Speybroeck, V.; Weckhuysen, B. M.; Beale, A. M., Determining the storage, availability and reactivity of NH3 within Cu-chabazite-based ammonia catalytic reduction systems. *Physical Chemistry Chemical Physics* **2014,** 16, 1639-1650.

[8] Korhonen, S. T.; Fickel, D. W.; Lobo, R. F.; Weckhuysen, B. M.; Beale, A. M., Isolated Cu2+ ions: active sites for selective catalytic reduction of NO. *Chemical Communications* **2011,** 47, (2), 800-802.

[9] CP2K Software package. http://cp2k.org/

Selective Catalytic Reduction of NO_x by ammonia: Unraveling the reaction mechanism through ab initio simulations

Tom Van Den Heede

Supervisor: Prof. dr. ir. Karen Hemelsoet
Counselors: ir. Kristof De Wispelaere, dr. ir. Jeroen Van der Mynsbrugge

***Abstract*: In light of tightening restrictions on NO_x emission in the near future, the Selective Catalytic Reduction of NO_x (SCR deNOx) abatement technology using ammonia as a reducing agent is a highly investigated research area. In earlier studies, several catalytic systems have been tested for the after-treatment of diesel exhaust streams and experiments have shown that Cu-SSZ-13, a chabazite-topology zeolite, provides an active, selective and stable option. The predominant active centre, an isolated Cu^{2+} ion, is hereby mostly positioned near the ring of the d6r subunit. In this thesis, ab initio calculations are performed on both periodic unit cells and finite clusters. The focus lies on the adsorption of NO and the influence of water addition on this adsorbed NO species. Moreover, the mobility of the Cu-ion is monitored by Molecular Dynamics simulations.**

***Keywords:* Selective Catalytic Reduction (SCR), $deNO_x$, density functional theory (DFT), heterogeneous catalysis, adsorption, Molecular Dynamics**

I. Introduction

Due to the presence of nitrogen components in fuels, a huge amount of nitroxides (NO_x) is released into the atmosphere. Once airborne, NO_x can react further into secondary products leading to detrimental effects on the environment such as acid rain and photochemical smog. Therefore, regulations on NO_x emission are continually becoming more stringent and thus additional abatement technologies are required. Because most of the NO_x emissions originate from diesel engine exhausts of mobile applications, a robust technology is required.

A popular technology is the Selective Catalytic Reduction (SCR) of NO_x with ammonia (NH_3) as reducing agent.[1] The hazardous NO_x is hereby converted into N_2 and H_2O. This catalytic system is installed near the diesel particulate filter (DPF) in heavy-duty vehicles, as shown in Figure 1.[2] Even though the NH_3-SCR deNOx technology is already applied in practice, the actual reaction mechanism behind the technology is still a point of discussion.[1] A thorough understanding of this mechanism is however crucial to create an intelligently designed catalyst to meet the upcoming restrictions.

Earlier studies have shown that metal-exchanged zeolites provide a catalytic system with excellent properties in terms of activity and selectivity. Metal exchange has been proven to greatly enhance the performance of the catalyst. Depending on the metal and topology selected, isolated ions, dimers or metal-oxide clusters have been observed.[1][2]

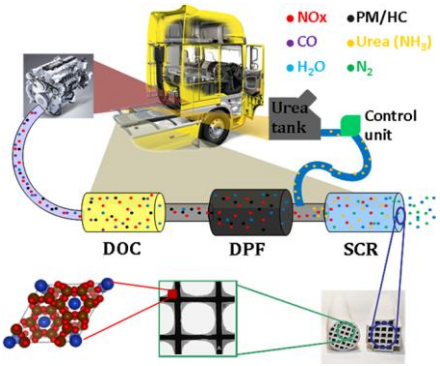

Figure 1: Installation of urea tank in heavy-duty vehicles. Decomposition of aqueous urea gradually produces ammonia for the SCR section of the diesel exhaust after-treatment.[2]

Recently, the focus has shifted towards zeolites with smaller pore windows, since these provide extra hydrothermal stability. This property is especially important for SCR catalysts because they are placed very close to the DPF, which can reach elevated temperatures above 600 K during the soot oxidation process. Both experimental [1][3][4] and theoretical [5][6][7] studies have focused on the use of Cu-SSZ-13 as catalyst material for the $deNO_x$ reaction. Cu-SSZ-13 has a chabazite topology, which consists of chabazite cages surrounded by double 6 membered ring (d6r) subunits. The catalytic centre, mostly isolated Cu ions, is generally presumed to reside near the top of the d6r subunit.[8]

II. Goal and scope

The main focus of this dissertation is on the adsorption of NO on Cu-SSZ-13 and subsequent interactions with additional water molecules, corresponding to the first steps of the reaction path proposed by Kwak et al. shown in Figure 2.[3] Particular attention goes to the geometrical characteristics of the optimized structure, the multiplicity of the adsorbed complex, the NO stretch frequencies and the charge distribution. Next, water molecules are added and the interaction of these molecules with the adsorbed species is thoroughly investigated. The coordination of the Cu ion and its corresponding mobility is monitored using ab initio Molecular Dynamics (MD) simulations. All results are obtained with quantum chemical methods and are linked with experimental results wherever possible.

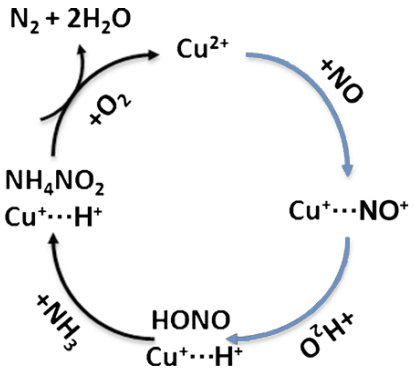

Figure 2: NH_3-SCR reaction pathway as proposed by Kwak et al. [3]

III. Methodology

To elucidate the mechanism behind the NH_3-SCR deNO_x reaction, mainly quantum chemical calculations based on Density Functional Theory (DFT) have been performed. The majority of the simulations consist of periodic calculations on a 36T unit cell (depicted in Figure 3, which represents the optimized geometry upon NO adsorption), using the CP2K software package [9] with a Gaussian Plane Wave basis set. The GGA-approximated PBE functional with D3 dispersion corrections was selected, along with GTH-PBE pseudo-potentials for every atom except Cu. The latter is described by a GTH-BLYP pseudo-potential because the PBE pseudo-potential is not parameterized for this atom.

Periodic calculations usually require long calculation times; hence several finite clusters were used as well, often in combination with an ONIOM-scheme. The high level consisted of the PBE0 hybrid functional, using a DGDZVP basis set, whereas for the low level the UFF force field was applied. The results obtained with these finite clusters were however unsatisfactory, due to lack of stability of the d6r subunits and the inability to correctly distribute the charges. Indeed, using a large 54T-cluster, a Cu^+ ion instead of a Cu^{2+} ion is observed as a result of finite-cluster effects. The analysis of the Cu-NO adsorption complex is therefore mainly based on the periodic calculations. Frequencies of the NO adsorbed complex were determined by a normal mode analysis to validate the results.

Further analysis of the interaction of the adsorbed NO species with water molecules has been done with ab initio Molecular Dynamics calculations, in which the potential energy surface is sampled with an NVT ensemble using the Nosé-Hoover thermostat and a time step of 1 fs. The same level of theory was applied as used for the static periodic calculations. Temperatures of 300 K and 600 K have hereby been investigated.

IV. Results and Discussion

Periodic geometry optimization of the initial adsorption proposed in Figure 2 shows that the Cu-ion is extracted from the upper ring of the d6r subunit towards the chabazite cage upon NO adsorption. The optimized geometry (shown in Figure 3) is in great correspondence with both experimental values [3] as with earlier theoretical research.[5] An NO bond length of 1.15 Å is obtained, as well as a Cu-N-O angle of about 142° for the energetically favoured singlet state. For this state, the adsorption energy equals 126 kJ/mol and the NO molecule is directed perpendicular to the face of the double 6-membered ring. The aforementioned values are fairly independent of the initial configuration. A second validation of the results is provided by the frequencies rather than the obtained geometry. The calculated characteristic NO stretch frequency of the Cu-adsorbed species equals 1952 cm^{-1} and is in good agreement with the 1948 cm^{-1} obtained by experimental IR measurements. [2]

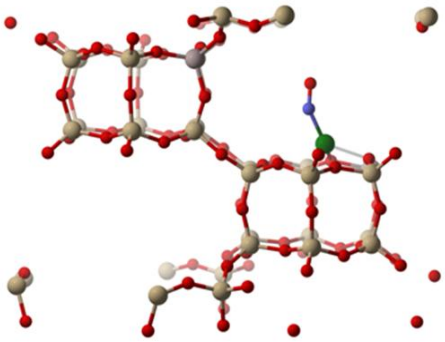

Figure 3: Optimized geometry of NO adsorbed on Cu-SSZ-13. The rhombohedral unit cell used in the periodic calculations is shown. (red:O beige:Si purple:Al green:Cu blue:N)

With the formation of HONO as the next intermediate in mind (see Figure 2), the interaction of water with the adsorbed NO species is also investigated. Mainly dynamic calculations on the periodic system have been used to monitor the positioning of up to 4 water molecules around Cu-NO in function of time. Again, the main focus is on the positioning of the Cu-ion. Analysis shows that the addition of the first two water molecules has the greatest influence, indicating that the third and fourth water molecule do not interact directly with Cu. This implies that the direct coordination shell of Cu includes NO, 2 water molecules and 1 or 2 oxygen atoms of the zeolite framework as depicted in Figure 4. The data shows that addition of water molecules results in the increase of the average Cu-N distance compared to the static optimized geometry without H_2O.

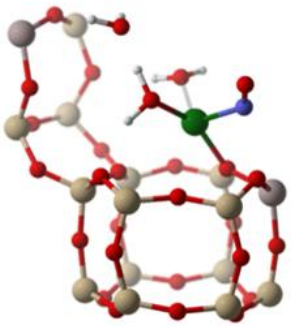

Figure 4: Detailed snapshot of the periodic MD simulation with 3 additional water molecules, indicating the presence of 2 water molecules in the coordination shell of the Cu atom.

The dynamic simulations provide a general view of the most commonly occurring configurations. For every number of water molecules, a snapshot is selected and this configuration is subsequently optimized. It is important to note that there are no guarantees that the selected snapshots are representative for the realistic situation. The total simulation time – maximum 10 ps – is rather limited to draw definitive conclusions. Nevertheless, a thermodynamic analysis of these optimized structures is performed to get an idea on the enthalpy and entropy contribution trends.

The results confirm that the first two water molecules bind more strongly to the Cu, illustrated by a strongly negative enthalpy change. Every H_2O addition is accompanied with an entropy decrease, especially for the second water of which the position is almost completely determined by the position of the first water molecule and the zeolite framework.

The introduction of additional water molecules decreases the interaction between the zeolite framework and the Cu ion, which is pulled towards the chabazite cage. This is accompanied by a mobility increase of the Cu centre, which is visualized by plotting the actual position of the Cu atom for every 100 timeframes. An example of such a plot is given in Figure 5 which contains the results of the dynamic simulation in the absence of water at a temperature of 600 K. Even without water molecules there is a significant mobility of the Cu ion at 600 K. The displacement is however focused in a favoured direction, towards a negatively charged oxygen framework atom next to one of the aluminium substitutions. Addition of water mainly allows deviations from this favoured direction, due to the introduction of attractive forces in multiple directions. Hence, the surface distribution spread gradually increases.

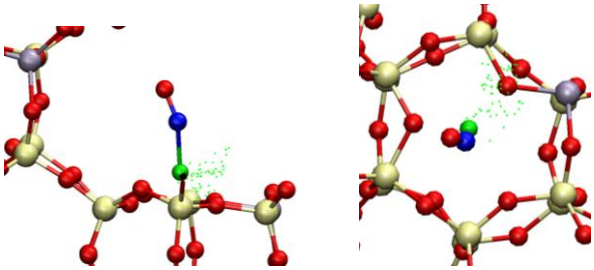

Figure 5: Visualization of the Cu-mobility in the absence of water at a temperature of 600 K. In total 83 dots are plotted since the simulation covers 8227 time steps.

The analysis of the Cu-mobility is in line with the analysis of the Cu-coordination and the results corresponding with the MD simulations at 300 K are shown in Figure 6. With increasing number of water molecules present, the coordination of the Cu with the zeolite framework (CN zeol) decreases, which implies an enhanced Cu mobility. The value below unity of the Cu-NO coordination number (CN NO) does however indicate that the threshold distance used to calculate the coordination numbers is too low. Hence, it is also expected that the actual value of CN water is closer to 2, i.e. the saturated Cu-coordination shell contains 2 water molecules.

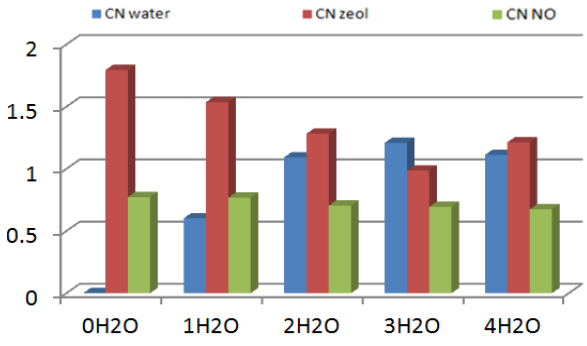

Figure 6: Coordination of Cu with water, zeolite framework oxygen atoms and NO throughout the MD simulations with increasing number of water molecules at 300 K.

Overall, it is shown that molecular dynamics simulations are a powerful tool to investigate a complex catalytic process and to provide molecular-scale insight which is hard to obtain experimentally.

V. Conclusions

To optimize the NH_3-SCR deNOx abatement technology, a detailed understanding of the reaction mechanism is required. Only then, it is possible to create an intelligently designed catalyst that is able to reduce the NO_x emissions in accordance with the regulations. The SCR-mechanism on Cu-SSZ-13 has therefore been investigated with DFT-based calculations, focusing on the NO adsorption and influence of additional water molecules. Periodic calculations have revealed the optimized structure of the adsorbed species, which is in excellent correspondence with earlier experimental and computational data. The NO molecule is positioned perpendicular to the face of the d6r subunit and the Cu is pulled towards the chabazite cage upon NO adsorption. Calculations on a smaller cluster model did not succeed in reproducing these results, due to finite-cluster effects. Periodic ab initio MD simulations have been used to assess the influence of the presence of water molecules on the adsorbed species. A Cu coordination shell containing NO, two water molecules and 1 or 2 oxygen atoms of the zeolite framework has been established. Introduction of additional water molecules leads to an increase of the Cu mobility.

Acknowledgements

The computational resources (Stevin Supercomputer Infrastructure) and services used in this work were provided by the VSC (Flemish Supercomputer Center), funded by Ghent University, the Hercules Foundation and the Flemish Government – department EWI. Prof. B. M. Weckhuysen (Utrecht University) and Dr. A. M. Beale (University College London) are also acknowledged for providing experimental data related to this research.

References

[1] Brandenberger, S.; Kroecher, O.; Tissler, A.; Althoff, R., The State of the Art in Selective Catalytic Reduction of NOx by Ammonia Using Metal-Exchanged Zeolite Catalysts. *Catalysis Reviews-Science and Engineering* **2008,** 50, (4), 492-531.

[2] Deka, U.; Lezcano-Gonzalez, I.; Weckhuysen, B. M.; Beale, A. M., Local Environment and Nature of Cu Active Sites in Zeolite-Based Catalysts for the Selective Catalytic Reduction of NOx. **2013**.

[3] Kwak, J. H.; Lee, J. H.; Burton, S. D.; Lipton, A. S.; Peden, C. H. F., A Common Intermediate for N2 Formation in Enzymes and Zeolites: Side-On Cu–Nitrosyl Complexes. *Angewandte Chemie International* **2013,** 52, (38), 9985-9989.

[4] Gao, F. H. K., Ja. Szanyi, Janos. H.F.Peden, Charles., Current Understanding of Cu-Exchanged Chabazite Molecular Sieves for Use as Commercial Diesel Engine DeNOx Catalysts - Springer. *Top Catal* **2013,** 56, *1441-1459*.

[5] Goeltl, F.; Hafner, J., Structure and properties of metal-exchanged zeolites studied using gradient-corrected and hybrid functionals. III. Energetics and vibrational spectroscopy of adsorbates. *Journal of Chemical Physics* **2012,** 136, (6), 061503.

[6] Goeltl, F.; Bulo, R. E.; Hafner, J.; Sautet, P., What Makes Copper-Exchanged SSZ-13 Zeolite Efficient at Cleaning Car Exhaust Gases? *Journal of Physical Chemistry Letters* **2013,** 4, (14), 2244-2249.

[7] Lezcano-Gonzalez, I.; Deka, U.; Van Yperen-De Deyne, A.; Hemelsoet, K.; Waroquier, M.; Van Speybroeck, V.; Weckhuysen, B. M.; Beale, A. M., Determining the storage, availability and reactivity of NH3 within Cu-chabazite-based ammonia catalytic reduction systems. *Physical Chemistry Chemical Physics* **2014,** 16, 1639-1650.

[8] Korhonen, S. T.; Fickel, D. W.; Lobo, R. F.; Weckhuysen, B. M.; Beale, A. M., Isolated Cu2+ ions: active sites for selective catalytic reduction of NO. *Chemical Communications* **2011,** 47, (2), 800-802.

[9] CP2K Software package. http://cp2k.org/

Table of contents

List of abbreviations

6mr	6-membered ring
CHA	Chabazite
CN	Coordination number
d6r	double 6-memberd ring
DFT	Density Functional Theory
DOC	Diesel Oxidation Catalyst
DPF	Diesel Particulate Filter
DZVP	Double Zeta Valence Polarized
EPR	Electron Paramagnetic Resonance
EXAFS	Extended X-ray Absorption Fine Structure
GGA	Generalized Gradient Approximation
GHG	Greenhouse gas
GPW	Gaussian Plane Wave
GTH	Goedecker-Teter-Hutter
GTO	Gaussian Type Orbital
HC-SCR	Hydrocarbon-assisted Selective CatalyticReduction
HF	Hartree-Fock
KS	Kohn Sham
LDA	Local Density Approximation
LEA	Low Excess Air
MC	Monte Carlo
MD	Molecular Dynamics
MM	Molecular Mechanics
MNDO	Modified Neglect of Diatomic Overlap
NH3-SCR	Ammonia-assisted Selective Catalytic Reduction
NOx	Nitrogen Oxides
ONIOM	Our own N-layered Integrated molecular Orbital and molecular Mechanics
PM3	Parametric Method 3
PM6	Parametric Method 6
QM	Quantum Mechanics
SCR	Selective Catalytic Reduction
SNCR	Selective Non-Catalytic Reduction
STO	Slater Type Orbital
UFF	Universal Force Field
XANES	X-ray Absorption Near Edge Structure
XC	Exchange and correlation

Chapter 1

Introduction

1.1 Negative impact of nitrogen oxides

Today the attention paid to the preservation of the environment reaches unprecedented extents. Politicians and the society in general are exerting a strong pressure on the consumers and the industry to minimize all detrimental emissions and pollutants. Nevertheless, a vast amount of pollutants ends up in the atmosphere. In Figure 1-1 the air pollution emission rates of certain polluting substances is compared. Even though this chart is based on data from 2006, the qualitative picture of the emissions remains unchanged.

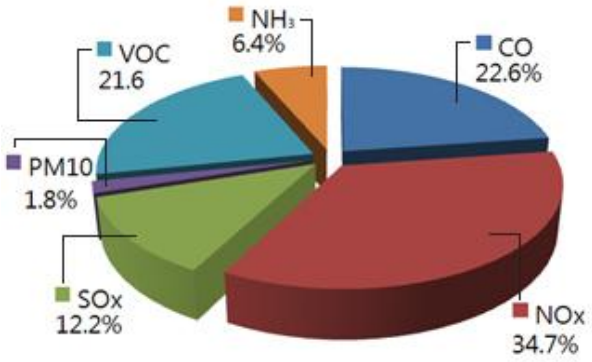

Figure 1-1: Relative share volumetric air pollution emission rate per substance [1]

The largest section of the chart is attributed to the emission of nitroxides (NO_x). It can be seen that NO_x emission accounts for 34.7 V% of the total emissions, which corresponds with 1274969 tonnes per year. Emissions of this proportion are bound to have a strong influence on air quality and the environment in general. Possible consequences include the formation of acid rain, photochemical smog and the depletion of the ozone layer. Furthermore nitrogen oxides are active greenhouse gases (GHG). Two of the aforementioned consequences are highlighted briefly in the subsequent sections.

1.1.1 Acid rain

Once in the atmosphere, NO_x can react with other natural components such as water vapour, effectively creating acidic products. The reaction of NO_2 with H_2O for example leads to the formation of nitrous acid (HNO_3). These products are dissolved in the water vapour and as a result the pH of the water can drop as low as 4. The rain formed by this acidified water causes damage to buildings and structures that come into contact. Evidently this acid rain can have an effect on the aquatic life in still waters as well.

1.1.2 Photochemical smog

The word 'smog' is a combination of the words smoke and fog. More specifically photochemical smog is used to describe a certain mixture of so called primary and secondary pollutants. Primary pollutants include nitrogen oxides and volatile organic compounds, which are both introduced into the atmosphere via vehicular emissions and industrial processes. Secondary pollutants are formed through reaction of primary pollutants with ultraviolet light. Examples of these secondary pollutants are harmful substances such as ozone, aldehydes and peroxyacetylnitrate.[2] While ozone in the stratosphere protects us from the dangerous radiation from the sun, ozone on ground level is toxic and can lead to headaches, fatigue and serious respiratory problems. Many densely populated areas that have to deal with a lot of traffic are exposed to the phenomenon of photochemical smog, due to a high production rate of primary pollutants. This creates an unhealthy environment and furthermore disturbs the view and image of the city.

1.2 Reduction of NO_x emissions

In Figure 1-2 the relative importance of NO_x producers is shown. About 28.8 wt% of the total NO_x production originates from stationary combustion processes, predominantly from the energy sector (15.7 wt%). However, the most extensive production is attributed to mobile sources, namely 32.7 wt% from on-road and 9.1 wt% from non-road sources. Especially diesel engines are very detrimental in terms of air pollution. Therefore, the main research is conducted to find commercial technologies which can be used to reduce the NO_x emission originating from these transport applications.

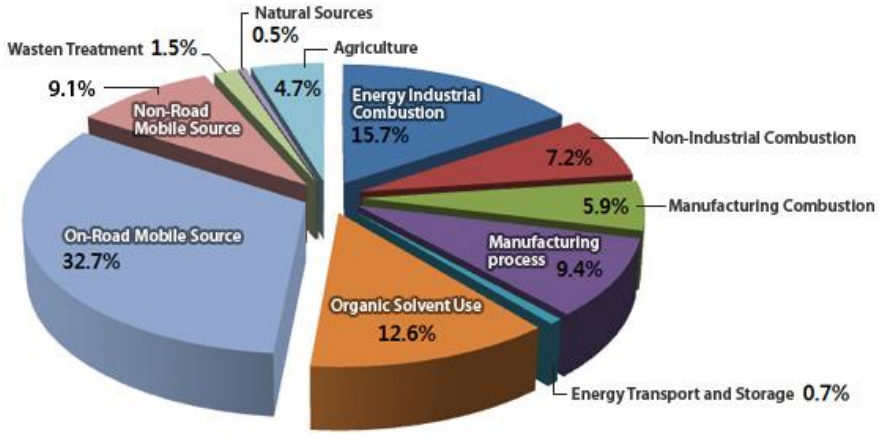

Figure 1-2: Comparison of the main NO_x sources (in wt%)[1]

Figure 1-3 presents the time-evolution of the legal restrictions concerning particulates and nitroxides.[2] These restrictions are plotted on the vertical and horizontal axis respectively and are expressed in g/kWh. In other words, the work [kWh] done by running an engine over a certain period may only lead to a limited mass production [g] of particulates and NO_x. A larger area on Figure 1-3, thus corresponds with more lenient restrictions. The Euro 6 norm, which was initially planned for 2013, will be introduced in two stages between 2015 and 2017; [2] and will apply among others to the sale of new vehicles.[3] Clearly supplementary (post-)treatment measures are required to keep the emission within boundaries. This stresses the importance of developing and optimizing catalytic technologies, allowing the conversion of hazardous components in the combustion gases into harmless molecules.

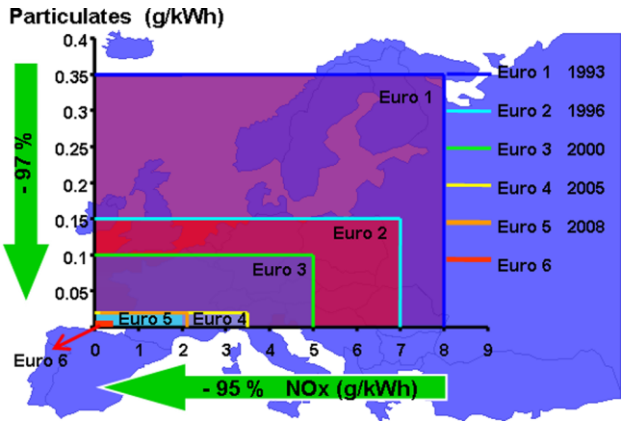

Figure 1-3: Evolution of the European legislation concerning emission of particulates and NO_x[3,4]

In the following, examples of technologies and methods which are being applied or studied are elaborated further.[5,6]

Hydrogenation units

The presence of nitrogen compounds in fossil fuels is the main cause for the emission of nitroxides into the atmosphere. Modern refineries are therefore equipped with standard hydrogenation units, which typically use a Co/Mo catalyst, eliminating most of the nitrogen from the fuels prior to the actual combustion. Unfortunately, the installation of these hydrogenation units does not suffice to respect the continuously more stringent European legislation.

Low excess air (LEA) combustion

A second method is a combustion modification for boilers, which reduces the amount of NO_x being formed during the combustion. The so called LEA combustion technique aims to lower the peak flame temperature - and hence the NO_x formation - by reducing surplus oxygen at the burner flame. This is done by reducing the amount of air introduced into the boiler until the optimal stoichiometry is reached. This technique is easily implemented since it only requires a single physical modification, i.e. adjustment of the combustion controller.

Staged combustion

When applying the staged combustion modification for boilers, the combustion process is divided in two zones. In the first zone, fuel is fired with a deficiency of air, i.e. less than the stoichiometric amount. This way a fuel-rich state is present near the primary flame. The rest of the combustion air is introduced in the second zone, where the combustion of the fuel is completed. Overall there is a hot first zone with a deficiency of O_2 and a second colder zone where the remaining O_2 is fed. In other words, the main NO_x producing factors, being high temperatures and high oxygen partial pressures, never occur simultaneously.

Selective Non-catalytic Reductions (SNCR)

SNCR systems are also designed to chemically reduce a portion of the NO_x emissions. The chemical reactions involved are however all gas phase homogeneous chemical reactions, in contrast to the catalytic version discussed in the next paragraph. The main variable to be optimized in order of obtaining a maximum efficiency is the reaction temperature. Unfortunately, large uniformity of gas

temperatures in combustion systems is difficult to obtain, hence the overall NO_x reduction efficiencies of SNCR systems are rather limited to 50% at best.

Selective catalytic reduction (SCR)

In an SCR system, exhaust gas is mixed with ammonia-containing air (other reducing agents than ammonia are also possible) and is subsequently passed over a catalyst. The catalyst is used to promote the reaction of NO_x and ammonia to form nitrogen and water. By introducing this catalyst, a properly designed and operated system can achieve NO_x reductions ranging from 50% to even 90%. The efficiency increase compared to the SNCR systems is of course slightly counteracted by the increase in capital and operating costs. Furthermore, the presence of the heterogeneous catalyst infers a complex system. Nevertheless, in light of the upcoming restrictions on NO_x emission, the advantage of the performance outweighs the disadvantages.

1.3 Aim of the dissertation

From the information provided above, it should be clear that the optimization of innovative processes such as the ammonia assisted selective catalytic reduction of NOx is crucial for obeying the continuously more stringent European legislation. More precisely, this technology should be implemented for the after-treatment of diesel vehicle exhausts, the main NO_x production source. In order of achieving high NO_x conversions and a high selectivity towards nitrogen and water, the selected catalyst and operating conditions should be a perfect match for the required reactions. This type of intelligent catalyst selection and design, based on structure-activity relations, is of course only possible if the reaction mechanism involved is known. This dissertation focuses on the catalytic active site in the ammonia assisted SCR on a Cu-SSZ-13 catalyst, since experiments have shown this could be an efficient choice. The main research is conducted with help of ab initio simulations, of which the basics are summarized in Chapter 3. Both static and dynamic simulations are performed. The Cu-SSZ-13 catalyst is hereby predominantly modeled using periodic unit cells. Results will focus mainly on the NO adsorption (Chapter 4) and the influence of H_2O addition (Chapter 5).

Chapter 2

Selective catalytic reduction of NO_x

As suggested in the previous chapter, the selective catalytic reduction (SCR) of NO_x technology can be applied to combustion gases to drastically decrease the residual NO_x concentrations of the exhaust. The general idea of the SCR of NO_x is to convert the nitroxides into harmless components, namely nitrogen gas and water, by contacting the combustion gases with a reducing agent on an intelligently designed catalyst. Lately, experiments have indicated that metal-exchanged zeolites proved to be very useful for this task. Other possible catalysts include noble metals and metal oxides. The main differences between these catalysts is highlighted in paragraph 2.2

The chapter starts off with a comparison of the most important reducing agents, i.e. hydrocarbons and ammonia. The latter is discussed in more detail, focusing on the most important reactions that can occur, after which a general mechanism is proposed.

2.1 Comparison reducing agents

At present, the main reducing agents being examined are hydrocarbons (HC-SCR) and ammonia or urea (commonly referred to as NH_3-SCR). The use of CO or H_2 as reducing agent is less popular, although it has been reported that the presence of hydrogen in HC-SCR enhances the low-temperature activity.[7] This can be useful since most SCR-catalysts operate better at temperatures of around 350 °C while the typical temperature range in lean exhausts of diesel engines is between 150 °C and 300 °C.[8] In this section, the advantages and disadvantages of the different reducing agents are discussed. Note that both options can be implemented simultaneously in a dual SCR system to combine the advantages (see Figure 2-1). During the first stage HC-SCR occurs and NH_3 is hereby produced as side product. The NH_3 produced is subsequently passed over the NH_3-SCR system in the second stage, leading to a more thorough reduction of the residual NO_x content.[8] In the remainder of this dissertation, however, the main focus will be solely on NH_3-SCR.

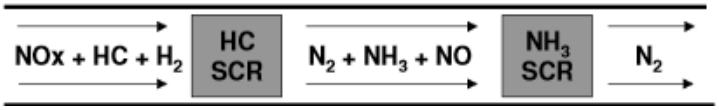

Figure 2-1: Dual SCR Concept [8]

2.1.1 HC-SCR

The use of hydrocarbons as reducing agents for the HC-SCR reaction seems to be a very attractive option since partially burned or unburned hydrocarbons are already available in the exhaust stream. König and co-workers from Volkswagen [9], who developed one of the first systems using this HC-SCR technique around 1985, used a Cu-exchanged mordenite catalyst for this. Later, other metals such as

Fe, Mn, Cr and V were tested but Cu was found to be the most effective one. An alternative was suggested by Smedler et al. [10] using an Ag/Al_2O_3 system at 400°C, with propane, propylene or alkenes as reducing agents. However, this second option proved to be unable to operate at lower temperatures. Over the years research has been able to lower this temperature requirement though, e.g. by addition of hydrogen or switching to a Pt/Al_2O_3 system. Nowadays, HC-SCR is mostly applied in light duty vehicles, whereas for heavy duty vehicles mostly NH_3-SCR is used.

2.1.2 NH_3-SCR

During the 1970s, NH_3-SCR was already being applied in stationary applications.[11] Due to the toxicity of ammonia, it is clear that direct storage of ammonia in pressurized vessels of motorized vehicles is highly discouraged. This would limit the use of NH_3-SCR to stationary combustion processes in an easy to control setting. Instead, for mobile applications (especially heavy duty vehicles) urea tanks can be installed, as shown in Figure 2-2. Via a control unit the required amount of ammonia is released by decomposing aqueous urea according to reactions (1) and (2):

$$(NH_2)_2CO \rightarrow NH_3 + HNCO \quad (1)$$

$$HNCO + H_2O \rightarrow NH_3 + CO \quad (2)$$

From these equations, it is clear that researching urea-SCR is equivalent to researching NH_3-SCR.

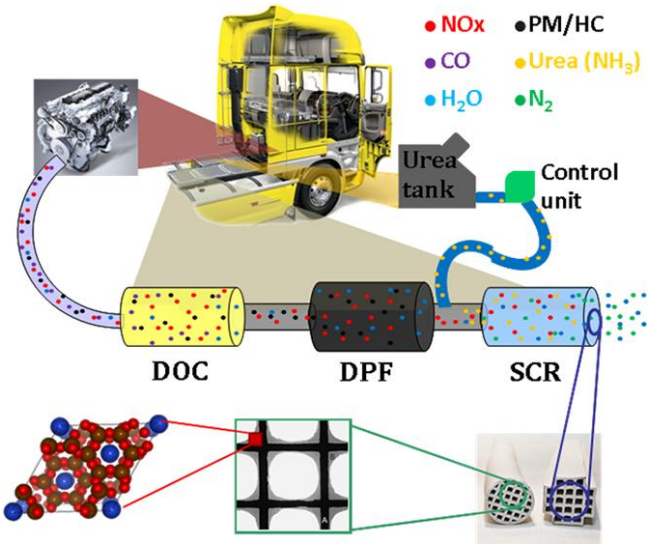

Figure 2-2: Concept of installing urea tanks in heavy duty vehicles [4]
DOC: Diesel Oxidation Catalyst - DPF: Diesel Particulate Filter

The basic SCR reaction using the released ammonia as reducing agent is described as follows:

$$4\,NH_3 + 4\,NO + O_2 \rightarrow 4\,N_2 + 6\,H_2O \quad (3)$$

The basic SCR reaction (3) can proceed faster in the presence of a 1:1 mixture of NO and NO_2, which is aptly referred to as fast SCR:

$$NO + NO_2 + 2\,NH_3 \rightarrow 2\,N_2 + 3\,H_2O \quad (4)$$

The explanation for this increased rate is that NO_2 is a much stronger oxidizing agent than O_2. In reality however, the NO_2 content in a typical diesel engine exhaust is far too low for the fast SCR to occur to a certain extent. This observation led to the implementation of exhaust gas recycling, hence increasing the amount of NO_2 in the feed. On top of that the diesel oxidation catalyst, designed to oxidize CO and unburned hydrocarbons in the exhaust, also provides extra NO_2. Nevertheless the remainder of this dissertation will focus on the presence of NO and not on NO_2.

As usual, reaching a maximal selectivity is hindered by several side reactions that can occur under typical SCR conditions. The most important side reaction (5) is the non-selective oxidation of ammonia itself into nitrogen or undesired nitrogen compounds such as NO_x and N_2O.[12]

$$4\,NH_3 + 3\,O_2 \rightarrow 2\,N_2 + 6\,H_2O \quad (5)$$

However, the extent of this reaction is fairly limited when using metal exchanged zeolites at temperatures between 200 °C and 400 °C.[13] The use of this catalyst type has many other advantages as well, and this is elaborated in more detail when discussing the catalyst selection in section 2.2.

Although certain NH_3-SCR systems are able to drastically decrease the residual NO_x content, there are a few drawbacks:

- Ammonia can react with sulphates present in the diesel, leading to the formation of ammonium sulphates. These components can accumulate, eventually causing irreversible damage to the catalyst.
- There is a chance that some of the NH_3 is not converted, which would imply toxic emissions coming from the vehicle exhaust. To counteract this potential NH_3 slip, oxidation catalysts are installed in form of a metallic substrate coated with platinum. As a consequence, residual CO and unburned hydrocarbons are oxidized as well. [14,15]

2.2 Catalyst selection

The following section provides extra information on the selection of an optimal SCR catalyst, based on several specific criteria. One of the most important aspects required for a commercially viable catalyst is the hydrothermal stability. This is easily understood when looking back at the practical implementation in mobile applications, depicted earlier in Figure 2-2. Due to the placement of the SCR-section after the diesel particulate filter, the catalyst needs to withstand temperatures over 650 °C during the soot oxidation processes.

First, a general overview is given of the catalyst types which have been investigated or tested thus far in practice. The types are compared in terms of performance, availability and synthesis ease. From this overview, it will become clear that the combination of high performance, i.e. activity and selectivity, and hydrothermal stability makes metal-exchanged zeolites an excellent choice as SCR-catalyst.

Section 2.2.2 is therefore devoted to this latter catalyst type. Special attention is paid to the influence of the zeolite topology and the selected metal. The final part (section 2.2.3) focuses on the catalytic properties of Cu-SSZ-13, which is potentially one of the best performing metal-exchanged zeolites for the NH_3-SCR reaction. In particular, different views on the location and nature of the active site are provided and compared.

2.2.1 General overview

Generally speaking, both HC-SCR and NH_3-SCR predominantly use noble metals, metal oxides or metal-exchanged zeolites as catalysts. An overview was recently provided by Deka et al.[4] As can be seen from Figure 2-3, noble metals are active even at low temperatures (around 150 °C). The downside of these catalysts is of course their high cost and the possible formation of N_2O (strong GHG). Metal oxides are less expensive but still very effective and are hence widely used for stationary SCR applications. Vanadium oxide for example, shows great catalytic properties but due to toxicity concerns of the volatile vanadia (above 650 °C) mobile applications are highly discouraged. Titania has been tested before as well, but in the end the rutile-anatase phase transition proved to be too troublesome due to possible catalyst deactivation. Fortunately the last catalyst type, being the metal-exchanged zeolites, combines high performance without the aforementioned problems.

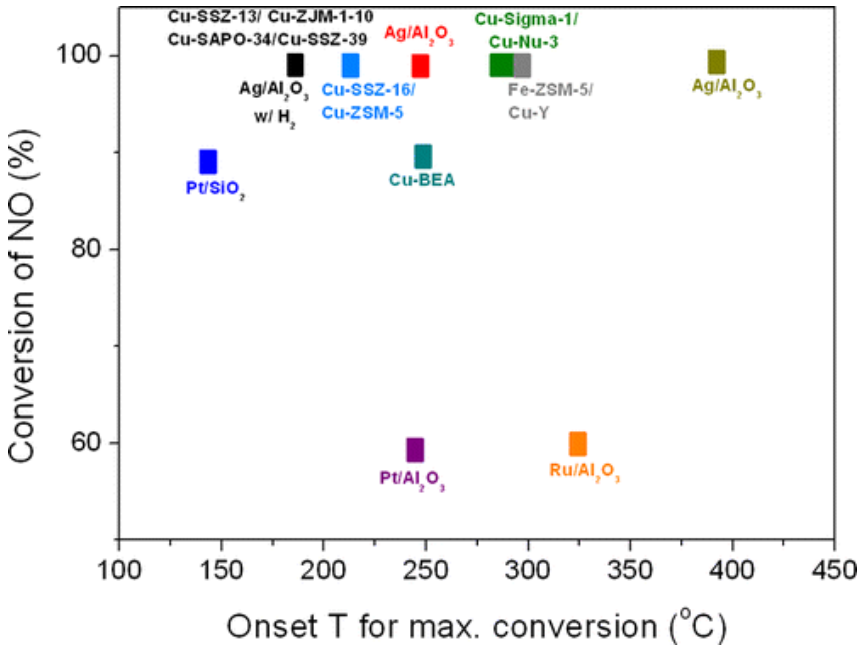

Figure 2-3: Comparison of conversion and activity for several SCR catalytic systems[4]

2.2.2 Metal-exchanged zeolites

Since the 1990s the importance of this class has increased continuously. Initially it seemed that lack of hydrothermal stability and resistance against poisoning would prevent commercialization of this type. However, recent more detailed studies have shown that some metal-exchanged zeolites are highly suitable for NH_3-SCR. The combination of high activity and nitrogen selectivity, a cheap production process and nontoxic properties makes them highly suited for mobile emission control.

Over the years, multiple combinations of metals and zeolite frameworks have been tested. In the following paragraphs, the most important possibilities concerning the zeolite topology and metal selection are mentioned and compared. Throughout the comparison of the topologies, some general

observations concerning the nature and roll of the active site(s) are provided. The influence of the selection on performance will be discussed, which will lead to the suggestion of using Cu-SSZ-13 as catalyst to be examined throughout the dissertation. Indeed, when looking at Figure 2-3 this catalyst clearly displays an excellent NO conversion, requiring only an onset temperature of about 180 °C. Despite having higher onset temperatures, Cu-ZSM-5 and Fe-ZSM-5 are used very frequently as well. Also in Figure 2-3, the catalysts mentioned for the HC-SCR can be found and it is seen that Pt/Al_2O_3 indeed offers lower temperature requirements compared to Ag/Al_2O_3, albeit at the expense of the maximum obtainable NO conversion.

Comparison topologies

Concerning the zeolite framework, the most extensively studied options are Y (FAU framework), mordenite (MOR framework), Beta (BEA framework), ZSM-5 (MFI framework) and most recently SSZ-13 (CHA framework). To get a first idea of the diversity, the topologies of the CHA, MFI and BEA framework are represented schematically in Figure 2-4, with indication of the pore window sizes and maximum molecule dimensions within the cage. In practice, the trend is hereby shifting to zeolites with smaller pore windows (mainly CHA structure) resulting in an increased hydrothermal stability. Large pores can contain more hydrocarbons, which can thermally destroy the catalyst when exposed to excessive heat.[13] Furthermore, small pores decelerate the net dealumination rate, increasing the life span of the catalyst to a large extent. For each topology, the presence of the metal, i.e. cation-exchanged zeolites, had a beneficial effect on the activity, since the transition metal ion acts directly as a redox catalytic centre.

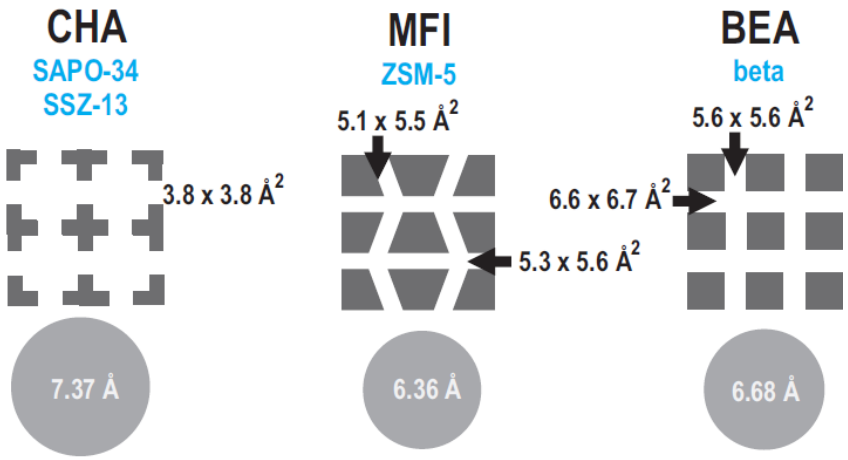

Figure 2-4: Schematic overview of the CHA, MFI and BEA framework with indication of pore sizes and maximum cage dimensions

In the following, the topology of the FAU, ZSM-5 and SSZ-13 framework is discussed in more detail. Again referring to Figure 2-3, these topologies are among the best available catalytic systems in terms of activity and maximum conversion. A recent overview of their main properties was also given by Deka et al. [4]

- Y (FAU)

The crystal structure of FAU is given in Figure 2-5 and it can be seen that the main structure consists of two subunits, being a sodalite cage (sod) and a double 6-membered ring (d6r). Molecules with a spherical diameter of up to 11.24 Å can reside within the supercage. However diffusion is only possible for molecules with maximum dimensions below 7.37 Å. In Figure 2-5 (b), possible Cu locations are indicated as blue dots. These positions were determined with help of crystal and powder XRD studies and it was stated that the relative importance of each position is among others dependent on the Si/Al ratio. A second factor influencing the actual position is the interaction with molecules in the process stream. This is a common observation for all topologies and this effect is discussed more elaborately for the CHA framework hereafter. Studies performed by Kieger et al. [16] suggested $[Cu\text{-}O\text{-}Cu]^{2+}$ species are the main active site present in Cu-Y and CuO clusters and Cu ions were only observed in minor concentrations.

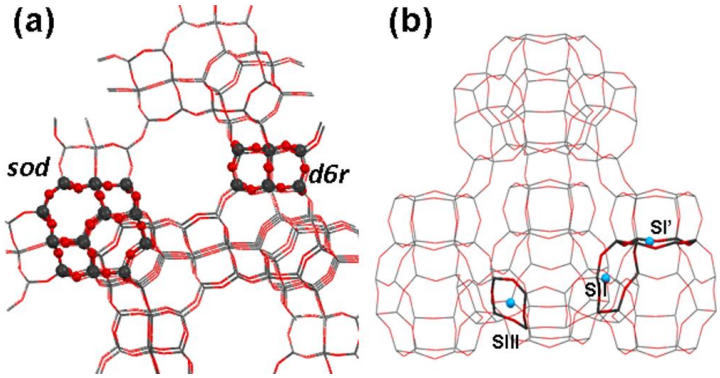

Figure 2-5: Crystal structure of FAU framework
(a) indication of the sodalite cage (sod) and double 6-membered rings (d6r) subunits
(b) indication of the Cu positions within the framework as determined by XRD studies

- MFI (ZSM-5)

In Figure 2-6 the crystal structure of a catalyst with a MFI framework is shown. A classical and widely used example is the Cu/Fe-ZSM-5 catalyst. The subunits indicated on the figure form a combination of straight and zigzag channels, with maximum inclusion dimensions limited to about 6.36 Å (see also Figure 2-4). Diffusion along the larger channels is possible for molecules with dimensions below 4.7 Å, while the smaller channels can only handle molecules up to 4.46 Å. On Figure 2-6 (b), 5 different cationic positions can now be distinguished, which were again determined through XRD studies. The complex nature of the subunits and the many possible Cu locations complicate the evaluation of this catalyst and more specifically the interaction/coordination of the Cu-species within the framework. Depending on the reaction conditions, e.g. moisture and temperature, both Cu^{+} as Cu^{2+} were observed as well as Cu-O-Cu species.[17] Recently the interaction of NO with Cu-ZSM-5 has been investigated with help of EPR and FT-IR spectroscopy to find the main surface intermediates involved in the SCR deNOx reaction.[18]

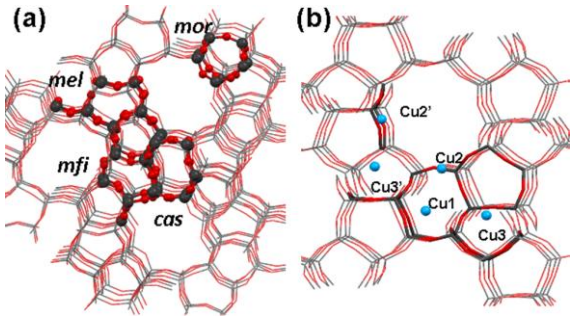

Figure 2-6: Crystal structure of MFI framework

- CHA (SSZ-13)

Figure 2-7 illustrates the structure of a CHA framework, which is composed of double 6-membered ring (d6r) and chabazite cage (cha) composite units. While the cage allows molecules up to 7.37 Å, the dimensions for possible diffusion along the axis is limited to 3.72 Å, which imposes significant restrictions compared to the topologies discussed above.

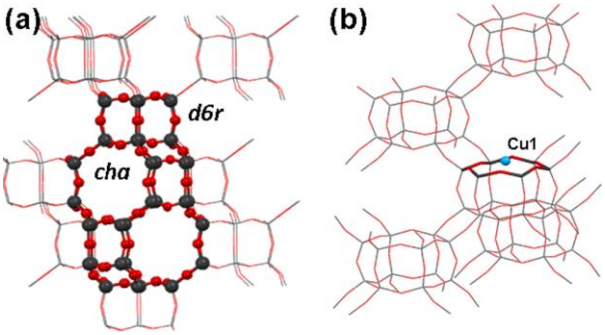

Figure 2-7: Crystal structure of CHA framework

In Figure 2-7 (b), it can be seen that a unique cation location is reported by Deka et al. [19, 20] on the face of the d6r subunit. In section 2.2.3, this location is investigated in more detail and it will be shown that interaction of the Cu-species with the reagents grants certain mobility to the Cu-species. The actual Cu-location has been a point of discussion for quite a while. Peden et al. [13] for example clearly proposed multiple possible positions, including positions near the centre of the large chabazite cage , in contrast with the findings of Korhonen et al. [20] and Korhonen et Al. The active site as proposed in Figure 2-7 (b), now only consists of isolated Cu^{2+} ions, which is highly beneficial as explained at the start of this section. Compared to Cu-ZSM-5, this results in a higher SCR activity, while contributing less to the NO decomposition side reaction.

In summary, the discussion above clearly illustrates why Cu-SSZ-13 with its CHA framework has gained so much attention in the last few years. This catalyst excels in terms of performance, due to the smaller pore windows, which increase the hydrothermal stability. Furthermore, the main Cu-species present are isolated monomers, implying a great combination of activity and selectivity. Also from a research perspective, Cu-SSZ-13 (CHA) is a very appealing option, since the (nearly) unique location of the Cu-species allows a more straightforward analysis of the computational results and thus provides a link with experimental data. XRD-diagrams for example, which would otherwise represent a volume average over several positions, are now more easily interpreted.

On the other hand, the unique location of the ion indicates that it is difficult to obtain high copper loadings in practice. Because of all aforementioned benefits, Cu-SSZ-13 was selected as model system for this dissertation and is investigated in more detail.

2.2.3 Cu-SSZ-13 as selected catalyst for NH_3-SCR deNO_x

Cu location

In Figure 2-8 (b) the crystal structure of a CHA framework is presented with indication of the possible Cu^{2+} cation positions. Copper position II, located within the face of the 6-membered ring hereby corresponds with the supposedly unique location proposed by Korhonen et al. Peden et al. state that smaller cations are predominantly present at position I and II in dehydrated samples. However, as stated before, interaction with molecules such as water can induce Cu-mobility. Position III located near the centre of the CHA cage is therefore also considered a possibility, as to maximize the coordination of Cu with e.g. water molecules. Larger cations such as Cs^+ are said to reside more at position IV, but this is of course less relevant in this research.

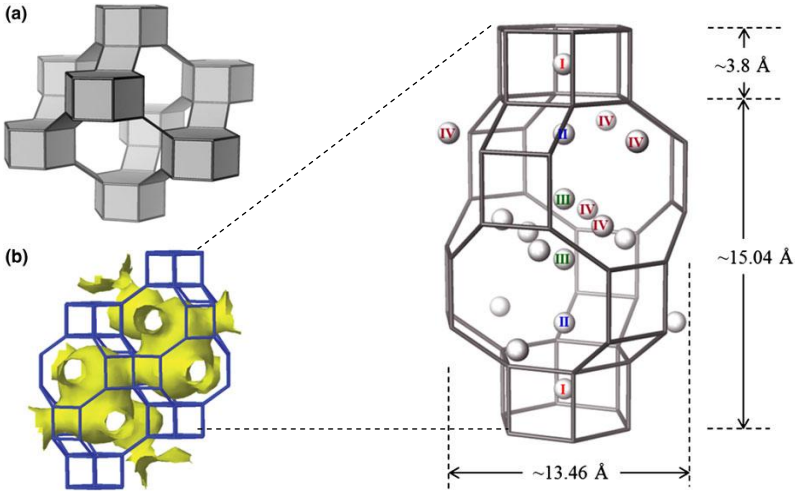

Figure 2-8: (a) Crystal structure of the CHA framework [4]
(b) Possible crystallographic positions of Cu^{2+} within SSZ-13 framework

A close-up of the local environment of the cation at the position mentioned by Deka et al. [19] is provided in Figure 2-9. The red balls indicated with an asterisk represent the three nearest neighbour lattice oxygen atoms to which the copper is coordinated. Rietveld refinement of high temperature XRD data showed that after calcination the average Cu-O distance was about 1.93 Å. The situation prior to the calcination is slightly different, since then a coordination of 4 oxygen atoms is reported at an average distance of 2.02 Å. Reduction of the coordination number during calcination is explained by the dehydration of the Cu^{2+}-ions, which is accompanied by a Cu^{2+} shift from the cavity above the d6r unit towards the face of the ring. A similar situation can be seen in Figure 2-10, where the opposite shift is caused by interaction of the cation with ammonia. In other words, Deka et al. also report that interaction with reagents grants a form of mobility to the cation, however they still attribute this to the same location. This shows that the word "unique" should be carefully interpreted.

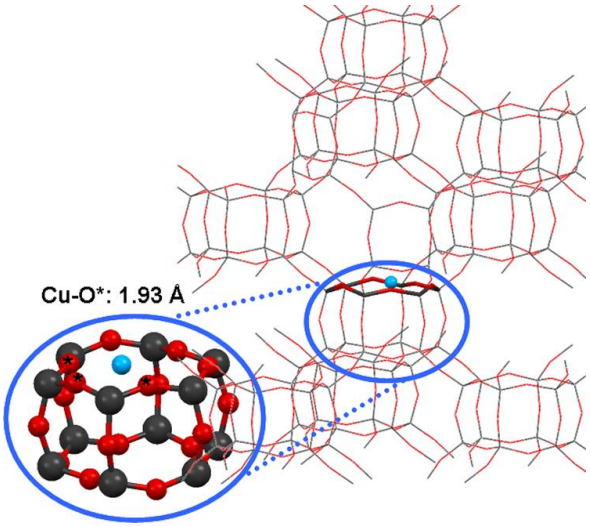

Figure 2-9: Local environment of Cu^{2+} in the d6r subunit of SSZ-13 [19]

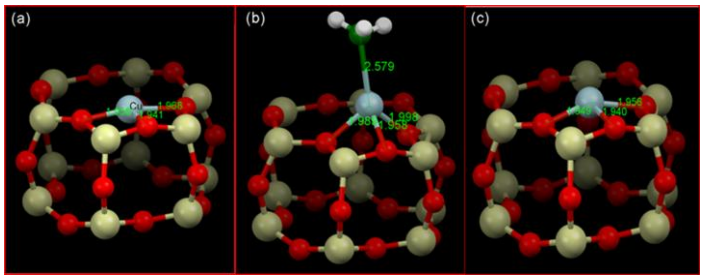

Figure 2-10: Relocation of the Cu ion as result of interaction with NH3 at ~125°C under SCR conditions [19]

Nature of the Cu-species

From the discussion of the metal-exchanged zeolites, in particular the chabazite topology zeolites such as Cu-SSZ-13, it was clear that isolated ions are the predominant species. So far, only Cu^{2+} has been mentioned in this regard, however due to changes in the local environment, Cu^{+} can occur as well. XAFS studies by Kispersky et al. [21] were performed on several catalysts, including Cu-SSZ-13, and it was found that a mixture of both oxidation states existed for all examined cases. For Cu-SSZ-13 under reaction conditions at 200 °C, it was stated that 15 % of the Cu species existed in the form of Cu^{+}. Later spectroscopic studies combined with theoretical data, suggested that for the fast-SCR reaction only Cu^{2+} was present.[22] Standard SCR conditions under a more reducing atmosphere, due to the absence of NO_2, did however allow a certain amount of Cu^{+} species to appear. IR measurements have been performed and confirm the presence of both Cu^{+} and Cu^{2+}.

Computational work with both Cu^{+} as Cu^{2+}, has been performed by Göltl et al.[23-25] Discussion of these results is however delayed to Chapter 4, where a direct comparison with the results of this dissertation can be made.

2.3 NH3-SCR: generalized reaction mechanism

There are still a lot of uncertainties related to the reaction mechanism involved in the NH_3-SCR of nitroxides. What has been generally accepted though is that the nitrogen formed during the reaction is formed by combining one nitrogen from the ammonia and one nitrogen from the nitroxide. This was established by performing experiments with isotopically labelled reactants.[26] The reaction mechanisms being considered should take this into account.

Figure 2-11 illustrates possible reaction pathways and the key intermediates. Most of the reaction mechanisms proposed start with the oxidation of NO to NO_2. This step is often opted as the rate determining step. The formed NO_2 can follow several paths, one of which consists of the disproportionation to NO_3^- and NO^+. Alternatively NO_2 can react with other NO molecules to form N_2O_3. The reaction between the latter and ammonia leads to the formation of NH_4NO_2, which can decompose easily into nitrogen and water. The latter step is facilitated by the presence of a Brönsted acid site, making zeolites an excellent choice. The focus in this dissertation will however be on the further reaction of the disproportionation product NO^+ with water, to form HNO_2. In turn, this molecule reacts with ammonia to form the same intermediate NH_4NO_2. The two routes mentioned - NO_2 disproportionation and the N_2O_3 formation route- are believed to be the most important for metal-exchanged zeolites.

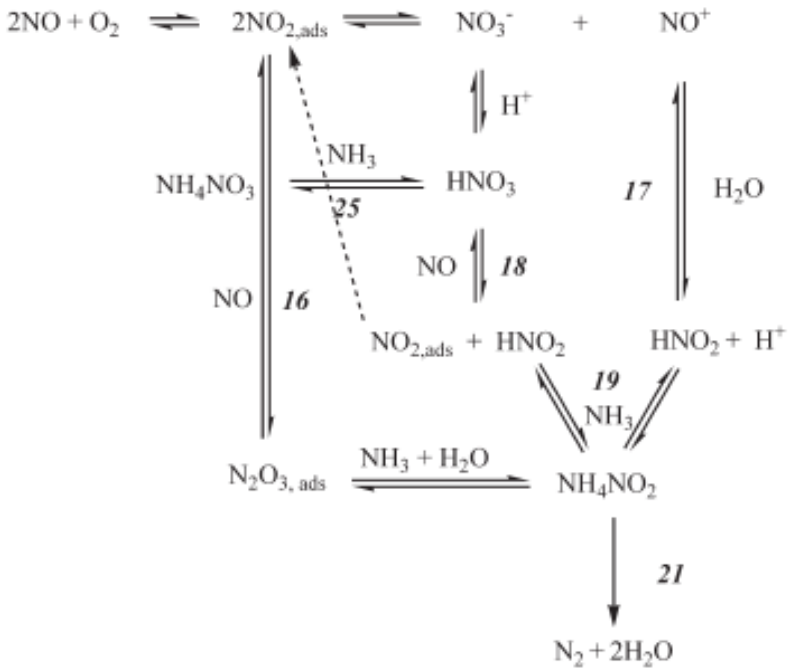

Figure 2-11: Overview reaction mechanism with formation of the NH_4NO_2 intermediate [27]

Note that the overview of Figure 2-11 is far from complete, since interaction with the active site is not taken into account explicitly. Furthermore, it was assumed that all NO was oxidized initially, which is not necessarily the case. Indeed, the review of Peden et al. [13] mentions a second route, with the possibility of only having half of the NO oxidized. The cycle shown in Figure 2-12 was proposed in the same review, for the low-temperature standard NH_3-SCR reaction in the presence of isolated Cu ion monomers. Evaluation of this mechanism is thus most relevant for the selected Cu-SSZ-13, as

follows from the discussion of the nature of the active site in sections 2.2.2 and 2.2.3. Note that this route corresponds with reaction arrows 17, 19 and 21 of the disproportionation route proposed in Figure 2-11.

Figure 2-12 suggests that both NH_3 and NO are adsorbed on the Cu species and that during the adsorption of NO the Cu^{2+} is reduced to Cu^{+}. Water subsequently reacts with the adsorption complex, by heterolytically breaking one of the H-O bonds. The OH^{-} part of the water molecule reacts with the adsorbed NO^{+} to form adsorbed nitrous acid (HONO), while the proton presumably reacts with the zeolite framework. Finally, as discussed earlier NH_4NO_2 is formed, which decomposes into N_2 and H_2O. Regeneration of the active site is supposedly done by oxidation of the proton to form a second water molecule.

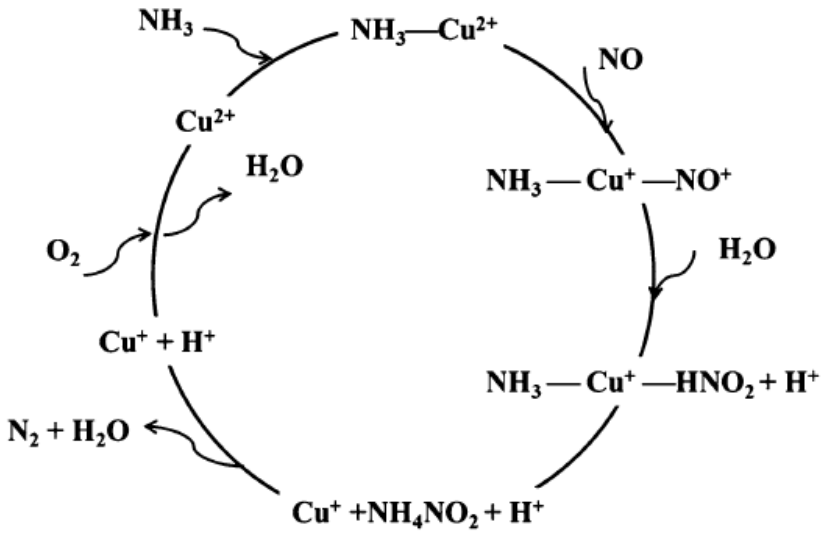

Figure 2-12: Proposed low-temperature cycle for the standard NH_3-SCR reaction in the presence of isolated Cu ion monomers. [13]

Chapter 3

Molecular modeling in heterogeneous catalysis

Chapter 2 was used to introduce the catalytic process and its selected metal-exchanged zeolite material, which will be investigated throughout this dissertation with help of molecular modeling. In this chapter, the theoretical background behind molecular modelling and ab initio calculations will be summarized. The chapter thus serves as a quick refresher of the most important principles and the applied approximations. Moreover, some attention is paid to the programs and methods used to investigate the reaction mechanism.

3.1 Quantum chemical methods

3.1.1 Schrödinger equation

The core equation used in quantum mechanical simulations is the Schrödinger equation, established by the physicist Erwin Schrödinger in 1925. It provides a non-relativistic description of a quantum system. Both time-dependent and time-independent forms are given in equations (6) and (7) respectively.

$$\hat{\mathrm{H}}|\,\Psi(\boldsymbol{r},t)\rangle = i\,\hbar\frac{d}{dt}|\,\Psi(\boldsymbol{r},t)\rangle \qquad (6)$$

$$\hat{\mathrm{H}}|\,\Psi(\boldsymbol{r})\rangle = E\,|\,\Psi(\boldsymbol{r})\rangle \qquad (7)$$

The time-independent form is probably the best known and represents the eigenvalue problem, which is solved to obtain the energy E of a system described by the wave function Ψ, by using the Hamiltonian operator $\hat{\mathrm{H}}$ acting on the eigenfunction Ψ. This wave function is determined by the positions of the electrons and the atomic nuclei. In a many-body system consisting of n electrons and N atomic nuclei, these positions are commonly denoted as $\mathbf{r_i}$ (i=1..n) and $\mathbf{R_j}$ (j=1..N). The Hamiltonian operator can now be written in terms of these positions as:

$$\hat{\mathrm{H}} = -\sum_i \frac{1}{2}\nabla_i^2 - \sum_j \frac{1}{2\,M_j}\nabla_j^2 + \frac{1}{2}\sum_{i_1\neq i_2}\frac{1}{|\boldsymbol{r_{i_1}}-\boldsymbol{r_{i_2}}|} + \frac{1}{2}\sum_{j_1\neq j_2}\frac{Q_{j_1}Q_{j_2}}{|\boldsymbol{R_{j_1}}-\boldsymbol{R_{j_2}}|} - \sum_{i,j}\frac{Q_j}{|\boldsymbol{r_i}-\boldsymbol{R_j}|} \qquad (8)$$

In this equation, M_j and Q_j are the mass and charge of the j^{th} atomic nucleus expressed in atomic units.

Solving equation (7) hence provides all energy eigenvalues and corresponding wave functions. This equation can thus also be used to find the wave function Ψ_0 corresponding with the ground-state, by using a variational principle. The ground-state is the state where the energy functional $E(\Psi)$ reaches a minimum value:

$$E[\Psi] \geq E[\Psi_0], \quad (9)$$

where:

$$E[\Psi] = \langle \Psi | \hat{H} | \Psi \rangle. \quad (10)$$

By systematically changing positions of nuclei and electrons, one can continuously decrease the value of the energy functional until a minimum value is reached or until the energy decrease is below a convergence threshold value. This iterative procedure ultimately leads to the most stable configuration of the systems being considered.

3.1.2 Solving the Schrödinger equation

Intuitively, one can see that solving the Schrödinger equation is a very challenging task. In fact, obtaining an exact solution of many-particle problems is not feasible; hence several approximations are commonly used. In this section the Born-Oppenheimer approximation and density functional theory calculations are introduced. A detailed discussion of these approximations is beyond the scope of this dissertation and can be found elsewhere [28, 29]. Herein, the focus will be on the practical implementation used in this research, namely the selection of basis sets leading to a good approximation of the wave function of the system.

Born-Oppenheimer approximation

In the Born-Oppenheimer approximation, the motion of electrons and nuclei is described separately. This approximation is valid since the mass of an electron is much smaller than the mass of an atomic nucleus, which implies that electrons move much faster than atomic nuclei. The motion of the electrons is thus determined by the external potential generated by the nuclei at fixed positions. In terms of the wave function, the global wave function is now rewritten as the product of an electron and a nuclear wave function. This way, electronic wave functions and energy levels now depend parametrically on the positions of the atomic nuclei.

Density Functional Theory

Generally speaking, the electronic Schrödinger equation cannot be solved analytically for many electron systems, so one must use techniques such as density functional theory (DFT) to approach the wave function. This method tries to describe the system in terms of the electron density $\rho(\mathbf{r})$ function rather than the classic wave function, as is done in Hartree-Fock (HF) and post-HF methods.[30] The equivalency of these representations has been proven in the Hohenberg-Kohn theorems.[31] Of course, this only shifts the problem of finding a wave function to finding a suitable density functional. The practical implementation of DFT was proposed by Kohn and Sham and consisted of using n non-interacting electrons with an identical density as the exact solution.[32] By introducing one-particle wave

functions Ψ_i for these independent electrons, the density could be rewritten as shown in equation (11). These one-particle wave functions are referred to as Kohn Sham (KS) orbitals.

$$\rho(\boldsymbol{r}) = \sum_i |\Psi_i(\mathbf{r})|^2 \qquad (11)$$

Of course, a description of the system by non-interacting electrons is far from accurate or realistic, so during the calculations so-called exchange and correlations (XC) corrections are taken into account. In practice, the total energy $E_{tot}[\rho(\boldsymbol{r})]$ of the interacting system is then determined as follows:

$$E_{tot}[\rho(\boldsymbol{r})] = T_{ni}[\rho(\boldsymbol{r})] + E_H[\rho(\boldsymbol{r})] + E_{ext}[\rho(\boldsymbol{r})] + E_{XC}[\rho(\boldsymbol{r})] \qquad (12)$$

$$T_{ni}[\rho(\boldsymbol{r})] = -\frac{1}{2}\sum_i \int d\boldsymbol{r}\, \Psi_i^*(\mathbf{r})\nabla^2\Psi_i(\mathbf{r}) \qquad (13)$$

$$E_H[\rho(\boldsymbol{r})] = \frac{1}{2}\int d\boldsymbol{r} \int d\boldsymbol{r}' \frac{\rho(\boldsymbol{r})\,\rho(\boldsymbol{r}')}{|\boldsymbol{r}-\boldsymbol{r}'|} \qquad (14)$$

$$E_{ext}[\rho(\boldsymbol{r})] = \int d\boldsymbol{r} v_{ext}(\boldsymbol{r})\rho(\boldsymbol{r}) + \frac{1}{2}\sum_{I\neq J}\frac{Q_I Q_J}{|\boldsymbol{R}_I - \boldsymbol{R}_J|} \qquad (15)$$

Note that the positions of the nuclei in equation (15) appear as parameters instead of variables, in accordance with the Born-Oppenheimer approximation.

The contributions in the equation above are respectively the kinetic energy T_{ni}, the Hartree energy E_H, energy from the external potential E_{ext} and the exchange and correlation correction E_{XC}. The functional form of the first three contributions is given in equation (13) to (15). While the exact functional form of the first three contributions is known, this is not the case for E_{XC}. In principle DFT should be considered an exact formalism, however in practice approximations for the unknown E_{XC} functional need to be used. Therefore approximations are introduced by switching to functional forms often based on experimental data.

One type of approximation is the local-density approximation (LDA) which, as the name suggests, calculates a value for the exchange correlation functional in terms of the density at the coordinate where the functional is evaluated. In this dissertation however, the generalized gradient approximation (GGA) is mainly applied, which not only uses the electron density but also the density gradient at the given point. By incorporating the gradient into the calculation of the functional, the accuracy increases as is shown in Figure 3-1, which represents the so-called Jacob's ladder [33,34]. There it can be seen that depending on the sophistication of the variable used to describe the functionals, the accuracy of the calculations can be altered. Note that the electron density in this figure is denoted as n. The highest accuracy can be achieved with Hyper-GGA, which uses the exchange-energy density ε_x.[35] An important class within Hyper-GGA are the so-called hybrid functionals, which incorporate both exact Hartree-Fock exchanges, as well as exchange and correlation from e.g. empirical values. The most commonly used hybrid functional is probably B3LYP [36,37], which is obtained by combining a GGA exchange functional from Becke with correlation functionals from Lee, Yang and Parr.[38] Three parameters are used to give weights to the different contributions. Slightly less accurate compared to Hyper-GGA is the Meta-GGA, which utilises the Laplacian of the electron density or the kinetic energy density τ, but is not discussed in more detail.

In this dissertation the PBE-D3 method is chosen for the periodic calculations. The hybrid functional PBE0 (PBE1PBE), which consists of 25 % exchange and 75 % correlation, is used for the cluster calculations.[39,40] PBE is short for Perdew, Burke and Ernzerhof which provided the gradient-corrected correlation functional in 1996.[41,42] This functional does not require empirical parameters. D3 on the other hand, indicates that dispersion corrections were taken into account.[43] These corrections were proposed by Grimme and consist of a set of 3 parameters, specific for each functional. The addition of these corrections allows a better description of the long range van der Waals interactions, which are otherwise inadequately described within the GGA approximation of the XC functional.[44, 45]

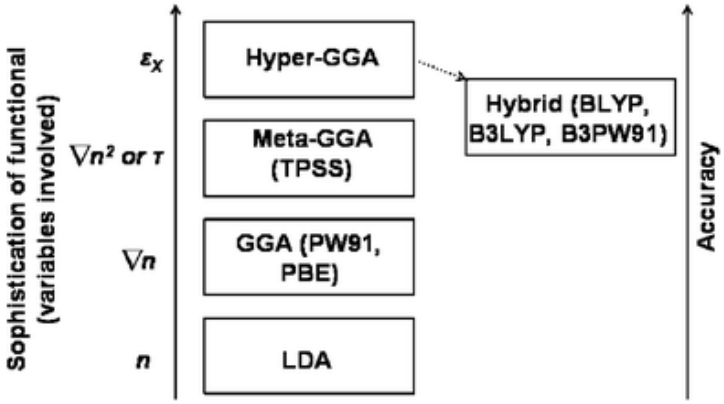

Figure 3-1: Scheme of Jacob's ladder depicting various exchange correlation approximations in function of increasing sophistication and accuracy [34]

The principles covered thus far are already sufficient to understand how a geometry optimization is performed. This iterative procedure is shown in Figure 3-2.

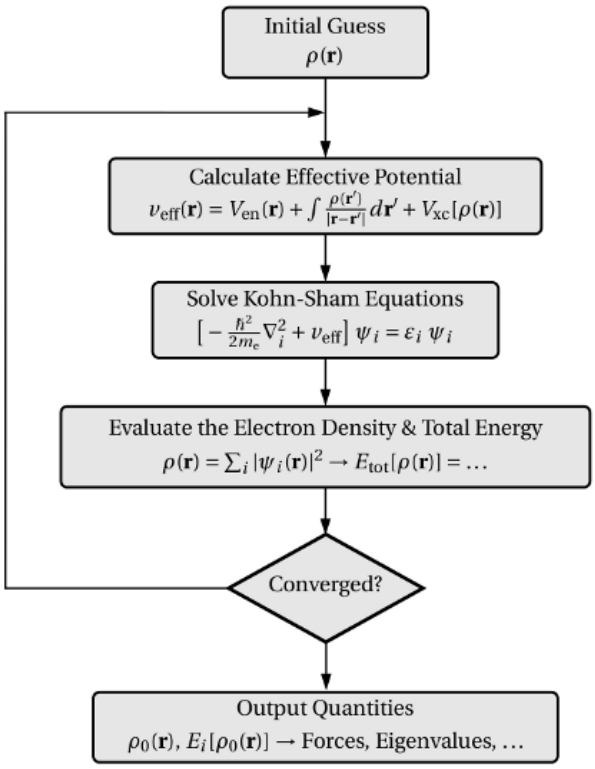

Figure 3-2: Iterative procedure leading to the ground state properties through a variational principle [46]

Basis sets

The KS orbitals introduced earlier are usually written as a weighted linear combination of a set of standardized (parameterized for every atom) atomic orbital functions:

$$\Psi_{\mathrm{i}}(\mathbf{r}) = \sum_{k} C_{ki} \Psi_{\mathrm{k}}^{\mathrm{AO}}(\mathbf{r}) \qquad (16)$$

The weight, i.e. contribution, of each function is determined by coefficients C_{ki} which are adjustable during the self-consistent Kohn-Sham-DFT procedure. The atomic orbitals $\Psi_{\mathrm{k}}^{\mathrm{AO}}(\mathbf{r})$ on the other hand remain a fixed linear combination of so-called Slater Type Orbitals (STO) or alternatively primitive Cartesian Gaussian functions (Gaussian Type Orbitals):

$$STO = \frac{\zeta^3}{\pi^{0.5}}\, e^{(-\zeta r)} \qquad (17)$$

$$GTO = \frac{2\,\zeta}{\pi^{0.75}}\, e^{(-\zeta r^2)} \qquad (18)$$

It is important to note that both are localized around the position of the atomic nucleus and have an exponential decay determined by a ζ - value and the electron-nucleus distance. The main difference between these GTO and STO, is that the electron-nucleus distance is squared for GTOs. As a result the multiplication of two GTOs centred on different atoms results in a finite sum of GTOs centred on a point along the axis between these two atoms. While the use of STOs is physically more correct, GTOs allow much faster calculations despite requiring additional basis functions.

A second alternative way of expressing the KS orbitals, is as a linear combination of plane waves. Doing so increases the numerical efficiency of the integration by allowing the use of fast Fourier transformations.[47] The natural wave periodicity and infinite extent make this approach ideal for periodic simulations. When using plane waves however, the rapid oscillations in the coordinate space cannot be described correctly without using an enormous basis set.

Finally, a third way of describing KS orbitals is by using Gaussian Plane Waves (GPW), which are a combination of the former two alternatives.[48-50] The electron density is thus represented in two different ways. A first representation consists of a series of contracted Guassian functions, which are centred around the atoms. The second representation uses a weighted expansion of plane waves. The weighting coefficients are chosen as to obtain two identical densities, which allows a straightforward conversion between the two representations. As a result, electrostatic interactions are described in a very efficient way. Gaussian Plane Waves are implemented in the Quickstep algorithm, which is applied in the CP2K software package.[50] For the periodic calculations in this dissertation a Double Zeta Valence Polarized (DZVP) MOLOPT basis set with plane wave cut-off of 300 Ry is selected for all atoms. It is thus possible of having a linear combination with two different ζ values, which allows a more flexible approach since some electrons have a wider range than others.

Pseudo-potential approximation

One way to remedy the use of an enormous plane wave-based basis set is to employ the pseudo-potential approximation, which distinguishes deeply-bound electrons, i.e. core electrons, from electrons with an energy close to the Fermi level, i.e. valence electrons.[51] Since the core electrons

predominantly cover a limited area around the atomic nucleus, these are rather insensitive to external influences, e.g. the vicinity of another atom for the formation of a chemical bond. Because of this, a smaller basis set can be used for the valence electrons, while the core electrons are described by pseudo-potentials. In addition, this pseudo-potential is selected in such a way that the highly oscillating part of the valence electron wave function in the vicinity of the core is smoothened. An illustration of this approximation is provided in Figure 3-3. For the calculations in this dissertation, GTH-PBE pseudo-potentials were used for all atoms, except for Cu for which no PBE pseudo-potential was available.[52, 53] GTH-BLYP pseudo-potentials were hence selected instead.

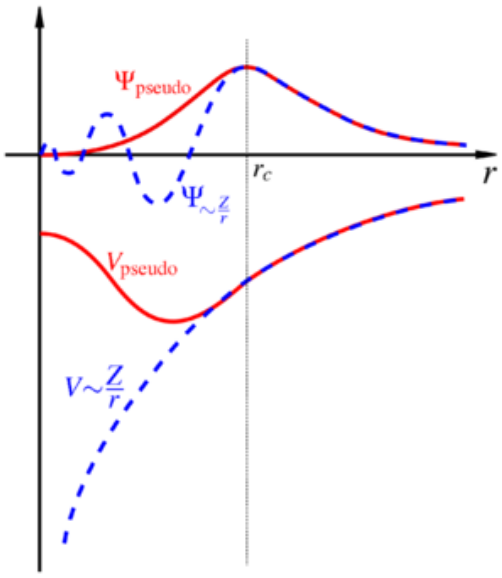

Figure 3-3: Smoothening of the valence electron wave function as a result of the pseudopotential approximation

3.2 Molecular Mechanic methods

Throughout the calculations in this dissertation, several ONIOM schemes are applied. This means that the system under consideration is basically divided in two main parts. One part is described by high level of theory quantum mechanical (QM) calculations as discussed in section 3.1, while the second part of the system is described by classical molecular mechanics (MM). Within the MM model, the system is described as a group of atoms which are connected through elastic bonds and are described by the equations of Newton.[54] As is illustrated in Figure 3-4, MM techniques are usually applied to describe systems on a larger time and length scale. In other words, switching over from QM to QM/MM methods decreases the computational cost at the expense of a decreasing accuracy of the electron description.

Each application requires the development of its own force field. In practice, the functional form of these force fields contains certain parameters which should be fitted to experimental data. The most popular force fields are however only fitted to a select group of atoms.[55] Some force fields aim to be as widely applicable as possible. An example of this is the universal force field (UFF) [55], of which the parameters are determined only by the element, its hybridization and connectivity and simple relations.

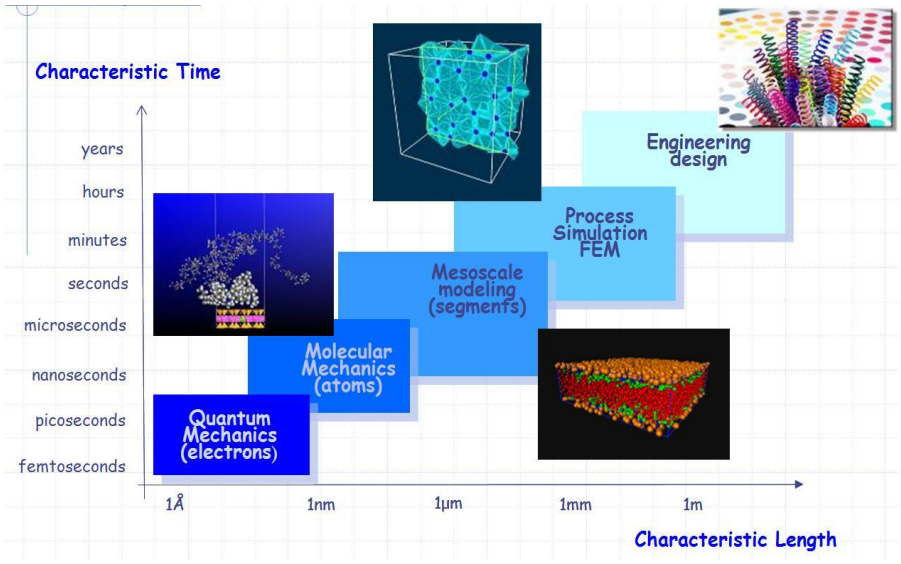

Figure 3-4: Comparison characteristic time and length scales for several modeling techniques [54]

3.3 Modeling the zeolite catalyst material

In this section, the information regarding the simulated systems is described. Firstly, the unit cell used in the periodic calculations is presented. Secondly, the most important finite clusters used in the dissertation are discussed. This also includes information on the applied ONIOM-schemes.

3.3.1 Periodic calculations

Periodic calculations have the tendency of having a high computational cost, but offer a broad view by taking the entire environment of the system into account. The computations are performed with the CP2K software package.[56, 57] The rhombohedral unit cell which is used for the Cu-SSZ-13 material is represented in Figure 3-5. This (empty) unit cell consists of 109 atoms, including 36T-sites and the corresponding cell parameters can be found in Table 1. The isolated Cu^{2+}, located just above the top ring of d6r subunit, is indicated as a green dot. To counter-balance the double positive charge of the Cu^{2+}, two Si atoms were substituted by Al atoms which are indicated as violet dots. Overall this leads to a Si/Al ratio of 17.

Table 1: Cell parameters of the rhombohedral unit cell of Cu-SSZ-13 shown in Figure 3-5

	Å		
A	13.558	0	0
B	-6.779	11.742	0
C	0	0	14.808

In Figure 3-5 the 2 Al atoms are clearly located in separate d6r units. Earlier computational research by Versaevel et al.[58] indeed suggested that both Al are not in the same d6r unit. This observation was based on energetic calculations combined with EPR data on the structures shown in Figure 3-6. Results showed that the position of the Al atoms influences the final Cu-O distances, although not all O atoms are susceptible to much change. Moreover, the positioning of the Al atoms in separate d6r units is also in agreement with experimental spectroscopy data of Korhonen et al. [20]

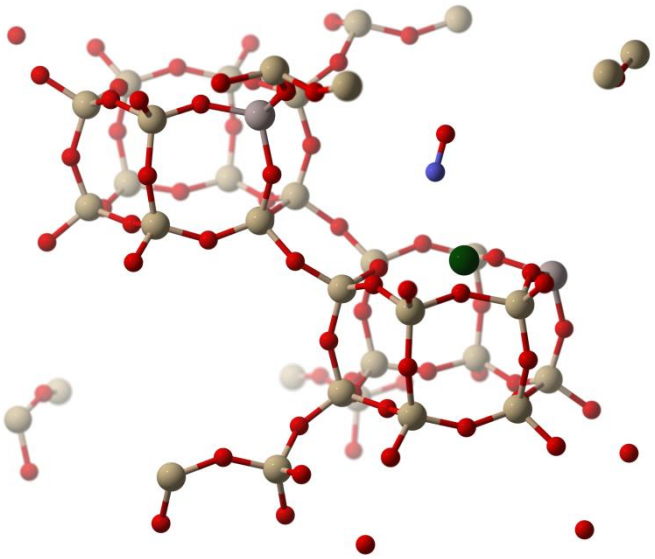

Figure 3-5: Unit cell used for the periodic CP2K calculations (Colour-code dots: red = O, white= Si, violet = Al, green= Cu)

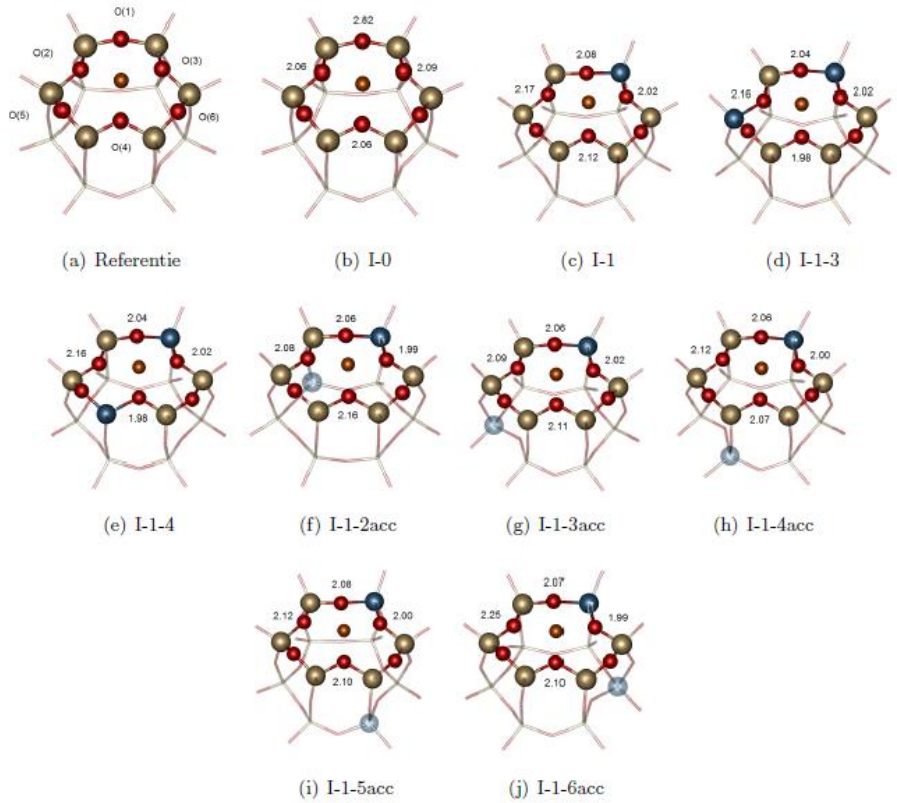

Figure 3-6: Possible locations of the Al atoms (in blue) within the d6r subunit [58]
Nomenclature I-a(-b): a is the index of the first Al atom, b is the index of the (optional) second Al atom Each 6-membered ring contains 6 indices, starting with 1 at the position shown in (c) I-1, and going up to 6 in a counter-clockwise direction. The suffix acc is used to indicate if the second Al atom is positioned in the opposite 6-membered ring

3.3.2 Cluster calculations

When performing ab initio calculations there is always a trade-off between the speed of the computations and the accuracy of the system description. Evidently, the size of the system being considered is a key factor in the resulting computational cost. The key is to eliminate all redundant atoms, while still maintaining a good configuration and electronic environment of the active site(s). Large finite clusters can be used for this purpose. These are usually extracted from the periodic structure of the investigated material. The dangling bonds are then substituted by hydrogens which are given an infinite mass. A normal procedure is however to first fix all the atoms except for the hydrogens, after which the position of these hydrogens is optimized. Subsequently the situation is reversed and the hydrogens are finally fixed to allow relaxation of the grid within a rigid hydrogen frame.

In a first attempt a subsystem of 8 d6r units (96T) was selected in a three-fold layer configuration, which is shown in Figure 3-7 (a).

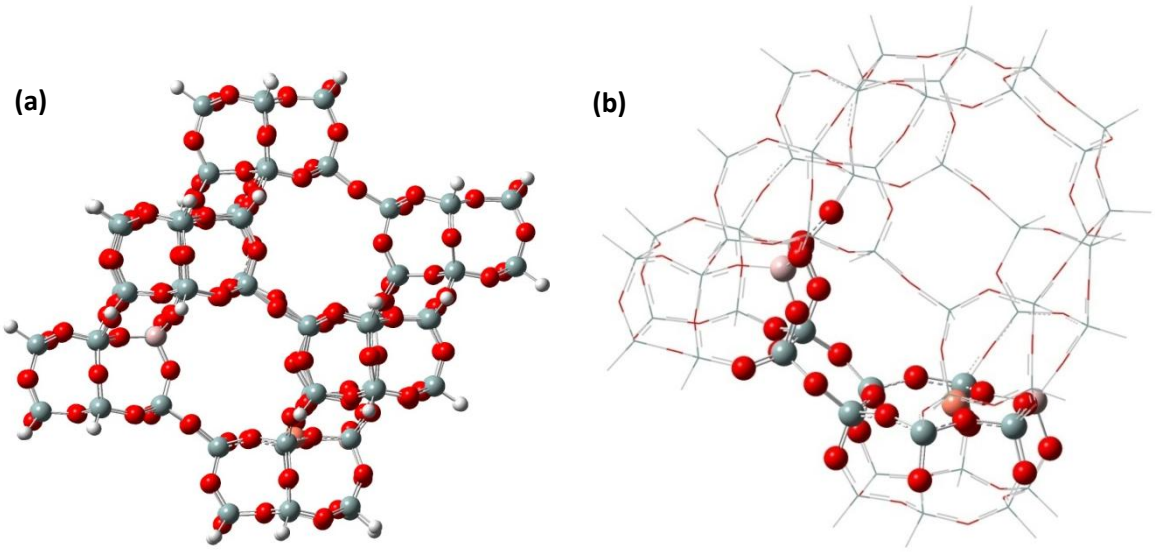

Figure 3-7: (a) Finite 96T-cluster extracted from the periodic structure
(b) ONIOM scheme of the extended 54T double 6-membered ring
low level: indicated with sticks - high level: indicated by colour-coded balls
red: O - silver: Si - pink: Cu – violet: Al - white: H

To reduce the computational cost of the calculations and to minimize possible complications with collapsing d6r units, the system is reduced to the two d6r units containing Al, extended with one large chabazite cage. This final system consisting of 54T-sites is shown in Figure 3-7 (b). An ONIOM-scheme is hereby applied, in which only the top-layer of the d6r-unit and an extension towards the second Al-atom remains in the high level of theory region. The high level is still described by PBE0 functionals. For the low level on the other hand the universal force field (UFF) scheme was selected. Other more accurate semi-empirical schemes such as PM3, PM6 and MNDO were tested as well, but did not lead to satisfactory results. Either very large deformations of the d6r units were observed (PM3/PM6) or the scheme simply was incompatible with the system due to a lack of parameterization of the Cu (MNDO). Furthermore, the D3-dispersion correction which are used in the periodic simulations, were omitted since this is rather difficult to implement within an ONIOM-scheme.

Note that despite all the efforts of reducing the simulation time and mitigating stability issues, getting the simulation to work is still a tedious task requiring a very specific input file.

3.4 Sampling the potential energy surface

Static calculations can provide very useful information and often have the advantage of allowing more complicated calculation methods, such as charge schemes. The downside of using static calculations exclusively is the danger of winding up in a local minimum on the potential energy surface, which can lead to biased short-sighted results. Dynamic calculations have the inherent advantage of allowing extensive sampling on the energy surface, which is of course invaluable in systems where the exact molecular configurations of e.g. reaction intermediates or adsorption complexes are unknown.[59] In this dissertation, both static and dynamic simulations are performed. The latter are becoming increasingly popular in heterogeneous catalysis [60], but their use is by no means a routine procedure.

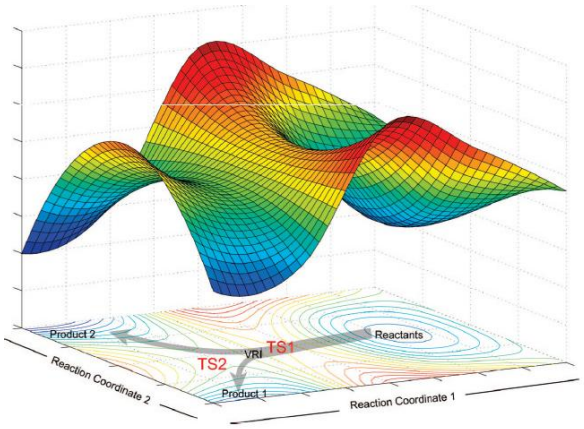

Figure 3-8: Potential energy surface exposed during sampling

In practice, distinction is made between stochastic methods such as the Monte Carlo (MC) method and deterministic methods such as Molecular Dynamics.

Monte Carlo

The stochastic MC-approach consists of the random exploration of the configuration space with help of an iterative procedure. First an initial set of atomic coordinates is specified after which a random atom is selected and given a random displacement. This new set of coordinates is accepted if there is a decrease in potential energy ($\Delta E < 0$) or if $e^{(-\Delta E/k\ T)} < R$, with R a random number in the range [0,1] and k and T, the Boltzmann constant and temperature [K] respectively. If none of these conditions is met, the displacement is rejected and either way a next random atom is selected to repeat the procedure. Due to the stochastic nature, no information on the time evolution of the system can be obtained, meaning that rates are not accessible. Stochastic methods are however not applied within this dissertation research.

Molecular Dynamics

Where the stochastic Monte Carlo method was based on the selection of several random numbers, the Molecular Dynamics (MD) method provides a deterministic alternative towards the sampling of the surface. MD methods are termed deterministic since the state of the system at any future time can be

predicted from its current state. The motion of every particle can be determined by using Newton's 2nd law, once the forces are calculated; either by force fields or by quantum mechanical calculations. Numerical integration of the equations of motions then leads to new velocities and new positions after a certain discrete time increment. The selection of the time increment depends mainly on the phenomena one wants to investigate. The timeframe of a collective vibration for example is 1 ps (10^{-12} s), while bond vibrations occur within a time frame of 1 fs (10^{-15} s). In other words, if you want to model the individual bond vibrations your time increment should be below 1 fs.

Specifically for this dissertation, MD simulations are performed with a time increment of 1 fs. The strength of these simulations is that the forces were calculated by ab initio calculations rather than by force fields, making the simulations very intensive yet also very accurate.

Thermodynamic ensembles

A dynamic simulation can be run in several modes. Standard MD simulations sample the NVE ensemble, meaning that the number of particles, volume and respectively energy remain constant. However, it is often interesting to impose certain conditions such as temperatures and pressures, e.g. to investigate the temperature dependency of thermodynamic properties. In this dissertation only NVT and NVE ensembles are used. A common practice in the study of heterogeneous catalysis is to run a NPT simulation first, to check how much the volume varies when sampling over the energy surface. However, a small volume range can be expected in the (periodic) system under consideration, due to the large dimensions of the cage compared to the reactants present. Hence, this volume equilibration step can be omitted.

In order to sample a NVT or canonical ensemble, a thermostat needs to be implemented. Popular methods include velocity rescaling, Nose-Hoover thermostats and Langevin thermostat. The first two methods are now discussed briefly. *Velocity rescaling*, which is the easiest one to implement, starts with determining an instantaneous temperature T_{inst} as function of the particle velocities v_i through:

$$\frac{3N}{2} k_b T_{inst} = \frac{1}{2} \sum_{i=1}^{N} M_i v_i^2 \qquad (19)$$

Because of thermal fluctuations however, T_{inst} deviates from the absolute temperature T. In a next step, the velocities are therefore rescaled as to obtain the target temperature according to:

$$v_i \rightarrow v_i' = \sqrt{\frac{T}{T_{inst}}} v_i \qquad (20)$$

The second option is to use the *Nosé-Hoover thermostat*. Implementation of this method is less straightforward but allows sampling the real canonical ensemble. With this method, a new variable 's' is introduced which effectively works as a heat bath, resulting in a kinetic energy alteration of the system. This kinetic energy change is compensated in the Lagrangian by introducing an extra potential energy term. During the MD simulation the Euler-Lagrange equations are subsequently integrated, while the corresponding Hamiltonian acts as the conserved quantity. In the periodic MD simulations of this dissertation, the Nosé-Hoover thermostat was selected.

Chapter 4

Adsorption of Nitric Oxide

The first step in the SCR deNO_x reaction is the adsorption of the reagents. In this chapter the adsorption of NO is discussed, which corresponds with the blue arrow in Figure 4-1. The reaction path being studied involves the formation of a so-called Cu-nitrosyl complex [Cu^+-NO^+], which is a key intermediate of the disproportionation route discussed in section 2.3. The existence and relevance of this complex has been extensively proven with help of IR spectra measurements, which will be used to validate the simulation results. [61]

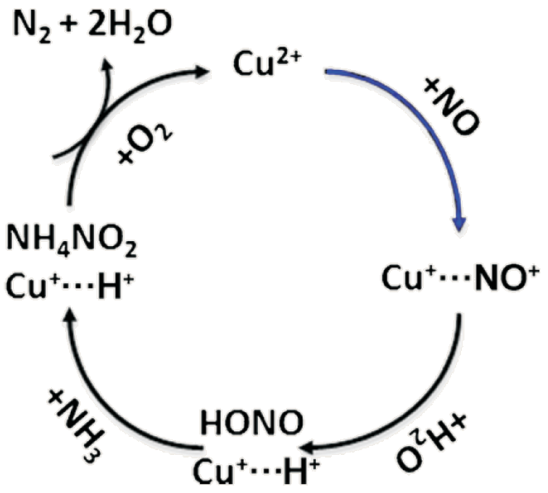

Figure 4-1: Reaction pathway with formation of the copper nitrosyl complex as proposed by Kwak et al. [61]

This chapter includes the results obtained from the geometry optimization of the adsorbed NO species by means of periodic calculations, in which two sets of calculations are performed. The first set of simulations focuses on the multiplicity which should be used during the simulation. A second set of simulations allows evaluating the dependency of the optimized geometry on the initial configuration. Furthermore, the influence of accounting for the periodic environment of the catalyst material is investigated by also simulating the NO adsorption for a smaller finite cluster.

Besides geometric properties such as the Cu-N distance, Cu-N-O angle and position of Cu relative to the framework, also the NO adsorption energy is determined. This is done by combining the energies of the optimized structures with the ones from the empty cluster and gas phase NO molecule. The analysis of the vibrational spectrum and charge distribution within the system is provided at the end of the chapter.

4.1 Geometry optimization

The main points of interest related to the NO adsorption are the Cu position relative to the framework, the Cu-N distance and whether or not a linear Cu-N-O configuration is valid. The latter would correspond to an angle α of 180° in Figure 4-2. Earlier experimental work by Kwak et al.[61] on Cu-SSZ-13 suggests a side-on adsorption formation on Cu^{+}, meaning the NO molecule is more or less positioned parallel to the face of the 6-membered ring (6mr). During the course of this dissertation research, new experimental data became available. Deka et al.[62] employed High Resolution Powder Diffraction (HRPD) and EXAFS experiments on cryo-cooled samples to investigate the configuration and suggested that the NO molecule is positioned perpendicular to the plane.

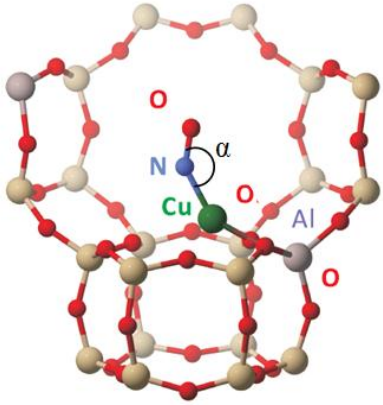

Figure 4-2: Optimized geometry of the NO adsorbed complex on Cu-SSZ-13 using periodic PBE-D3 simulations

It is also interesting to compare the experimentally obtained values with values obtained by earlier ab initio research by Göltl et al. albeit on a smaller system only consisting of a single d6r unit.[25] An overview of these configurations is given in Figure 4-3. As can be seen in Table 2, a set of 5 functionals was tested for both Cu^{+} and Cu^{2+}. PW91 and PBE are examples of functionals using the GGA-approximation, while the other functionals (PBE0, HSE03 and HSE06) are of the hybrid class. The latter should thus lead to more accurate results according to Jacob's ladder (see Figure 3-1). Simulations for Cu^{2+} were also performed on two different configurations. In Figure 4-3 (b) the Al substitutions are situated in the same 6mr of the d6r unit, in contrast to the second Figure 4-3 (c).

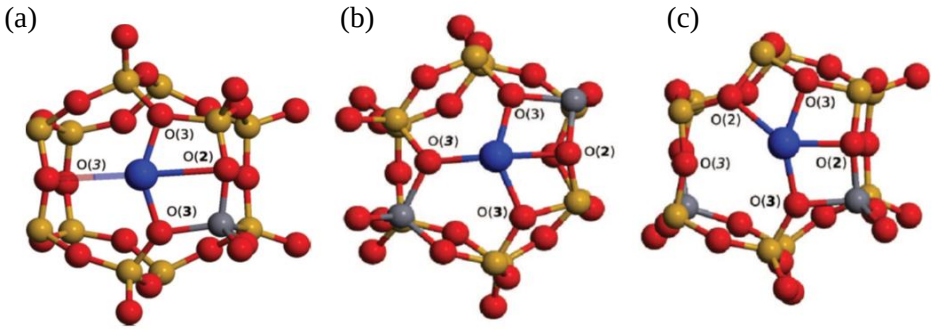

Figure 4-3: Comparison configurations used in the research of Göltl et al. [23]
(a) Configuration 1 for Cu^{+}
(b) and (c) Configurations 1 and 2 for Cu^{2+}

When comparing the results for Cu^{2+}, a wide variation is observed for the Cu-N distance, the observed N-O stretch frequency and especially the adsorption energy. There is a very strong dependency on the selected functional, where the greatest differences are caused by switching over from GGA to hybrid functionals. Changing the positioning of the Al substitutions leads to substantial alterations as well, even for identical functionals. This shows that all results -experimental or through simulations- should be compared with caution. The main interest in this dissertation is therefore limited to the PBE column, as this functional was selected here. Since earlier work by Versaevel et al.[58] suggested both Al are in a different 6mr, the most relevant results for this research are highlighted in the table.

Table 2: Comparison results of the adsorption complex obtained by Göltl et al. [23, 25] with highlighted results used as reference throughout the dissertation

Configuration I	Cu^{+}	**PW91**	**PBE**	**PBE0**	**HSE03**	**HSE06**
|Cu,N|	Å	1.76	1.76	1.78	1.78	1.78
|N,O|	Å	1.18	1.19	1.16	1.17	1.16
α(O,N,Cu)	°	144.6	143.7	144.0	143.4	143.8
$\Delta E_{adsorption}$	kJ/mol	-125.2	-123.4	-84.4	-86.4	-85.6
ν_{N-O}	cm^{-1}	1805	1825	1976	1972	1977
Configuration I	Cu^{2+}	**PW91**	**PBE**	**PBE0**	**HSE03**	**HSE06**
|Cu,N|	Å	1.86	1.86	2.04	2.04	2.05
|N,O|	Å	1.15	1.15	1.14	1.14	1.14
α(O,N,Cu)	°	131.8	131.8	127.1	126.9	127.6
$\Delta E_{adsorption}$	kJ/mol	-109.0	-96.6	-26.0	-28.5	-22.0
ν_{N-O}	cm^{-1}	1921	1942	2106	2101	2103
Configuration II	Cu^{2+}	**PW91**	**PBE**	**PBE0**	**HSE03**	**HSE06**
|Cu,N|	Å	1.80	1.80	1.96	1.96	1.97
|N,O|	Å	1.15	1.15	1.14	1.14	1.14
α(O,N,Cu)	°	136.9	137.0	131.3	131.3	131.6
$\Delta E_{adsorption}$	kJ/mol	-143.9	-136.9	-62.0	-76.2	-60.5
ν_{N-O}	cm^{-1}	1929	1952	2112	2108	2113

4.1.1 Influence of multiplicity

In this section, the computational results concerning the adsorption of NO on Cu-SSZ-13 are discussed. More precisely, the determination of the adsorption energy and the optimal geometry of the configuration were determined in terms of the selected multiplicity and the exact content of the CP2K/Gaussian input file. First, the electron configuration of Cu and Cu^{2+} is given in Figure 4-4, to understand the considered multiplicities. After interaction with NO, which has an unpaired electron itself, the multiplicities obtained are 1 for the electron configuration on the left (singlet, no unpaired electrons) or 3 (triplet, 2 unpaired electrons) for the picture on the right.

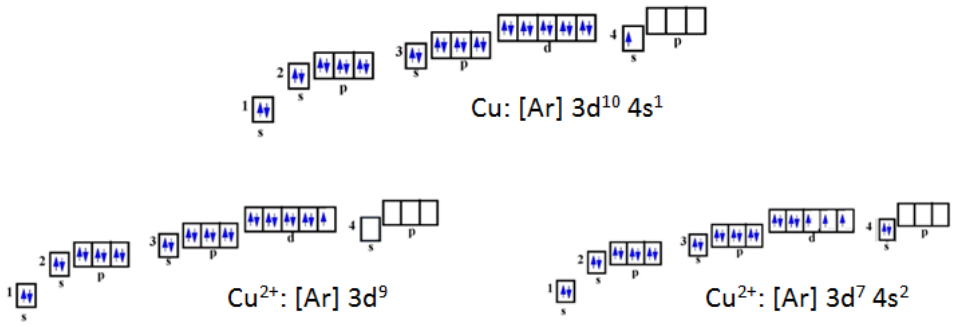

Figure 4-4: Possible electron configurations for Cu (top) and Cu^{2+} (bottom)

When performing periodic calculations with CP2K, it is possible to enable the local spin density (LSD) option. Turning this option on, implies that electrons with a different spin occupy orbitals with a different energy. It is therefore important that the LSD option is turned on in situations with an odd number of electrons, e.g. for the empty Cu-SSZ-13 framework having a multiplicity 2.

In total, 4 geometry optimizations were simulated, because of the selection between 2 multiplicities and the optional usage of the LSD keyword in the input file. The main results of the optimized structures are shown in Table 3 and Figure 4-5 respectively. To clarify, β represents the dihedral angle between Cu and the top layer of the double 6-membered ring.

Table 3: Results for testing the multiplicity and local spin density specification
M1 refers to the singlet, whereas M3 refers to the triplet configuration

		M1	M1 - LSD	M3 - LSD
|Cu,N|	Å	1.77	2.82	2.00
|N,O|	Å	1.15	1.14	1.17
α(O,N,Cu)	°	142.0	138.0	131.2
β(Cu, d6r)	°	23.72	9.08	15.19
$\Delta E_{structure}$	kJ/mol	0	57.94	49.79
ΔE_{NOads}	kJ/mol	-126.7	-68.7	-76.9

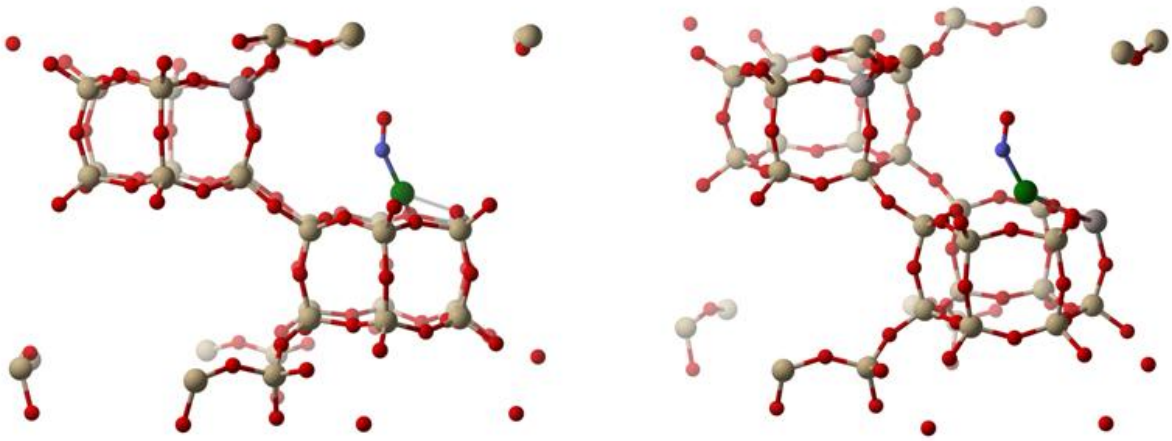

Figure 4-5: Unit cell structure of the optimized NO adsorption geometry (singlet without LSD)
(Colour-code red: O beige: Si violet: Al green: Cu blue: N)

As could be expected the results obtained for the singlet without LSD and the triplet with LSD are almost exactly the same, hence the results of the latter are not included explicitly in Table 3. On the other hand, the results of the LSD simulations were less comparable, yet usually showed the same trend relative to the simulations without LSD.

From Table 3, it is clear that the simulation results without LSD are energetically favoured, and hence the combination of multiplicity 1 and no LSD is selected as reference during the remainder of the research. Results of this latter combination are also more in correspondence with the results reported in Table 2. The angle reported by Göltl et al. is somewhat lower, but nearly identical N-O and Cu-N distances were reported (PBE configuration 2 in Table 2). Moreover, the adsorption energy from the simulation of the singlet without LSD is in rather good agreement with the reported adsorption energy, although a difference of about 10 kJ/mol remains.

4.1.2 Influence of the initial configuration

An important aspect to be investigated in ab initio calculations is the dependency/influence of the selected initial configuration. This is especially true for static calculations where the possibility of ending up in a local minimum exists (see section 3.4). Therefore, 3 different starting structures were tested and compared in terms of optimized geometry and calculated adsorption energy. Figure 4-6 represents the initial configurations of which the geometry has been optimized. Note that these 3 pictures are cut-out from the actual unit cell as shown in Figure 3-5, to highlight the change near the active centre.

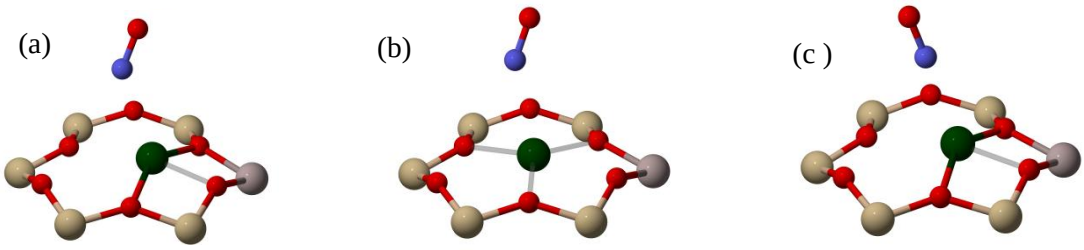

Figure 4-6: Detail of the change of the active site, used to determine the influence of the initial configuration (a) reference (b) centralized Cu position (c) linear structure (Colour-code red: O beige: Si violet: Al green: Cu blue: N)

Figure 4-6 (a) is taken as reference, since the copper position for that configuration is in close agreement with previous studies.[13,19, 22] Figure 4-6 (b) then represents the initial configuration which was used to determine the influence of the copper ion, being the green ball, which is now in a more centralized position. Finally the Cu-N-O angle was adapted to mimic a linear adsorption mode as shown in Figure 4-6 (c). The optimized structure of the reference is shown in Figure 4-2, where the nomenclature of the table is defined. Table 4 contains the most important results obtained after optimization of the three configurations. From Table 4 it can be concluded that the difference between the optimized geometries in terms of initial Cu position is very small. This is of course a comforting result.

In summary, NO is positioned rather perpendicular to the face of the d6r. Upon adsorption, the Cu is pulled out of this plane.

Table 4: Influence of the initial configuration on the optimized geometric properties (singlet, no LSD)

Initial configuration		Reference	Cu-shift	Linear
|Cu,N|	Å	2.82	2.87	2.60
|N,O|	Å	1.13	1.14	1.14
α(O,N,Cu)	°	137.6	143.0	173.4
β(Cu, d6r)	°	8.21	4.74	10.21
Optimized geometry				
|Cu,N|	Å	1.77	1.77	1.75
|N,O|	Å	1.15	1.15	1.15
α(O,N,Cu)	°	142.0	139.5	154.0
β(Cu, d6r)	°	23.72	23.33	27.04

4.1.3 Influence of the active site environment

The results discussed so far in 4.1.1 and 4.1.2 corresponded to periodic calculations. As mentioned earlier, calculations on a smaller finite cluster using an ONIOM scheme were executed as well to reduce simulation time. An extended 56T-cluster was used and the applied ONIOM scheme is indicated in 3.3.2). In Figure 4-7, the optimized geometry of NO adsorbed in this cluster is shown and one can observe a substantial difference compared to the periodic calculations. Significant deviations are found in the calculated Cu-N-O angle and in the Cu-N distance (see Table 5). In the cluster the Cu is also situated much closer to the face of the d6r unit, as illustrated by the much smaller dihedral angle β.

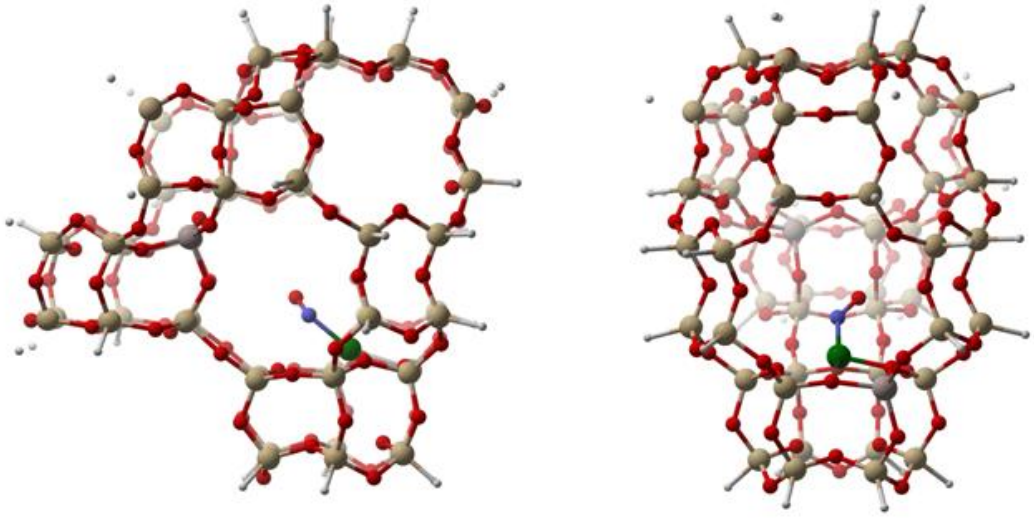

Figure 4-7: Different perspectives of the optimized cluster geometry

The largest difference is however given by the angle between the Cu-N bond and the face of the d6r unit. In the cluster calculation the NO molecule seems rotated somehow, i.e. the oxygen of the NO is no longer facing upwards, while the nitrogen is closer to the face of the d6r unit.

Table 5: Influence of the active site surroundings on the optimized geometry (periodic values were taken from the singlet simulation without LSD)

		periodic	cluster
|Cu,N|	Å	1.77	1.93
|N,O|	Å	1.15	1.11
α(O,N,Cu)	°	142.0	133.3
β(Cu, d6r)	°	23.72	7.013

In summary, the values obtained through the cluster calculations deviate to a great extent from the periodic simulations. This could thus influence calculations further along the SCR process. However, problems with the stability of the cluster prohibited further examination. A water molecule was added to the system, aspiring to analyse the formation of HONO, and this configuration was optimized while still keeping the exterior hydrogen atoms fixed. Unfortunately the interior system contracted almost instantaneously upon optimization which led to large deformations of the structure. All bonds between the exterior hydrogens and the interior framework were ruptured throughout this deformation. A possible explanation for the structure instability is the use of an asymmetric high level within the ONIOM-scheme, which can lead to artificial dipole moments and charge imbalances. Future work should therefore be devoted towards finding a better suited combination of finite cluster and ONIOM-scheme.

4.2 Frequency analysis

As the discussion earlier suggested, IR measurements are a valuable tool in the determination of the intermediates which are present during the reaction. Calculating the frequencies and comparing them with experimentally determined frequencies is therefore required in order to validate the results. One set of IR measurements was provided by Kwak et al.[61] and the data can be found in Figure 4-8. The observation of the NO stretch of Cu^{2+}-NO at about 1950 cm^{-1} was one of the main reasons for investigating the NO adsorption reaction pathway. To clarify, when talking about the Cu^{2+}-(NO) stretch, this refers to the NO bond stretch of the species adsorbed on the Cu. Both periodic and cluster simulations were performed to calculate the frequencies and the results are of course compared with the values reported in Figure 4-8 and with the values reported by Göltl, which were given earlier in Table 2.

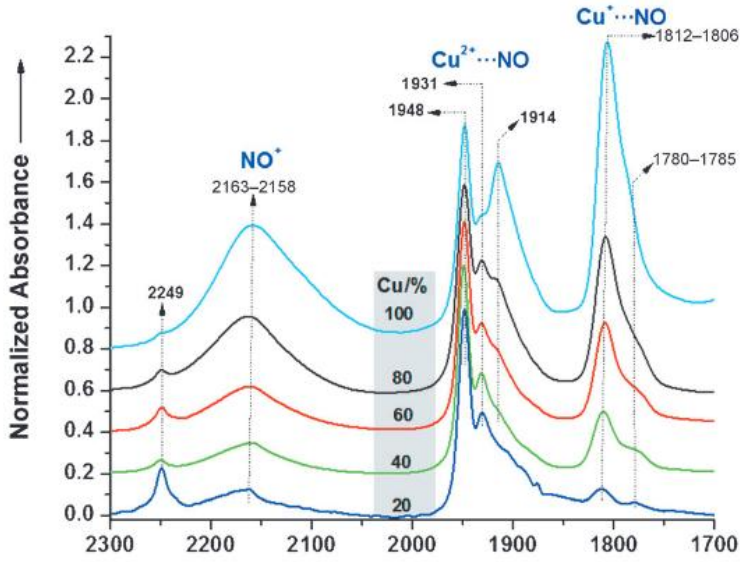

Figure 4-8: Experimentally determined IR spectrum at various copper loadings [61]

4.2.1 Periodic calculations

The data obtained from the vibrational analysis includes a list of encountered frequencies, together with the corresponding intensity and force constant of that specific vibration. Here, the main interest is in the high frequency range, since low frequencies (400 cm^{-1}-1500cm^{-1}) are mostly attributed to framework vibration modes acting as fingerprint of the zeolite.[63] The spectrum which was obtained is hereby illustrated in Figure 4-9. Two regions of relatively low frequencies dominate the spectrum. When taking a closer look however, one can also distinguish a small intensity increase at a frequency of 1952 cm^{-1}, which corresponds with the NO stretch of Cu^{2+}-NO. The excellent agreement between this value and the 1948 cm^{-1} found in Figure 4-8, means that this vibration can be used to monitor the proceedings of the reaction. Of course the values from Figure 4-8 were obtained by *in situ* spectrum measurements; hence the influence of the other reactants on the calculated spectrum should be investigated as well. Future research can aim towards researching the frequencies found for the other intermediates in order to interpret additional IR measurements.

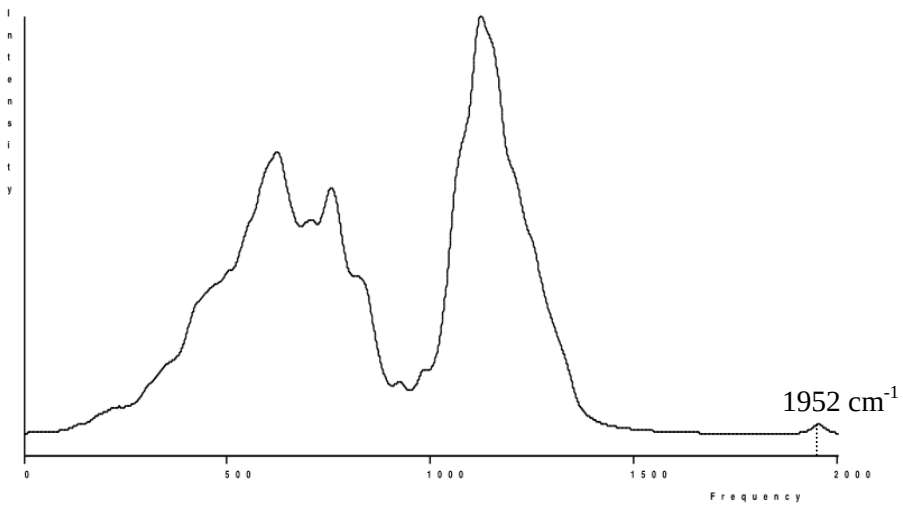

Figure 4-9: IR spectrum obtained by the periodic vibrational analysis (frequency on x-axis expressed in cm^{-1})

4.2.2 Cluster calculations

To get a better understanding on how the environment of the catalytic centre affects the obtained spectrum, a frequency analysis was performed on small finite clusters as well. Because of the relatively large cage, one might expect that the influence on the frequency corresponding to the NO stretch is minimal. This paragraph thus covers the simulation results obtained after reduction of the system to the top-ring of the d6r unit.

The calculations which have been discussed so far in 4.1 corresponded with periodic calculations with unit cell as shown in Figure 3-5. When going over to the subselection of the double 6-membered ring, the second aluminium in the system disappears. As a consequence the Cu^{2+} ion only experiences a single counter charge of 1 Al substitution. Earlier research with charged systems however did not always lead to correct results, so this simulation should be analysed with caution. A first calculation is done on the charged system, after which a second Al atom is introduced to the system. The selected Al positions are indicated on Figure 4-10, which contains the optimized geometries for a single (a) and double (b) Al substitution. For the optimization of these small clusters PBE0 (PBE1PBE) hybrid functionals were selected using a DGDZVP basis set. D3-dispersion corrections were applied as well to allow a proper comparison with the results from the periodic calculations.

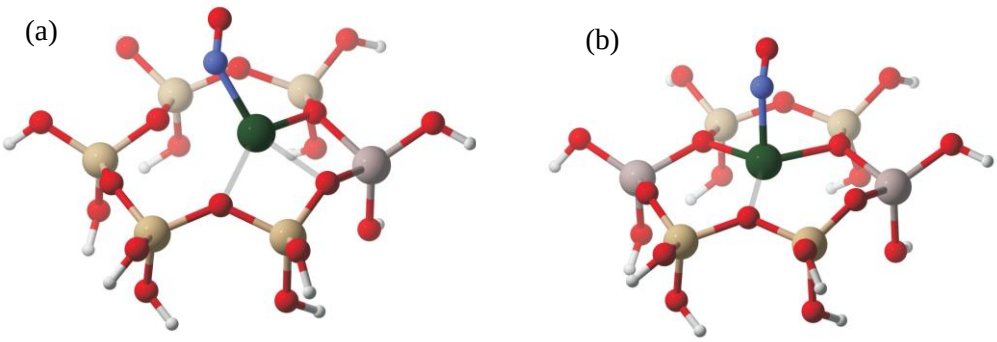

Figure 4-10: (a) optimized NO-geometry in case of a single Al substitution
(b) optimized NO-geometry in case of a double Al substitution

The reader is reminded to the fact that during optimization, hydrogens are given an infinite mass and locked position. However, this time the final hydrogen positions were set manually and thus are not the consequence of a geometry optimization. This was done to ensure there was no interference of the hydrogens with the NO stretch. The hydrogens attached to the top layer were therefore set pointing away from the active site, while the hydrogens from the bottom layer were set in a circle as to form hydrogen bonds with the next oxygen.

- 1Al: net positive charge

Figure 4-11 contains the IR spectrum obtained for the cluster with 1 Al substitution. Similar to Figure 4-9, the highest intensities are obtained for frequencies within the 1000-1400 cm^{-1} range. The shape of the peaks is however more visible, in contrast to the envelope which was observed in the periodic case. Naturally, the main interest for this dissertation is to see whether or not the Cu-NO stretch frequency has shifted by a substantial amount. This is clearly the case since the peak frequency obtained is now at 2112 cm^{-1}, which is far removed from the experimentally

obtained value. Note that this value is identical to the value obtained by Göltl et al as can be seen in Table 2.

- 2Al: neutral system

In Figure 4-10 (b), the optimized structure is depicted with indication of the Al positions in purple. While the initial structure of this geometry differs only in the substitution of the second aluminium, the optimized structure shows great deviations. This is of course no surprise, since the positively charged Cu-ion now tries to achieve a balance by interacting with both substituted sites at once. The difference in position is quantified by measuring the typical Cu-O distances and comparing them with the ones obtained from the periodic calculations. Despite the large geometric differences between Figure 4-10 (a) and (b), the obtained spectra are quite similar. The Cu-NO frequency is now situated at 2169 cm^{-1}, meaning that the addition of a second Al atom induces an extra shift of about 57 cm^{-1}.

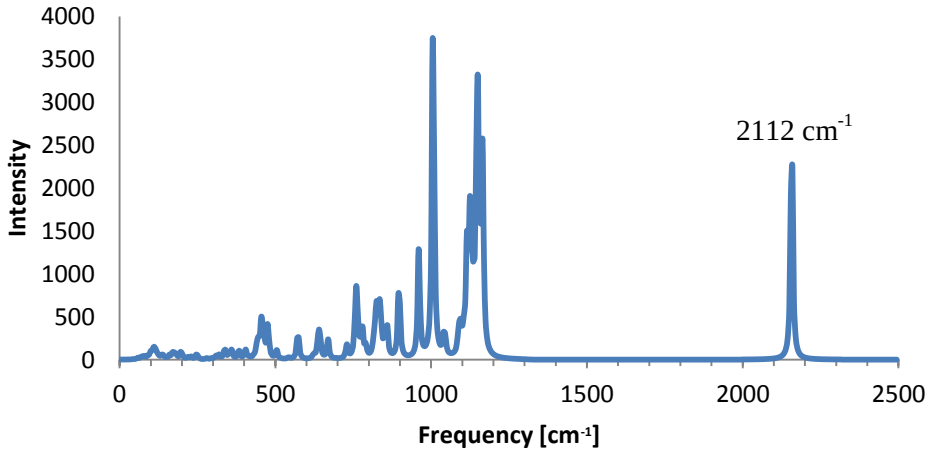

Figure 4-11: IR spectrum obtained for the system with 1 Al substitution

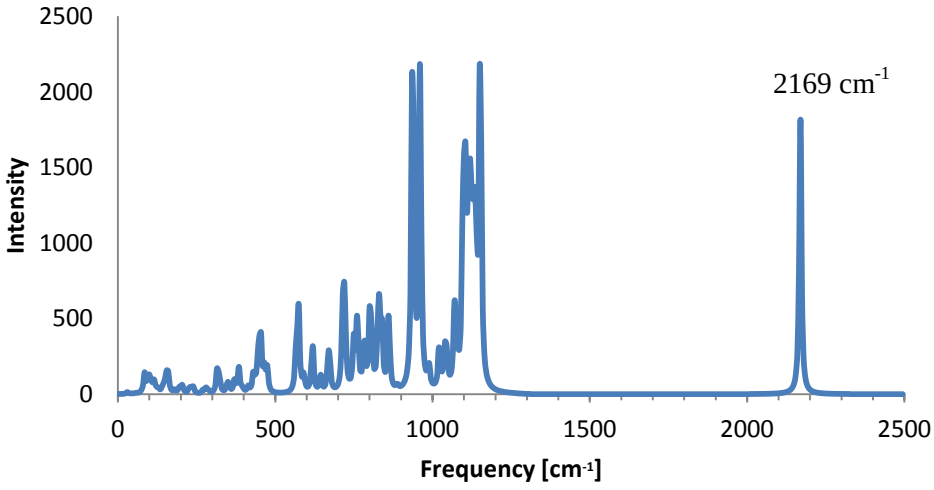

Figure 4-12: IR spectrum obtained for the system with 2 Al substitutions

4.3 Charge distribution

An important aspect to understand the reaction mechanism is to know how the charge is distributed at every step of the process. In this section the influence of the NO adsorption on the charge distribution is thus investigated. The main interest is to see whether or not (or to what extent) Cu^{2+} is reduced to Cu^{+} through interaction with the NO molecule. Secondly, the charges within the NO molecule itself will give information on how NO will interact with other molecules. This increases the insight gained to obtain a correct analysis of the results in Chapter 5. Finally the spin density is discussed here as well.

Table 6 presents the charges obtained from the Natural Population Analysis (NPA)[64]. This generally gives better results than the standard reported Mulliken values (Table 7), especially when using metal atoms. The main difference is that NPA accounts for the natural mass and electronegativity of every atom, whereas Mulliken basically divides the electron density between two atoms in equal parts independent of the inherent electron affinity. The values in the 'before' column correspond with the individual molecules, so evidently the N and O charges cancel each other out. The values in the 'after' column on the other hand correspond to the adsorbed Cu-NO species. According to this data the charge of every atom increases upon adsorption. This is in contrast with both expectations and earlier findings [4, 13], where it is stated that the Cu^{2+}-ion should be reduced to Cu^{+} throughout the process. Some of the positive charge would end up mostly on the nitrogen of the NO molecule, which would lead to enhanced interaction with oxygen atoms from water molecules. This could be an explanation for the superior performance of copper-exchanged zeolites over standard zeolites, in terms of activity and selectivity.

Table 6: Comparison NPA atomic charges before and after NO adsorption

	before	after
Cu	0.86	0.91
N	0.22	0.32
O	-0.22	0.04

Table 7: Comparison Mulliken atomic charges before and after NO adsorption

	before	after
Cu	0.61	0.71
N	0.09	0.24
O	-0.09	0.11

A closer inspection of the reported Cu-charge before adsorption, indicates that Cu^{+} is already present prior to the adsorption. This is confirmed by investigating the natural electron configuration calculated by the normal population analysis. The configuration [Ar] 4s(0.11) 3d(9.93) 4p(0.08) 4d(0.01) 5s(0.01) is obtained for the Cu-species without NO, where the value between brackets shows how many electrons occupy the respective orbitals. It is seen, that -apart from minor numerical effects- 10 electrons occupy the 3d orbitals, resulting in a closed shell species. Since [Ar] 3d(10) corresponds with the configuration of Cu^{+}, this infers that the finite cluster is incapable of providing a proper charge distribution. The extra positive charge is mainly distributed over the exterior hydrogen atoms, which were introduced to deal with the dangling bonds (see section 3.3.2).

The former discussion confirms that periodic systems are favored for the description of the NO adsorption. Indeed, the periodic simulations allow a correct description of the charges and spin density. The spin density can be visualized and this is shown in Figure 4-13 for the periodic calculations on the original Cu-SSZ-13 model. As expected, the spin is predominantly focused on the Cu-species, implying the presence of Cu^{2+}.

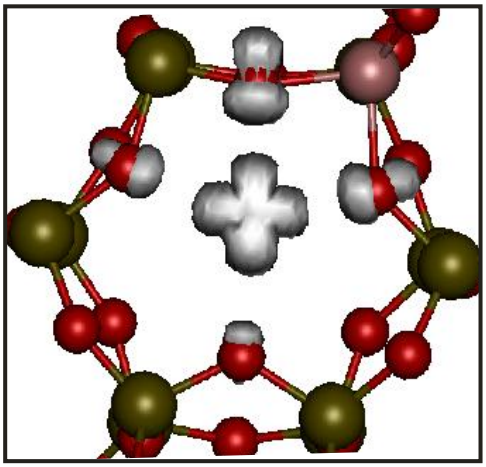

Figure 4-13: Spin density mapping for the periodic calculations on the original Cu-SSZ-13 model

Chapter 5

Reaction of adsorbed NO species with water

We theoretically examined the geometric and electronic state of the adsorbed NO in Chapter 4, so the next logic step is to simulate the reaction/interaction with water (see Figure 4-1). The main goal, in terms of the elucidation of the reaction mechanism, is to find out the optimal coordination of the copper with respect to surrounding water molecules. Next, we try to find the transition state leading to HONO as the next intermediate. The calculations discussed in this chapter, are predominantly periodic CP2K calculations. Since it is intuitively less clear how the molecules will position themselves, the focus of section 5.1 is on dynamic simulations as explained in section 3.4. Snapshots of preferential states, i.e. frequently observed during the sampling of the potential energy surface, are investigated in more detail in section 5.2. This chapter provides a thermodynamic analysis of the coordination sites and also focuses on typical Cu-positions in function of time, temperature and coordination.

5.1 Influence of additional water molecules on the Cu location and coordination

Before investigating the reaction of NO with H_2O to form HONO, it is important to determine the exact state of the reactants. Chapter 4 had a rather limited view on the adsorption, since NO was the only molecule present in the zeolite framework. Actual process conditions, however, lead to a complex mixture of NO, NO_2, H_2O, NH_3, unburned hydrocarbons and several other species within the cage. In this dissertation, the interaction with up to 4 water molecules is taken into account, with the objective of finding the HONO transition state in mind. It is thus assumed that water is sufficiently available in a typical diesel exhaust stream. Besides the water naturally present in this stream, water is also produced throughout the SCR deNO_x reaction, so this is a valid assumption. In the subsequent paragraphs several aspects are treated and compared for each number of water molecules. In Figure 5-1, the initial configurations of the 4 simulation sets are presented. The position of NO corresponds with the optimized geometry obtained during the static calculations in Chapter 4.

The successive configurations were constructed by adding an extra water molecule, while maintaining the position of the water molecules already present. Even though the importance of the initial structure of the molecules is less significant for MD simulations, one should avoid situations where molecules are too close to each other. This problem was encountered when the third water molecule was added too close to the NO, resulting in an instant repulsion of the NO, which consequently lost interaction with the copper ion. Simply increasing this water NO distance was sufficient to ensure a normal simulation.

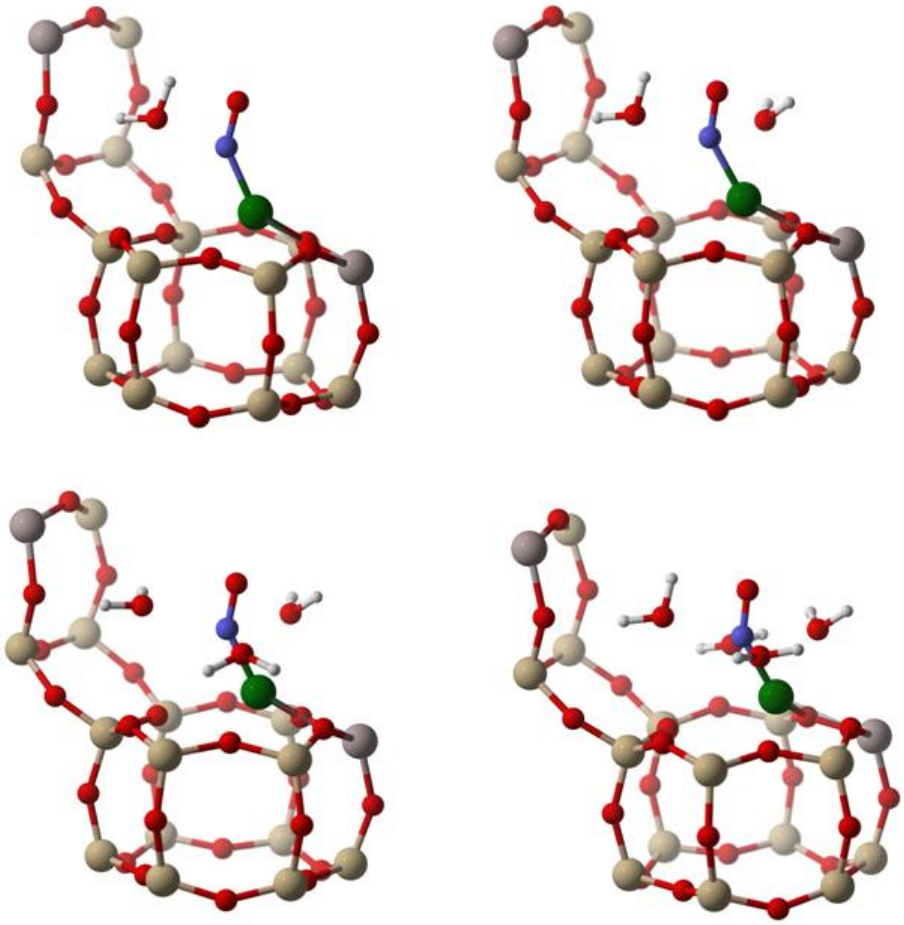

Figure 5-1: Initial structures for the periodic MD simulations with successive addition of water molecules to the NO adsorbed CU-SSZ-13 complex

5.1.1 Assessing the quality of the MD simulations

As mentioned earlier in paragraph 3.4 a dynamic simulation is performed using ab initio Molecular Dynamics, while upholding a time step of 1 fs. Ideally, a total run length of about 20 ns is necessary to get a representative idea of the most occurring configurations. Due to time constraints however, at most 10 ps were simulated. It is important to check if and when the system is equilibrated. This is done by monitoring the temperature in function of time and by indicating at which step the simulated temperature corresponds with the imposed temperature. The analysis should be based on results of simulations after this specific time step. A second indicator for the quality of the simulations is the conserved quantity, which was introduced in paragraph 3.4 as well. The variation of the conserved quantity needs to be compared with the variation of e.g. the potential energy. The variation of the latter should be at least one order of magnitude larger compared with the conserved quantity. This convergence analysis is only discussed for the case with 1 water molecule at an imposed temperature of 300 K, see Figure 5-2. The results of the other simulations are treated analogously and the main data is presented in Table 8. For the corresponding plots the reader is referred to Appendix A-I.

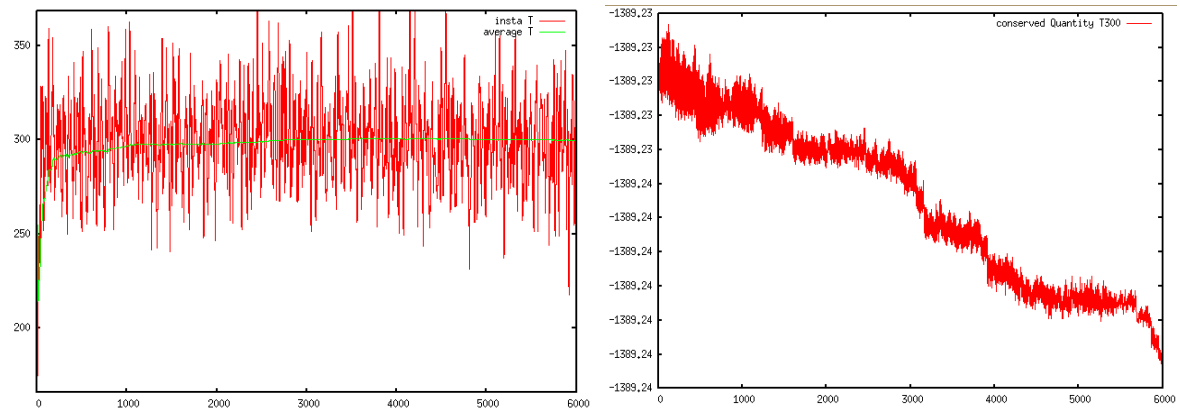

Figure 5-2: Evolution of the instantaneous (red) and average (green) temperature (left) and conserved quantity (right) in function of time, to evaluate the periodic MD simulation with 1 H_2O at 300 K

From Figure 5-2, one could graphically decide how many simulations should be omitted during the analysis of the data. A more systematic approach was used, by looking at the first time step for which the average temperature was within 98 % of the imposed temperature. The resulting equilibration times ($t_{equilibrated}$) can be found in Table 8. For the final analysis these numbers were rounded up to the nearest multiple of 100 just to be safe. So for the simulation with 1 water molecule at 300 K for example, the first 800 simulations were omitted.

Table 8: Data required to evaluate the quality of the MD simulations

	$T_{imposed}$ [K]	$t_{equilibrated}$ [fs]	Δ conserved quantity [a.u.]	ΔE_{pot} [a.u.]
$1H_2O$	300	787	0.005	0.15
	600	486	0.006	0.36
$2H_2O$	300	128	0.010	0.10
	600	727	0.013	0.30
$3H_2O$	300	184	0.004	0.31
	600	398	0.012	0.28
$4H_2O$	300	318	0.005	0.36
	600	13	0.010	0.39

The final columns of Table 8 show that the variation of the conserved quantity is at least 1 order of magnitude smaller than the range of the potential energy. Hence it can be concluded that no specific problems occurred during the simulations.

5.1.2 Influence of additional water molecules on Cu-NO complex

First the average Cu-N distance and angle between the Cu, N and O-atoms as obtained by the MD simulations are analyzed for the reference case with 1 additional water molecule at 300 K. The influence of both the temperature and the amount of water molecules taken into account is discussed later in this paragraph.

Reference case: 1H_2O at 300 K

Figure 5-3 and Figure 5-4 contain the graphs for the time evolution of respectively the |Cu,N| distance and Cu,N,O angle. From these figures, average values of 1.80 Å and 139° are obtained respectively. When comparing these values with the values of the static optimization of the pure NO adsorption (1.77 Å and 142°), only small variations are noticeable. Interaction of the water molecule with the Cu-species decreases the bond strength of Cu and NO. Therefore it is expected that the |Cu,N| distance will increase when adding extra reactants to the system.

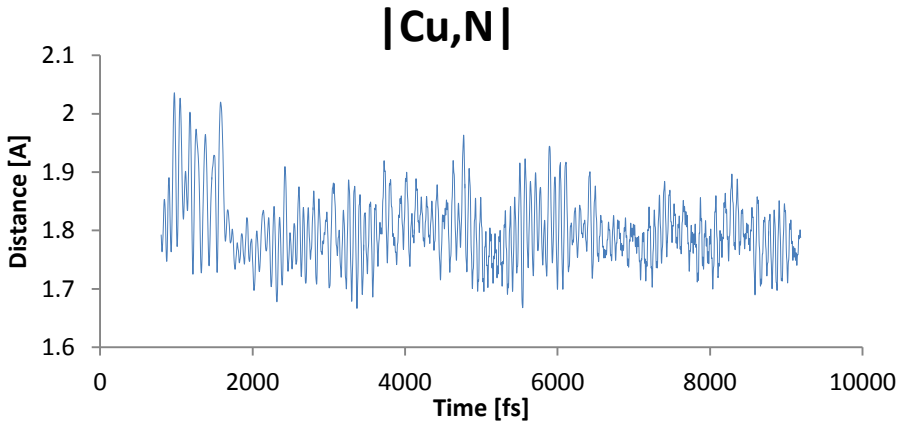

Figure 5-3: Time evolution of the Cu-N distance for the reference case with one additional H_2O molecule at 300 K

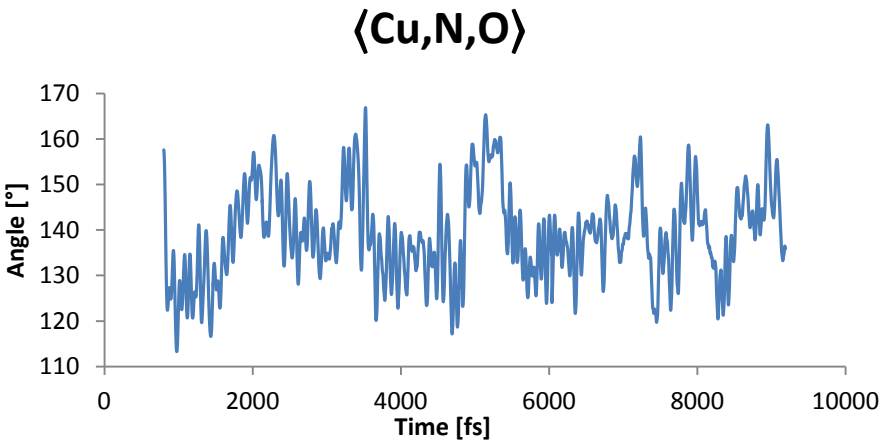

Figure 5-4: Time evolution of the Cu-N-O angle for the reference case with one additional H_2O molecule at 300 K

Comparison with other simulations

In Figure 5-5, the average Cu-N distance is given in function of the number of added water molecules at both 300 K and 600 K. The result for 4 water molecules at 600 K is not included, since this MD simulation encountered some problems leading to values which were clearly not in line with the other results - the average Cu-N distance had a value over 6 Å. This was due to the starting geometry for the MD simulation, where one water molecule was too close to the NO, resulting in runaway of the NO molecule.

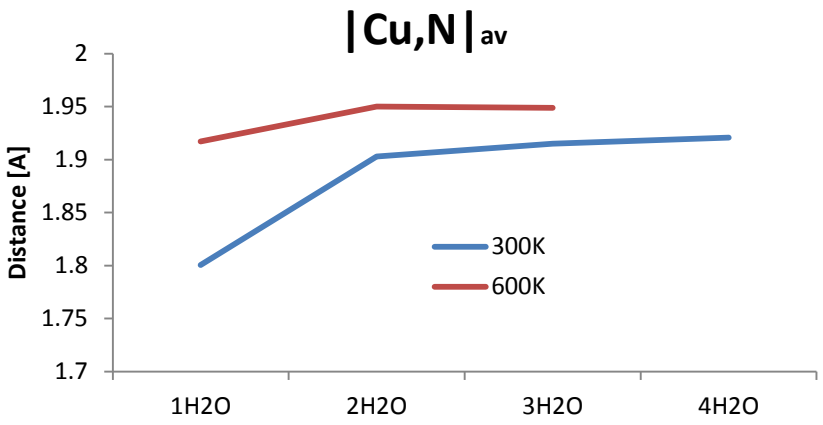

Figure 5-5: Average Cu-N distance at 300 K and 600 K in terms of number of water molecules added

A first observation is that the average distances at elevated temperatures are systematically higher than for lower temperatures. The second observation is mostly noticeable in the results at 300 K, where $|Cu,N|_{av}$ increases with the addition of water molecules. This change is most significant when going from 1 to 2 water molecules and seems to level off when adding more H_2O. Addition of respectively 1 and 2 water molecules thus has a greater influence on the coordination with the copper ion. This implies that the Cu ion is preferentially surrounded by NO, 2 water molecules and oxygen atoms of the zeolite framework. At 600 K however, the distance decreases slightly when adding a third water molecule. This is possibly explained by the influence of entropy factors. Higher temperatures mean that the contribution of the entropy to the Gibbs free energy increases. A decreasing |Cu,N| distance, i.e. stronger interaction between Cu and NO, can thus be explained by a slightly decreasing coordination of the water. A geometric investigation of possible hydrogen bond formation is thus advised.

The second point of interest which was investigated, is the angle between the Cu, N and O atom. These results are displayed in a similar way, in Figure 5-6. This time both temperatures clearly behave according to the same trend. The absolute value of the observed angle is however lower at 600 K, except for the case with two water molecules where the values more or less match. The absolute values corresponding to Figure 5-5 and Figure 5-6 can be found in appendix A-II.

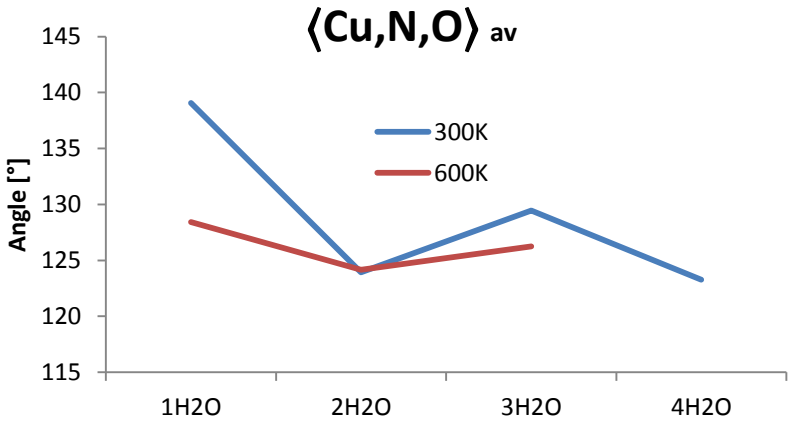

Figure 5-6: Average Cu-N-O angle at 300 K and 600 K in terms of number of water molecules added

5.1.3 Influence of additional water molecules on Cu-coordination

During the static simulations in section 4.1, it was established that the Cu was pulled towards the chabazite cage upon NO adsorption. By decreasing the interaction with the zeolite framework, it is expected that the mobility of the Cu-NO complex increases. This aspect is discussed thoroughly in section 5.1.4. To understand the influence of water addition on the Cu-mobility however, it is required to know how the Cu-coordination with the zeolite framework depends on the number of water molecules present. In this paragraph the Cu-coordination is investigated by introducing 3 separate coordination numbers for respectively the NO molecule, additional water molecules and all oxygen atoms of the 6mr from the top of the d6r subunit. The definition of the Cu-coordination number (CN) is given by following formula:

$$CN_i = \sum_{G_i} s_{ij} \qquad (21)$$

in which G_i corresponds to one of the three atom groups, i.e. NO, the water molecules or the zeolite framework oxygen atoms. The formula for s_{ij} is given by:

$$\begin{cases} 1 \quad \text{for} \quad \delta_{ij} > 0 \\ \dfrac{1-\left(\frac{\delta_{ij}}{r_0}\right)^n}{1-\left(\frac{\delta_{ij}}{r_0}\right)^m} \quad \text{for } \delta_{ij} > 0 \end{cases} \qquad (22)$$

where δ_{ij} is defined as $|r_i-r_j|-d_0$.

In this dissertation d_0 was set as zero, meaning δ_{ij} represents the distance between Cu and one of the atoms of the three groups under consideration. Since distances are always positive, only the formula for $\delta_{ij} > 0$ is applied. The shape of this function is as such that for $\delta_{ij} << r_0$, s_{ij} is very close to unity. A steep decrease from 1 to 0 is observed when δ_{ij} exceeds the r_0 value. In other words, the selection of an r_0 determines the scope of the coordination shell. Here a value of 2.2 Å is selected based on typical distances between Cu and O atoms of the zeolite framework, calculated from the simulations without H_2O. Standard values for n and m are 6 and 12 respectively so these values are used in this dissertation as well.

The influence of additional water molecules on the average coordination numbers at a temperature of 300 K is presented in Figure 5-7. A general trend is that the coordination with the zeolite framework decreases with increasing number of water molecules. For the simulation with pure NO ($0H_2O$) a two-fold coordination with the zeolite framework was observed. This gradually decreases to a value near unity when going from 0 to 3 water molecules. A small increase is seen for the addition of the fourth water molecule. As the zeolite cage is filled with water molecules there is less space available which could somehow force interaction of the Cu-ion with the zeolite framework. When looking at the blue bars representing coordination with water molecules, it is seen that the values are smaller than expected. The first water molecule is only attributed to the coordination shell for about 55% of the total simulation time. For 2 to 4 water molecules a value slightly higher than unity is observed. The CN_{water} trend thus confirms the inferior influence of the third and fourth water molecule; however the absolute values suggest that a larger value for r_0 value should have been used. Similar conclusions can be drawn from the green bars, representing the Cu-coordination with NO.

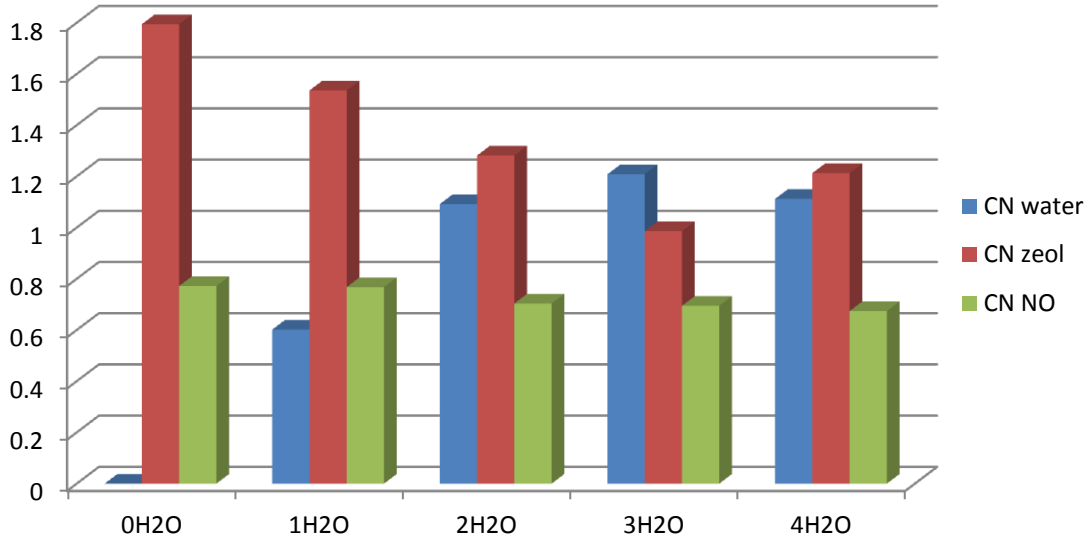

Figure 5-7: Coordination numbers as function of H_2O molecules at 300 K
$0H_2O$ corresponds to values from an MD simulation in the absence of water molecules

In Figure 5-8 the corresponding results for the simulations at 600 K are presented, where the results for 4 water molecules are omitted as explained earlier in section 5.1.2. Fairly similar trends are observed, except for the coordination with the zeolite framework. Clearly the simulation with one water molecule is not in line with the other results. Closer inspection of the simulation showed that combination of an elevated temperature and the position of the water molecule pulled the Cu-ion above the Al atom, leaving only a single zeolite oxygen able to interact with the Cu. The simulation time for this case was only about 4500 fs and should thus be extended further to obtain a better representation. The effect described above did not occur in the presence of multiple water molecules, because the individual attractions between Cu and H_2O tend to counter-act each other, i.e. attractive forces are exerted in multiple directions decreasing the absolute maximum displacement of the Cu-ion. This is of course related to the mobility of the Cu-ion, which is discussed next.

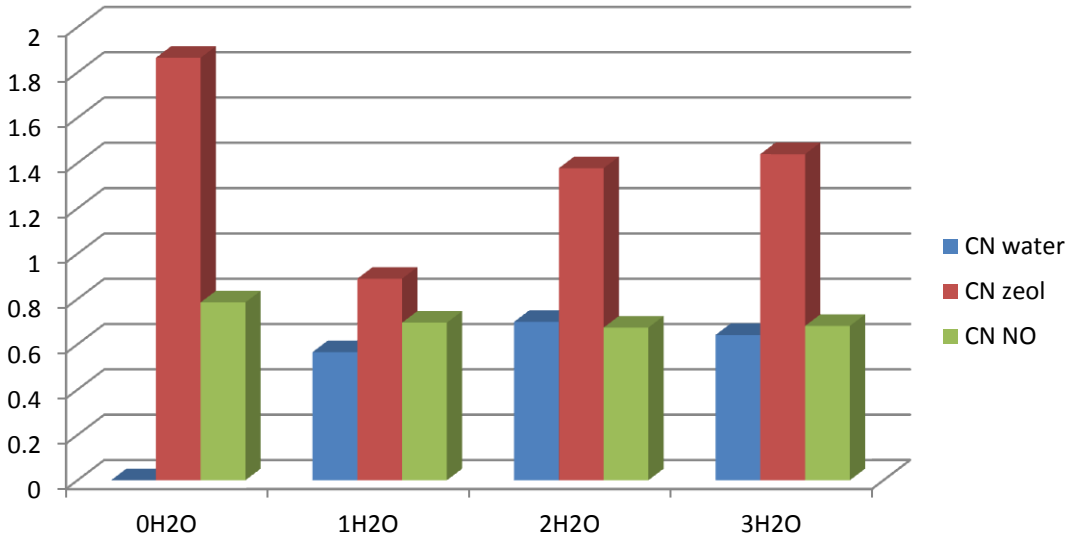

Figure 5-8: Coordination numbers as function of H2O molecules at 600 K
$0H_2O$ corresponds to values from an MD simulation in the absence of water molecules

5.1.4 Analysis of the Cu location and mobility of the active site

Influence of additional water molecules on Cu location

From the earlier chapters, it is clear that one of the major uncertainties within the SCR deNO_x mechanism is the location of the Cu-ion throughout the reaction pathway. Therefore the analysis mainly focuses on this aspect. In order of describing the Cu position precisely, the centre of mass of both the top and bottom ring of the d6r subunit is calculated for each frame. These centres are henceforth denoted as CM1 and CM2 respectively and are indicated on Figure 5-9. Plotting the distance between the Cu atom and CM1, as well as the angle between Cu, CM1 and CM2 describes the Cu position. The time evolution of the aforementioned properties is now discussed in more detail. First, the situation with one additional water molecule simulated at 300 K is examined and taken as the reference case. Later on, the sensitivity of the time evolution, in terms of selected temperature and number of molecules present, is investigated.

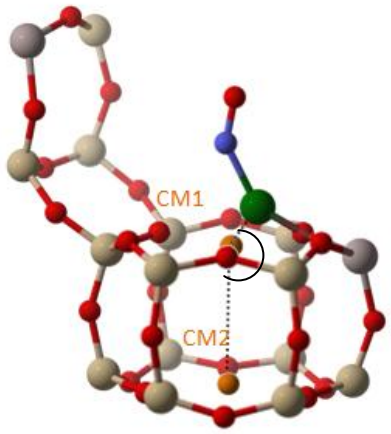

Figure 5-9: Indication of the centre of masses as orange dummy atoms used to monitor the Cu-position throughout the MD simulation

Reference case: 1H_2O at 300 K

Figure 5-10 depicts the time evolution of the distance between the Cu atom and CM1. Due to the nature of the MD simulation, an oscillatory behaviour is obtained around the average |Cu,CM1| distance of 2.09 Å. A maximum and minimum value of respectively 2.65 Å and 1.69 Å are observed; the range is thus 0.96 Å.

Our first interest is to see whether or not the Cu-ion stays more or less in the single position slightly above the top face of the d6r unit. An allowance threshold on the Cu-CM1 distance is introduced to determine what percentage in time the Cu is located near the aforementioned location. This threshold is set to 0.15 Å and is defined relative to the average distance of 2.09 Å obtained. Calculating the relative amount of time spent of the Cu within the threshold range leads to a total percentage of 49 % (see Table 9), demonstrating that the Cu-ion is quite mobile.

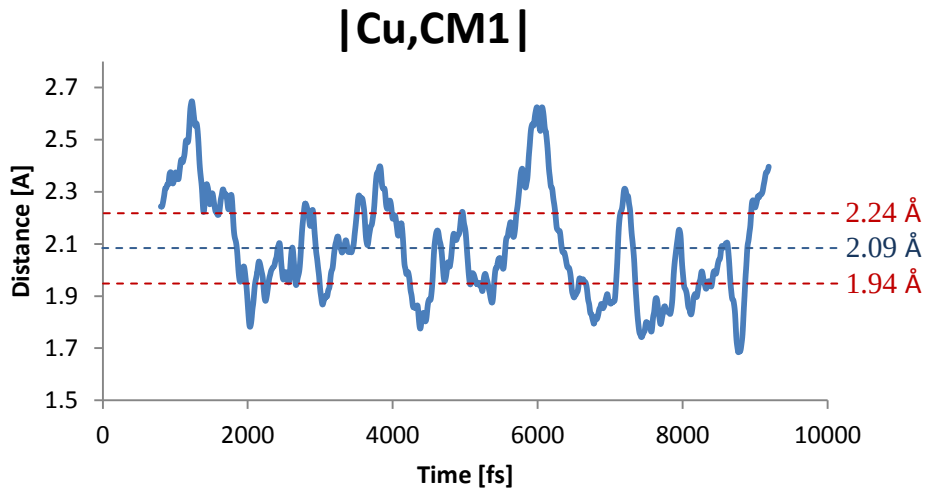

Figure 5-10: Time evolution of the distance between the Cu-ion and CM1 for the reference case with one additional H_2O molecule at 300 K

The evolution of the Cu-CM1-CM2 angle is shown in Figure 5-11. Here, the values are ranging between 134° and 152° with an average value of about 143°. To see if an increasing |Cu,CM1| is accompanied by an increasing Cu-CM1-CM2 angle, the correlation coefficient of these two data series was calculated and a value of 0.52 was obtained; hence no significant correlation is observed.

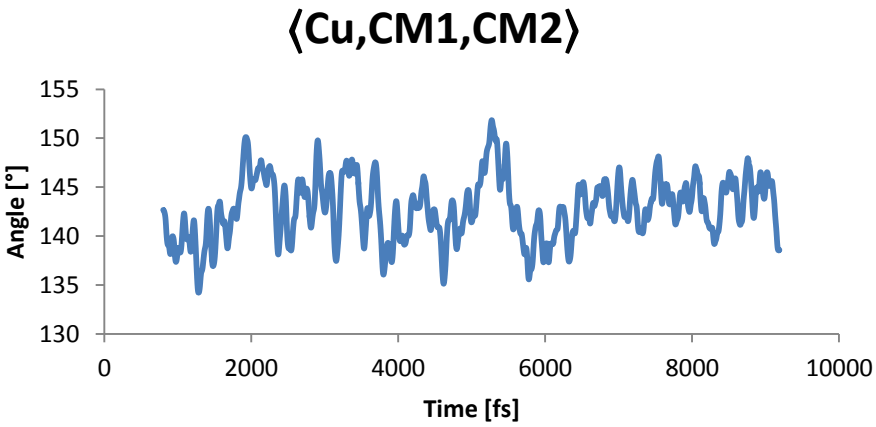

Figure 5-11: Time evolution of the angle between the Cu-ion, CM1 and CM2 for the reference case with one additional H_2O molecule at 300 K

Comparison with other simulations

The MD simulations with varying number of water molecules are all compared in terms of average geometrical properties. This is shown in Figure 5-12 and Figure 5-13 for the Cu-CM1 distance and Cu-CM1-CM2 angle respectively.

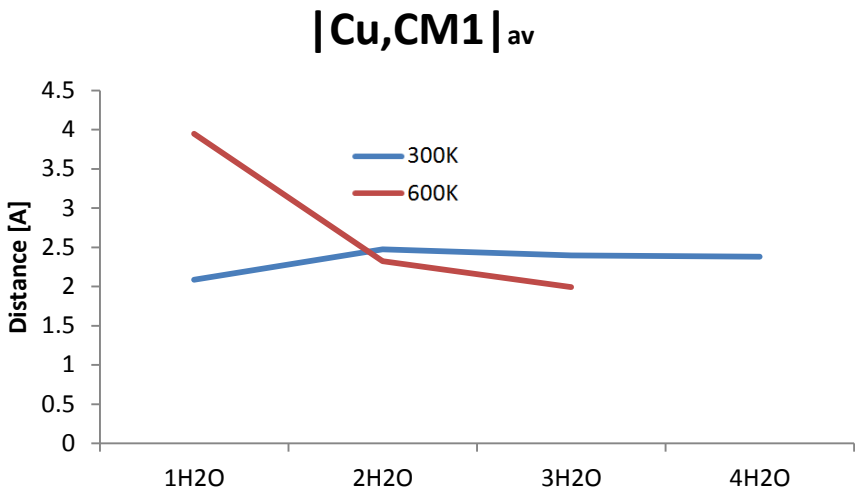

Figure 5-12: Average Cu-CM1 distance for varying number of water molecules at 300 K and 600 K

In Figure 5-12 it is seen that at 600 K a decreasing trend can be observed. Again, the change is most significant during the addition of the second water molecule, which causes |Cu,CM1| to drop from 3.95 Å to about 2.32 Å. In contrast, the addition of the third and fourth water molecule only decrease the distance by 0.32 Å and 0.07 Å, respectively. This is a first indication that a maximum Cu saturation is obtained with help of 2 H_2O molecules. The third and fourth molecule are interacting less with the Cu-ion and thus only have minor (indirect) effects.

At 300 K however, the situation is fairly different. There, the addition of the second water molecule induces an increase of the Cu - CM1 distance. The trend of the subsequent additions is however again similar to the situation at 600 K. During the simulations, a clear shift in the Cu-position can be observed at 600 K, going from a more or less centralized position within the top ring of the d6r subunit to a position straight above the Al atom present in this ring. A possible explanation might be that it is more easy for the Cu ion to escape the framework coordination at higher temperatures.

Table 9 contains the relative amount of time that the Cu is within the threshold range of the average position, as explained earlier. There is no steady decreasing or increasing trend noticeable. For both temperatures however, the percentage for 2 additional water molecules is the highest, indicating that this is most likely the most stable configuration. The decrease for the addition of the third and fourth water molecule, indicates that a higher mobility is obtained. This could be explained by the decreasing Cu-coordination with the zeolite framework and the competitive interaction of H_2O with the Cu-ion. The influence of additional water molecules on the mobility of the complex is elaborated later. Addition of the second H_2O is accompanied with an increasing percentage, which is intuitively less straightforward. A possible explanation is that the adsorbed complex containing 2 water molecules interacts more strongly with the zeolite framework, inducing stability to a certain extent. Naturally, the same could be said about the addition of the third and fourth water molecule. The data provided in Table 9 would then imply the competitive effect is more pronounced than the zeolite framework interactions. Of course the critical note on dynamic simulations still applies here; hence a larger set of longer simulations should be run to confirm these statements.

Table 9: Relative amount of time spent within a 0.15 Å radius of the average position

% within range	**$1H_2O$**	**$2H_2O$**	**$3H_2O$**	**$4H_2O$**
300K	49%	59%	37%	20%
600K	18%	51%	34%	/

Figure 5-13 shows the influence of the number of water molecules in the system on the average Cu-CM1-CM2 angle indicated in Figure 5-9. For both investigated temperatures an increasing trend can be observed for the addition of the first 3 water molecules. Combining the information from Figure 5-12 and Figure 5-13 shows that at 600 K, the decreasing Cu-CM1 distance is accompanied with an increasing Cu-CM1-CM2 angle, i.e. addition of water pulls the Cu almost above CM1. Also at 300 K, the addition of water induces a more centralized Cu-position. The absolute values corresponding to Figure 5-12 and Figure 5-13 can be found in Table A-II-1.

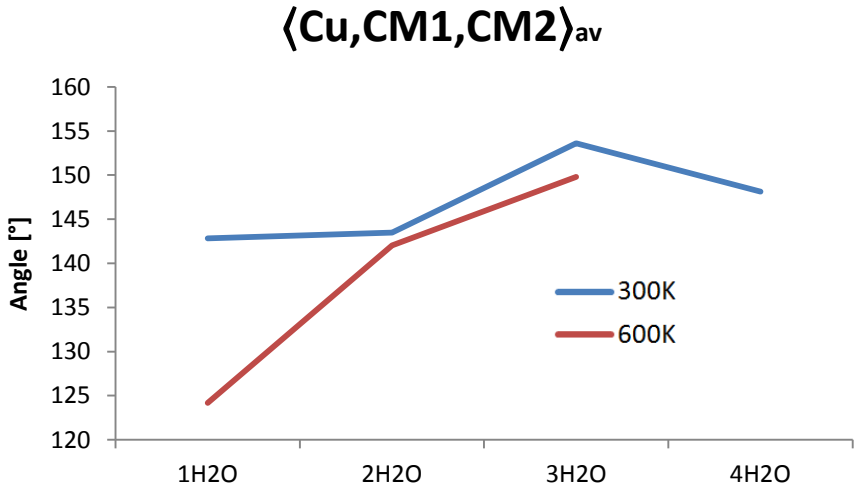

Figure 5-13: Average angle between the Cu-ion, CM1 and CM2 for varying number of water molecules at 300 K and 600 K

Influence of additional water molecules on mobility of the active site

As explained in the previous section, interaction between the Cu-ion and molecules within the chabazite cage decrease the coordination with the zeolite framework. Now, the effect on mobility is investigated. One might expect that a decreasing zeolite coordination automatically is accompanied with a mobility increase of the Cu-ion; however other complex effects with the surrounding water molecules need to be accounted for.

To visualize the Cu-mobility, the actual position is indicated by a green dot for every 100 frames (i.e. every 100 fs). While it is not possible to deduce the actual path throughout the simulation, the concentration and spread of the dots, provides information on respectively the most occurring positions and the all-round mobility of the ion. These plots are first compared for the MD simulations at 300 K with an increasing amount of surrounding water molecules. Later, the temperature dependency is discussed briefly.

Before analyzing the aforementioned plots, it is important to stress that the different cases did not run equally long. As shown in Table 10, the simulation with one water molecule at 300 K contains 9190 time steps, meaning 92 dots are plotted. The simulation with 2 water molecules on the other hand only contains 5863 time steps; hence this image will contain 34 less dots. This can lead to biased conclusions.

Table 10: Number of time steps [1 fs] included for every MD simulation

# time steps	**NO**	**1H_2O**	**2H_2O**	**3H_2O**	**4H_2O**
300 K	6191	9190	5863	7501	7500
600 K	8227	4959	3627	3728	/

Figure 5-14 contains the aerial view of the Cu-positions covered throughout the simulations at 300 K. The position of the NO and water molecules which are shown correspond with the last frame of the simulation and as such do not necessarily represent preferred configurations. It is seen that with increasing number of water molecules the area enclosed by all dots increases. Interestingly the displacement of the Cu-ion seems to be unidirectional for the case of 0, 1 and 2 H_2O molecules. The addition of the third and fourth H_2O induces displacement in multiple directions due to interaction with the H_2O already present and competitive interaction with the Cu-ion. This observation was used to exemplify the deviation of the zeolite coordination number for 2 water molecules at 600 K (see Figure 5-8).

In summary, the results discussed in 5.1.3 and 5.1.4 indicate that the Cu-mobility increases upon addition of extra H_2O molecules, due to a decreasing coordination with the zeolite framework.

Temperature dependency

So far only results at 300 K have been discussed. The behavior at elevated temperatures is also important, since this will give insights on the stability of the catalytic system. Figure 5-15 provides the side and top view of the Cu-position evolution in the absence of water at 300 K (left) and 600 K (right). Both top and side view indicate that the directionality of the Cu-displacement towards the oxygen is rather independent of temperature. The side views are indeed very similar, but the top view at 600 K indicates deviations from the line connecting the Cu and the oxygen. This increasing spread is a common observation at elevated temperatures.

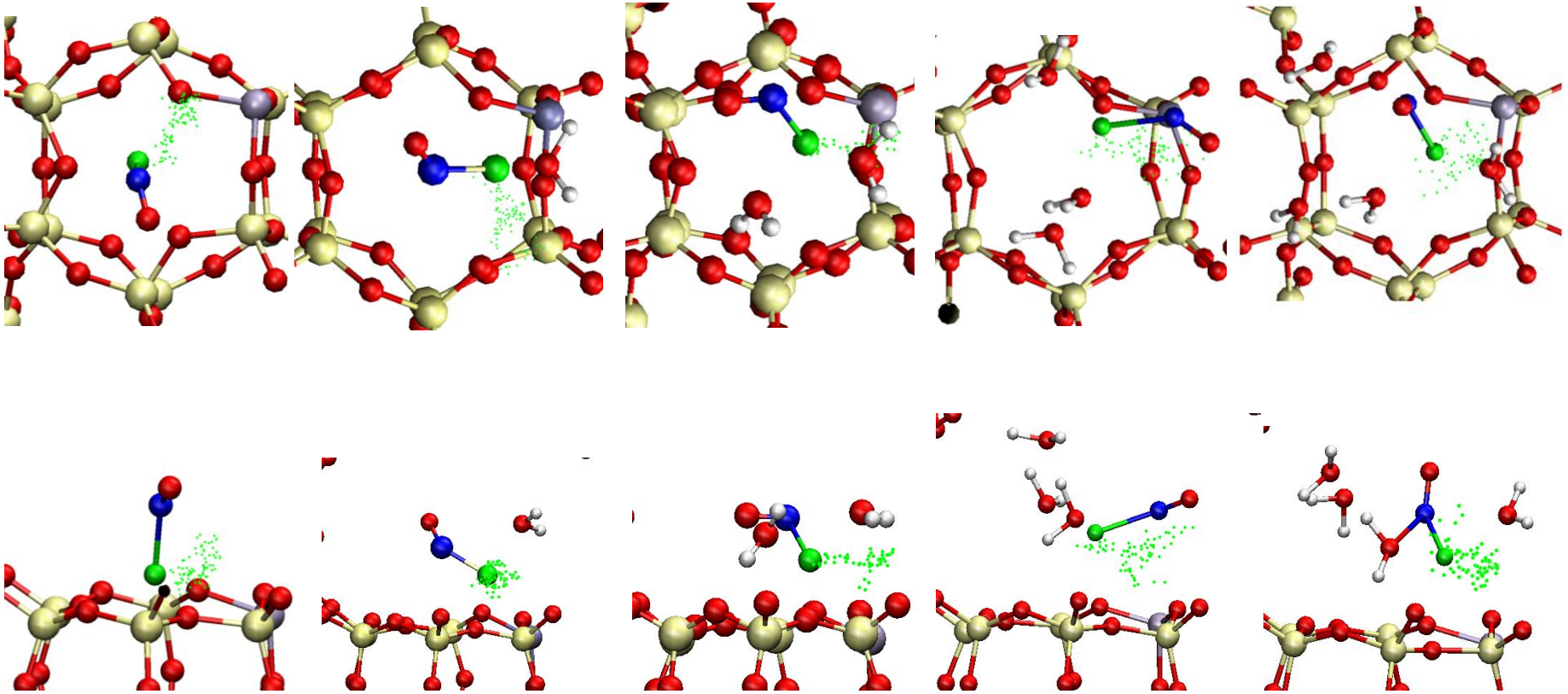

Figure 5-14: Top and side perspective for the MD simulations at 300 K. Illustration of the Cu-mobility as result of increasing number of water molecules (0 to 4 from left to right) The green dots represent the Cu-position at every 100 fs.

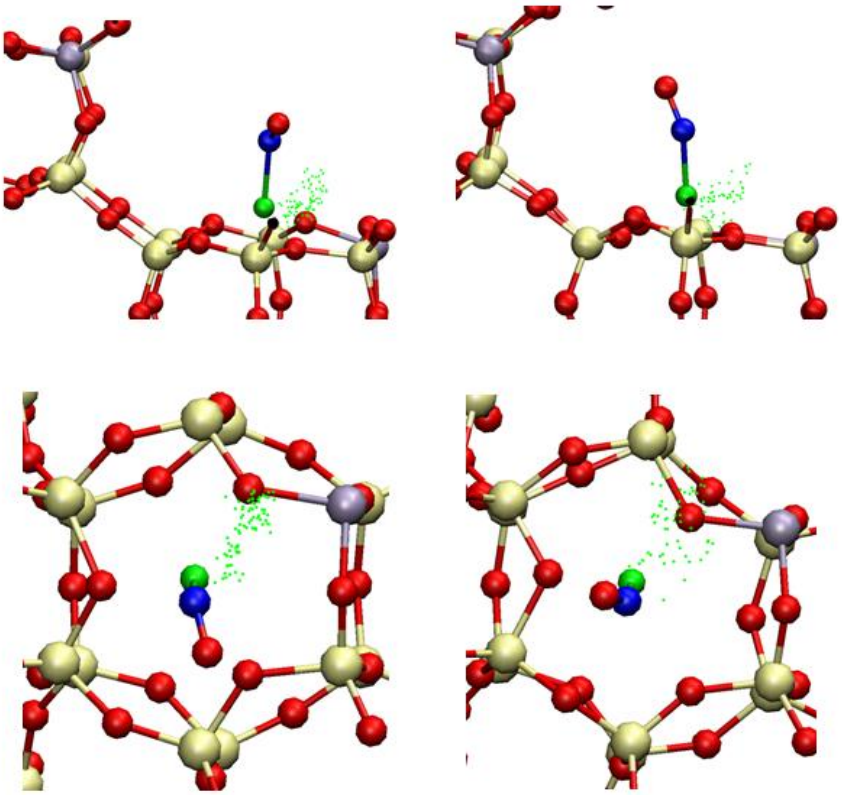

Figure 5-15: (left) side and top view of NO simulation at 300 K (right) side and top view of NO simulation at 600 K

5.2 Snapshot analysis

For each of the MD simulations at 300 K discussed above, a snapshot is taken from a 'representative' geometry. Of course it is always a bit arbitrary to pick out 1 frame out of several thousands. The selection of the representative geometry is done visually at first and once a rough idea is formed the final selection was based on energy factors. A geometry which corresponds with a relatively low energy, usually appears more frequently throughout the MD simulation, so this is a good methodology. The selected geometry is subsequently optimized with help of periodic CP2K calculations and the results will be discussed in paragraph 5.2.1. Finally, in order to assess the Cu-coordination a thermodynamic analysis at 93 K, 300 K and 600 K is performed, to evaluate the influence of the number of water molecules.

5.2.1 Geometry optimization

This paragraph covers the results of the geometry optimizations of the selected snapshots. The optimized geometry for each number of water molecules is presented in Figure 5-16. Note that only part of the unit cell is displayed to improve the clarity of the figures. Due to the snapshot selection procedure discussed above, i.e. selecting a frequently occurring geometry at relatively low energies, these simulations only needed a limited amount of iterations to converge. In other words, there is only a small difference between the initial and optimized structures. The geometric properties and energy of these optimized structures is presented in Table 11.

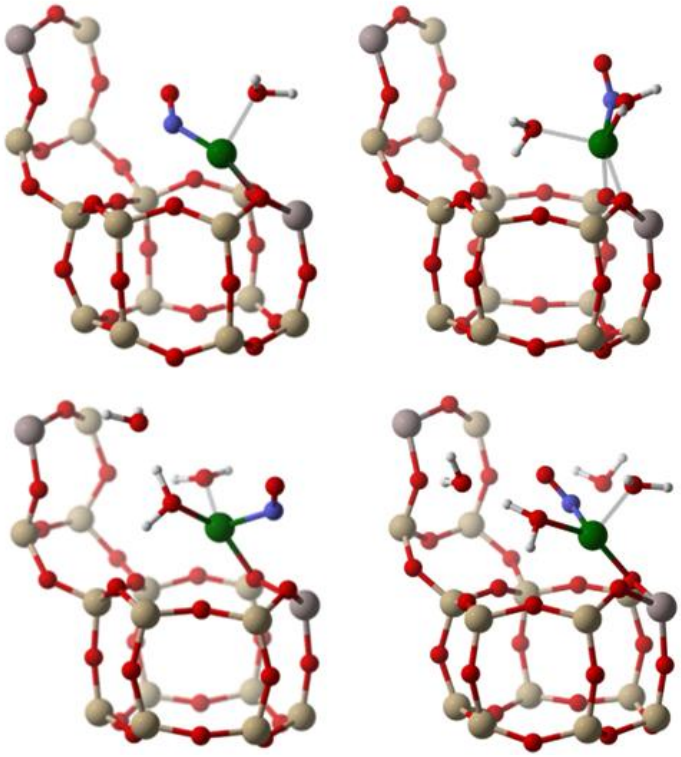

Figure 5-16: Optimized geometries from the MD snapshots

Table 11: Comparison geometric properties of the optimized MD snapshots

		1 H_2O	**2 H_2O**	**3 H_2O**	**4 H_2O**
|Cu,N|	Å	1.79	1.85	1.96	1.89
|N,O|	Å	1.14	1.14	1.14	1.15
⟨O,N,Cu⟩	°	133.2	122.0	128.0	121.6
β(Cu, d6r)	°	39.8	54.1	47.50	40.05

When comparing the data in Table 11 with the results of the ab initio MD simulations (Figure 5-5 and Figure 5-6), very similar trends can be observed. The reported Cu-N distance from Table 11 does however have a relatively high value, whereas the MD simulations showed that the results for 3 and 4 water molecules should be similar. This clearly illustrates that ab initio MD simulations can provide an accurate, yet broad description of the system.

5.2.2 Thermodynamic analysis

In this section the thermodynamic analysis of the optimized geometries is discussed. This analysis is done at 3 relevant temperatures 93K (-180°C), 300 K and 600 K. The former is done because samples investigated with help of e.g. high resolution powder diffraction, are usually cryo-cooled to this temperature in order to mitigate thermal vibrations. First the results at 93 K are discussed, after which the temperature dependency of each property is investigated.

Temperature 93 K

Figure 5-17 shows how the enthalpy change evolves for the subsequent addition of water molecules. The expected trend is to find a ΔH which continuously becomes less negative with every H_2O

addition. This would be explained by the fact that the first molecules are allowed to coordinate directly with the Cu complex, whereas the final molecules only form hydrogen bonds with other water molecules because the coordination shell of the Cu-ion is already saturated. The amount of molecules required to saturate this shell is of course not known a priori, but from the optimized geometries of Figure 5-16 one would expect 2 water molecules are sufficient to do so.

The trend observed in Figure 5-17 is indeed as expected, however the enthalpy change corresponding with the addition of the third molecule is still quite strongly negative. Judging from the optimized geometries one would estimate that the enthalpy change caused by the third addition is only about 20 kJ/mol per hydrogen bond formed. At first glance, only two hydrogen bonds are formed during this addition, hence a value of -40 kJ/mol would seem more logical. Of course Figure 5-16 can give a biased view, because the entire cage is not shown, so further interactions with the cage could still increase the negative enthalpy change.

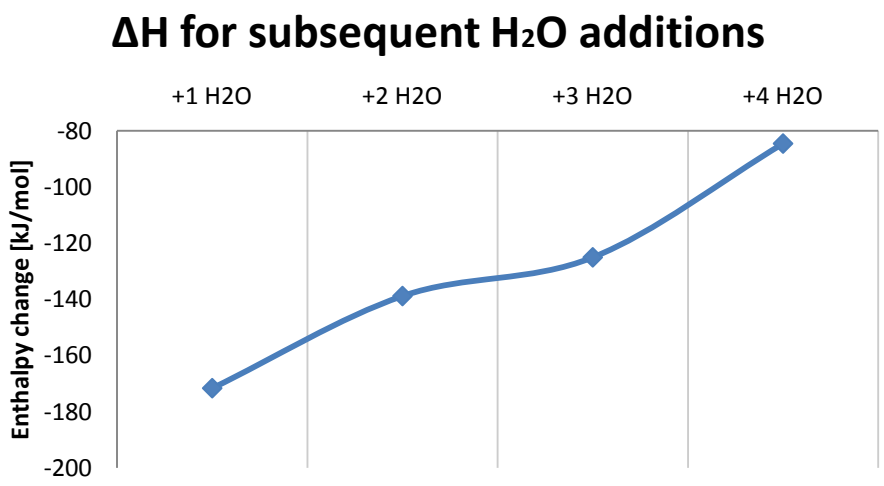

Figure 5-17: Enthalpy changes for the subsequent addition of H_2O

The dependency of the entropy on the number of water molecules added is given in Figure 5-18. Every addition is accompanied with an entropy decrease, but the strongest decrease is clearly visible for the second H_2O addition. A possible explanation is that the coordination of the first water molecule results in a fairly mobile Cu complex, i.e. for example still allowing a certain rotation of the water molecule around the Cu. For the addition of the second coordinated water molecule extra restrictions are imposed, of course due to the presence of the first water molecule, but also due to extra H_2O - framework interactions effectively anchoring the Cu complex to a certain extent. This is accompanied with a strong introduction of order and hence entropy decrease. Finally the entropy change for the third and fourth water molecule show a fairly equal intermediate value. The intermediate value is the result of the fact that these last H_2O molecules are able to roam more freely in the cage then the coordinated H_2O molecules (hence entropy decrease lower than $\Delta S_{+2\ H2O}$), which is counteracted somehow because now already two water molecules are present (hence entropy decrease higher than ΔS_{+1H2O}).

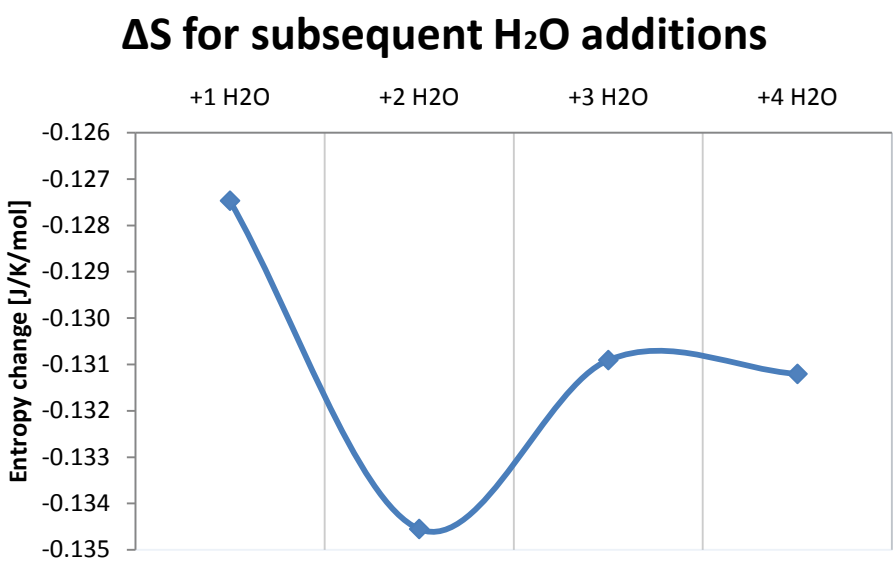

Figure 5-18: Entropy changes for the subsequent addition of H_2O

To conclude the thermodynamic analysis for 93 K, the information of the enthalpy and entropy change are combined to calculate the free energy change for every subsequent H_2O addition. The result is shown in Table 12. Due to the relatively small -TΔS contribution at 93 K, the free energy change is almost completely determined by the enthalpy changes.

Table 12: Results of the thermodynamic analysis at 93 K of the optimized snapshots from the MD simulation

[kJ/mol]	**+ 1 H_2O**	**+ 2 H_2O**	**+ 3 H_2O**	**+ 4 H_2O**
Δ H	-171.6	-138.8	-125.0	-84.5
-T Δ S	11.9	12.5	12.2	12.2
Δ G	-159.77	-126.3	-112.8	-73.3

Temperature dependency

Now that the behaviour of the thermodynamic properties at 93 K is explained, the analysis can be extended to compare the results with other temperatures of 300 K and 600 K. First the enthalpy changes are compared in Figure 5-19. The general trends are very similar for all investigated temperatures, however the enthalpy decreases are more noticeable with increasing temperature.

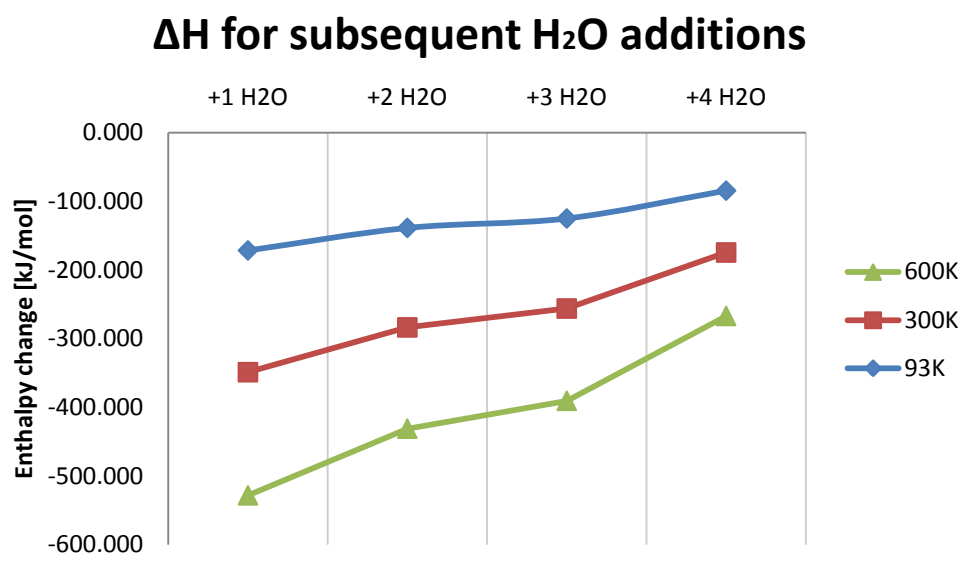

Figure 5-19: Temperature dependency of the enthalpy changes for the subsequent addition of H_2O

For the entropy as well, the changes are more expressed for the analysis at higher temperatures, as can be seen from Figure 5-20. Again the same interpretation is provided by the fact that higher temperatures induce higher mobility of the 'loose' molecules, leading to a much stronger contrast with the coordinated species.

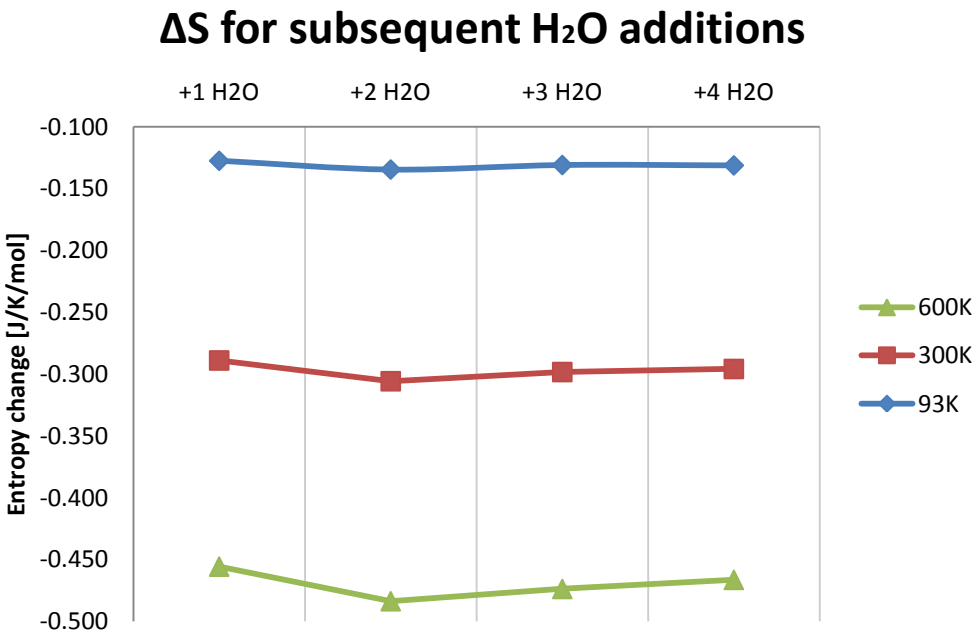

Figure 5-20: Temperature dependency of the entropy changes for the subsequent addition of H_2O

Due to the larger negative ΔS found at higher temperatures and the higher temperature itself in the T ΔS term of the free energy contribution, the influence of the entropy term increases drastically with increasing temperature.

Chapter 6

Conclusions

Restrictions on nitric oxide (NO_x) emissions are becoming continuously more stringent to mitigate the associated problems of among others acid rain and photochemical smog. The main sources of NO_x emission are diesel exhaust streams from mobile applications and hence a lot of research is conducted on this topic. One way of reducing the residual NO_x content in the exhaust stream is by the Selective Catalytic Reduction (SCR) with ammonia (NH_3) as reducing agent. This method, in which NO_x and NH_3 are converted into N_2 and H_2O, is already used in practice, even though many questions concerning the detailed reaction mechanism remain unanswered. A thorough understanding of this mechanism is however crucial in order to find structure-activity relations of the involved catalyst material. Only then an intelligent catalyst design is achievable to uphold the upcoming restrictions.

Earlier studies have shown that metal-exchanged zeolites provide a catalytic system with excellent properties in terms of activity and selectivity. It has been proven that the metal exchange greatly enhances the performance of the catalyst, however the nature of these metal catalytic centres remains a point of discussion. Depending on the metal and topology selected, isolated ions, dimers or metal-oxide clusters were observed. Recently, lot of attention has been given to Cu-SSZ-13, which has a chabazite topology consisting of chabazite cages surrounded by double 6 membered ring (d6r) subunits. These subunits and small pore windows greatly enhance the hydrothermal stability of the catalyst, which is essential since the SCR reaction takes place in close vicinity of the Diesel Particulate Filter which is oxidised frequently at elevated temperatures.

Experimental findings indicated that the dominant catalytic centre within Cu-SSZ-13 is given by an isolated Cu-ion, located on the top face of the d6r subunit. Therefore the interaction of NO with a Cu^{2+} ion was investigated using Molecular Modeling techniques. In a first stage, the pure adsorption of NO was modeled in order to determine the position of the Cu-species. Relevant distances and frequencies were used to validate the results by comparison with experimental data. In a second stage, the influence of additional water molecules on the Cu-position was investigated in more detail.

In order to elucidate the mechanism behind the NH_3-SCR deNOx reaction and in particular the initial adsorption of NO and subsequent interactions with additional water molecules, theoretical methods were used. The main part of the calculations consisted of periodic DFT-based calculations on a 36T unit cell, by using the CP2K software package with a Gaussian Plane Wave basis set. PBE functionals with d3-dispersion corrections are hereby selected and a pseudo-potential approximation is applied. Periodic calculations often require long calculations times. Therefore, several finite clusters were employed as well, often in combination with an ONIOM-scheme, where universal force fields were used to describe the low level. The results obtained with these finite clusters were however unsatisfactory, due to lack of stability of the d6r subunits and the inability to correctly distribute the charges. Indeed, based on a NPA analysis a Cu^{+} ion instead of a Cu^{2+} ion was observed throughout the

simulations as a result of computational cluster effects. The further analysis of the Cu-NO adsorption complex was therefore mainly based on the periodic calculations.

The periodic calculations of the NO adsorption geometry optimization shows that the Cu-ion was extracted from the upper ring of the d6r subunit towards the chabazite cage upon NO adsorption. The optimized geometry was in great correspondence with both experimental values and earlier theoretical research. An NO bond length of 1.15 Å was obtained, as well as a Cu-N-O angle of about 142° for the energetically favoured singlet state. For this state, the adsorption energy equals 126 kJ/mol and the No molecule is directed perpendicular to the face of the double 6-membered ring. The aforementioned values are fairly independent of the initial configuration. A second validation of the results is provided by the frequencies rather than the obtained geometry. The calculated characteristic NO stretch frequency of the Cu-adsorbed species equalled 1952 cm^{-1}, in good agreement with the 1948 cm^{-1} obtained by experimental IR measurements.

With the formation of HONO as next intermediate in mind, the interaction of water with the adsorbed NO species was investigated. Mainly dynamic calculations on the periodic system were used to monitor the positioning of up to 4 water molecules around Cu-NO in function of time. Again the main focus was on the positioning of the Cu-ion. Analysis shows that the addition of the first two water molecules has the greatest influence, indicating that the third and fourth water molecule do not interact directly with Cu. This was true for the position of the Cu-ion as well as for the geometric properties of the Cu-NO complex itself, meaning that the direct coordination shell of Cu consists of NO, 2 water molecules and 1 or 2 zeolite framework oxygen atoms. The data showed that addition of water molecules resulted in the increase of the average Cu-N distance compared to the static optimized geometry without H_2O.

The ab initio MD simulations provided a general view of the most commonly occurring configurations. Due to the limited simulation times there is however no guarantee that all representative states are sampled, so the results should be interpreted with caution. For every number of water molecules, a snapshot was selected and this configuration was subsequently optimized. A thermodynamic analysis of these optimized structures confirmed that the first two water molecules bind more strongly to the Cu, illustrated by the strong negative enthalpy change. Overall the interaction of Cu with water increased the Cu-mobility.

Even though the NO adsorption has now been studied extensively there is still a long way to go before the SCR deNOx reaction can be fully understood. Before going over to similar investigations regarding the following intermediates such as HONO and NH_4NO_2, the NO adsorption should be refined further. For instance, the presence of molecules other than water could have an effect on the state of the adsorbed NO and should thus be taken into account. Furthermore, while the results of the periodic cluster calculations seemed to match the experimental results very well, finding a stable finite cluster with a successful ONIOM-scheme would help to reduce calculation times substantially and would allow more advanced calculations. Then, once the state of all intermediates is thoroughly known, the kinetics of every reaction could be compared to finally determine the dominant reaction mechanism. Fortunately, recent advancement in e.g. the Nudged Elastic Band provide a way of calculating kinetic parameters for periodic systems.

Clearly, there are still several milestones to be achieved, but I am sure talented scientists will rise up to the challenge and will succeed in eliminating NO_x emissions to a great extent!

Appendix A

Additional data

APPENDIX A-I: Quality assessment of the Molecular Dynamics simulations (section 5.1.1)

Results used to check the quality/convergence of the Molecular Dynamics simulations corresponding with the interaction of the adsorbed NO species and a varying amount of water molecules. Two sets of imposed temperatures are used (300 K and 600 K).The evolution of the average and instantaneous temperatures (K) is shown as green and red curves respectively on the figures at the left hand side. On the right the evolution of the conserved quantity (a.u.) is plotted. Time on the x-axis is in fs.

1H2O

T300

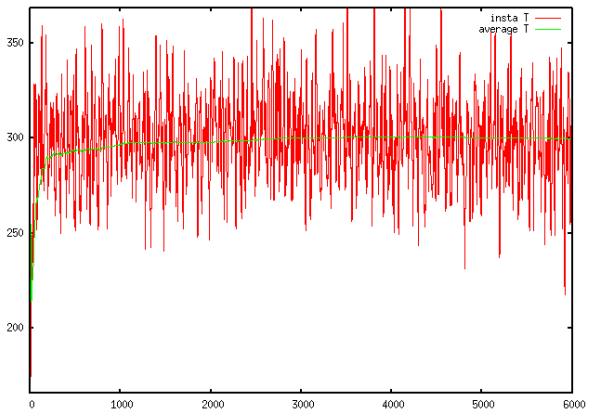

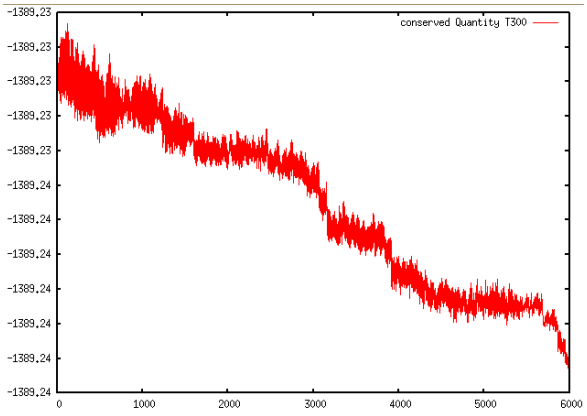

T600

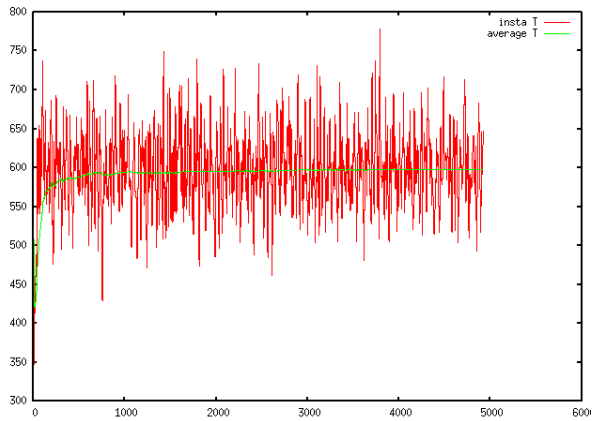

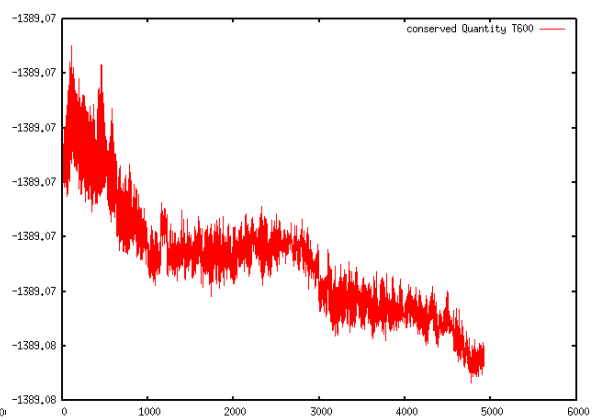

2H2O

T300

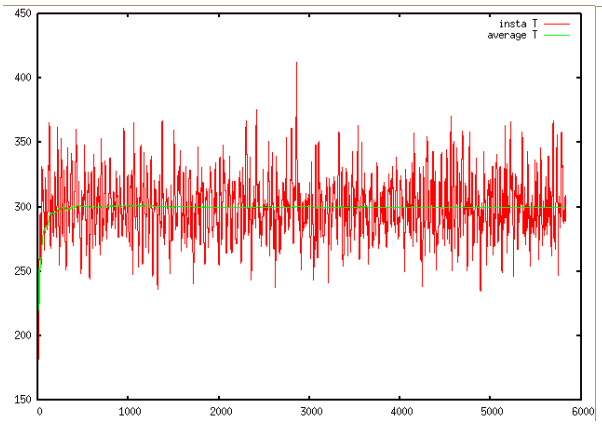

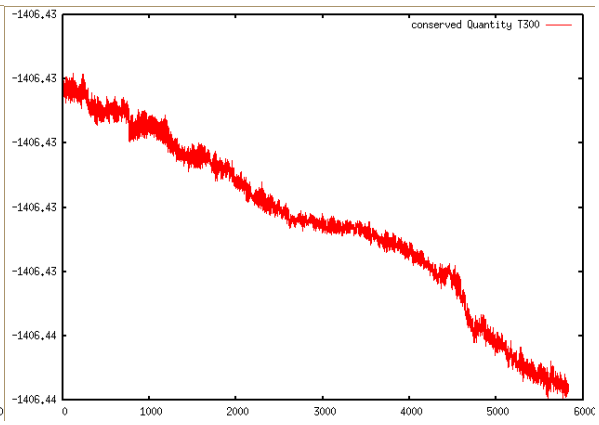

T600

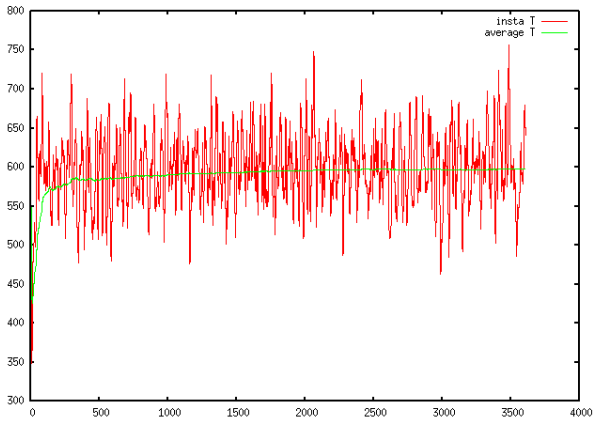

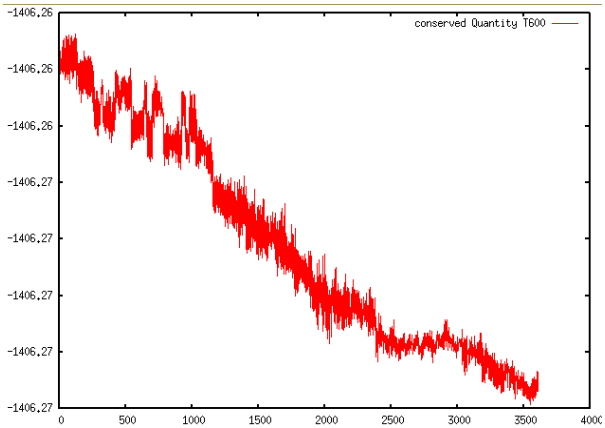

3H2O (posb)

T300

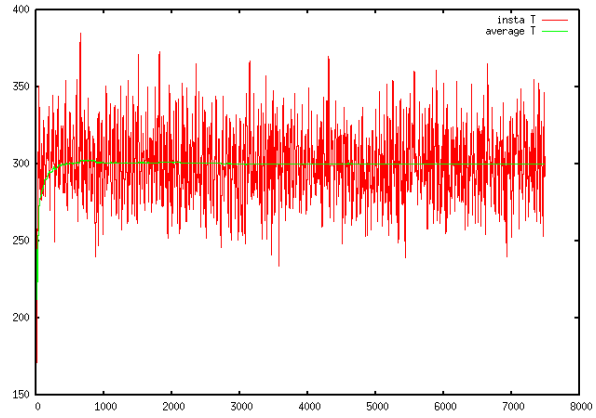

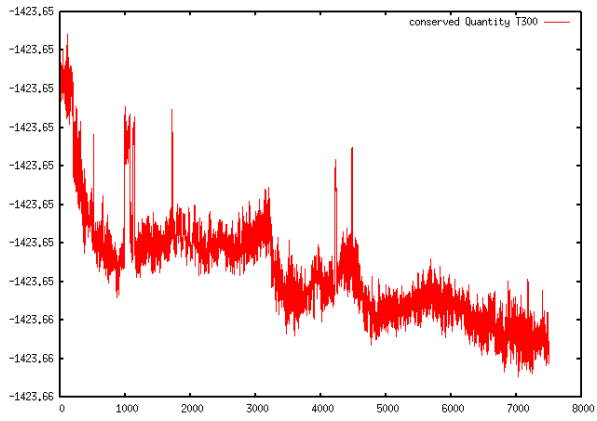

T600

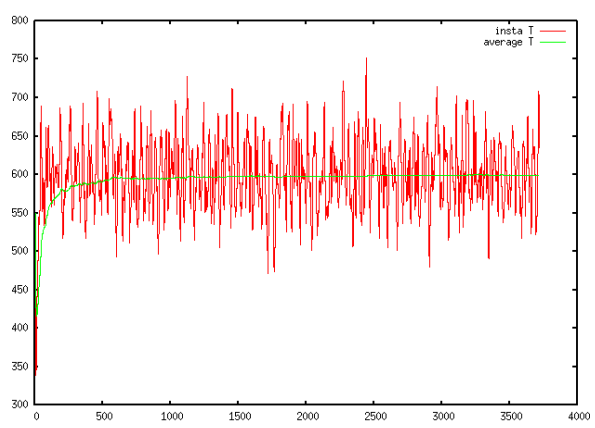

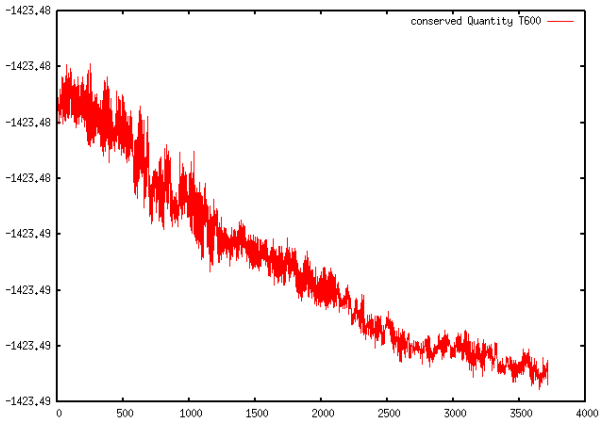

4H2O

T300

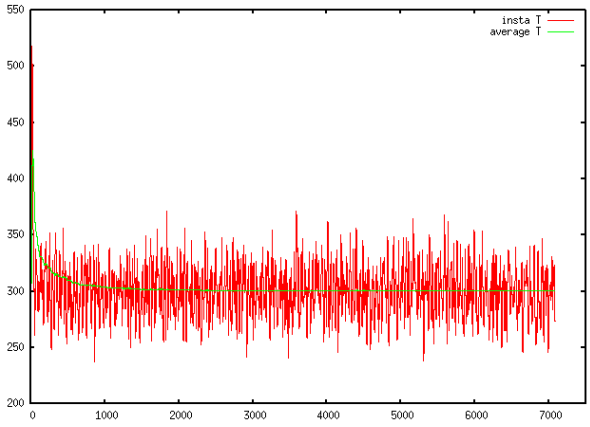

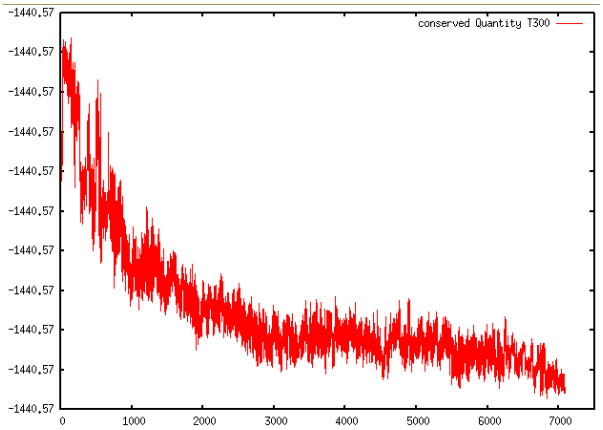

T600

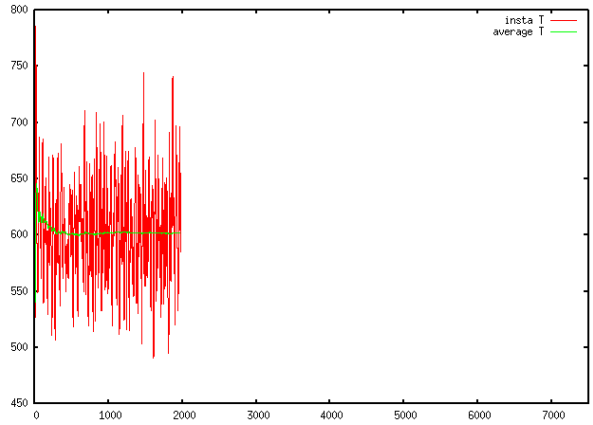

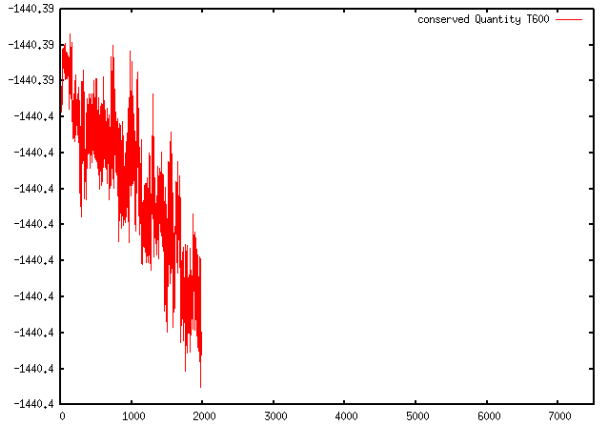

APPENDIX A-II: Comparison of the main results of the MD simulations modelling the interaction with a different amount of water molecules.

Table A-II-1: Comparison average Cu-CM1 distance and angle between Cu, CM1 and CM2 throughout the MD simulations

$\|Cu,CM1\|_{av}$ [Å]	**$1H_2O$**	**$2H_2O$**	**$3H_2O$**	**$4H_2O$**
300K	2.09	2.47	2.40	2.37
600K	3.95	2.32	1.99	1.93
⟨Cu,CM1,CM2⟩ [°]				
300 K	142.82	143.49	153.59	148.14
600 K	124.19	142.02	149.80	/

Table A-II-2: Comparison average Cu-N distance and angle between Cu, N and O throughout the MD simulations

$\|Cu,N\|_{av}$ [Å]	**$1H_2O$**	**$2H_2O$**	**$3H_2O$**	**$4H_2O$**
300K	1.80	1.90	1.92	1.92
600K	1.92	1.95	1.95	/
⟨Cu,N,O⟩ [°]				
300 K	139.07	123.94	129.46	123.28
600 K	128.42	124.15	126.24	/

Appendix B

Poster NCCC

This appendix contains a smaller version of the poster which was presented on the 11th of march during NCCC XV (XVth Netherlands' Catalysis and Chemistry Conference), 10th-12th march 2014, Noordwijkerhout (NL).

NH3-SCR of NOx: NO-adsorption on Cu-SSZ-13 using Ab initio simulations

Tom Van Den Heede[1], Jeroen Van der Mynsbrugge [1], Kristof De Wispelaere [1], Ines Lezcano-Gonzalez [2], Andrew M. Beale [2], Bert M. Weckhuysen [2], Veronique Van Speybroeck [1] and Karen Hemelsoet [1]

[1] Center for Molecular Modeling, Ghent University, Technologiepark 903, B-9052 Zwijnaarde, Belgium
[2] Inorganic Chemistry and Catalysis Group, Debye Institute of Nanomaterials Science, Utrecht University, Universiteitsweg 99, 3584 CA Utrecht, The Netherlands

Reduction of NO_x [1]

- Problems caused by NO_x emissions:
  - Acid rain
  - Photochemical smog
  - Ozon layer depletion
- Stringent EURO VI regulations upcoming for mobile sources: need for innovative and optimized processes/ catalysts → Selective Catalytic Reduction by ammonia (NH_3-SCR)
- Production of NO_x mostly originating from combustion processes in transportation applications (>40%)

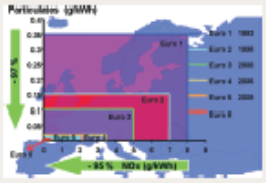

Catalyst selection: Copper-exchanged zeolite Cu-SSZ-13 (CHA topology) [3]

Advantages Performance:
- N_2-Selectivity
- Activity
- Hydrothermal stability

Research:
± unique location active site → ease of interpreting experimental and theoretical modelling data

Disadvantage
Difficult to obtain high Cu-loading

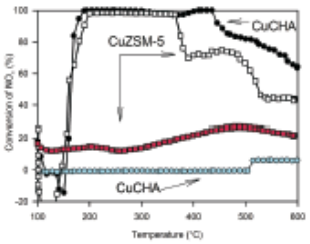

Proposed reaction mechanism [4]

- Experimental data has indicated the presence of copper-nitrosyl (Cu-NO) complexes
- Other intermediates are nitrous acid (HONO) and ammonium nitrite (NH_4NO_2)

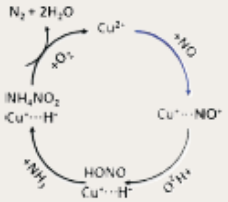

NO adsorption

Different starting structures for simulation

Influence initial Cu-N-O angle ↔ Influence initial Cu position ↔

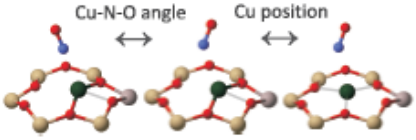

Properties optimized structures

E_{ads} [kJ/mol]	-128.15	-126.66	-128.21
α(O$_1$,N,Cu)	124.3°	126.8°	127.0°
|Cu,N| [A°]	1.75	1.77	1.77
β(Cu,O$_2$,Al,O$_3$)	128.5°	126.4°	126.6°

Influence initial Cu-position? Negligible
Influence initial Cu-N-O angle? Higher but still negligible
Triplet was considered as well → Similar geometry

Optimized geometry

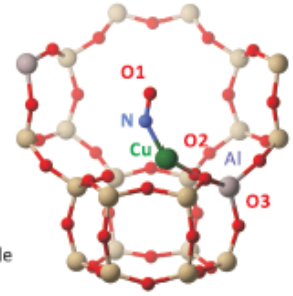

Optimized structure in good agreement with experimental results

Conclusion

- Optimized configuration NO adsorbed species is found and validated by comparing the obtained geometries and IR spectra
- Further research concerning other intermediates required

Process: Aftertreatment combustion gas by NH_3-SCR [1,2]

Global reactions:
$4\,NO + 4\,NH_3 + O_2 \rightarrow 4\,N_2 + 6\,H_2O$
$2\,NO_2 + 4\,NH_3 + O_2 \rightarrow 3\,N_2 + 6\,H_2O$
$NO + NO_2 + 2\,NH_3 \rightarrow 2\,N_2 + 3\,H_2O$

Toxicity issues NH_3 in mobile applications urea-SCR in heavy duty vehicles
$(NH_2)_2CO \rightarrow NH_3 + HNCO$
$HNCO + H_2O \rightarrow NH_3 + CO_2$

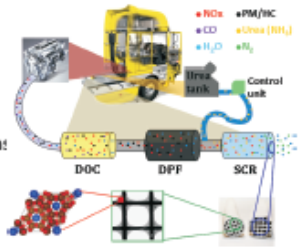

Characterisation of Cu-SSZ-13 [1,3]

- Chabazite topology with double 6-membered rings (d6r) and chabazite subunits (cha)
- Active site (Cu^{2+}) predominantly located on the face of the d6r unit facing the chabazite cage. Absolute location determined by presence of reactants and even moisture content. High Cu-loadings: $(Cu\text{-}O\text{-}Cu)^{2+}$ dimers observed in small amounts.

Research objectives

- Model NO adsorption using periodic DFT-based simulations
- Gain insights in the reaction mechanism and perform a kinetic analysis
- Evaluate the configuration and electronic state of the intermediates

Methodology

CP2K - periodic DFT-based simulations

PBE-functional with d3-dispersion correction
PBE based pseudo-potential

Gaussian (DZVP) and plane waves basis set

Distinction LSD/ no LSD should be made

Unit cell

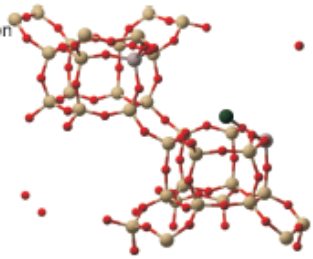

IR spectra calculations

- Periodic vibrational analysis using CP2K to obtain IR-spectrum: NO stretch frequency 1953 cm^{-1} → Correspondence with FTIR studies [4]
- Isolation of top half of d6r: [Gas phase PBE1PBE/DGZVP]

Advantage → More advanced methods for calculation of charge-distribution and IR-spectra (experimental validation)

Disadvantage → Loss of accuracy by omitting interaction with the cha cage (expanded in future work)

Relocation second Al to obtain charge-neutral configuration (non-periodic) [left]
→ Single Al atom tested as well to avoid large Cu displacements [right]

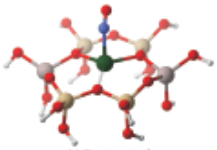

NO-stretch: 2169 cm^{-1}

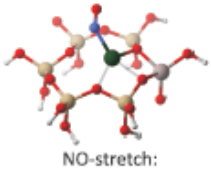

NO-stretch: 2157 cm^{-1}

References

[1] Deka,U., Lezcano-Gonzalez, I., Weckhusen, B.M. and Beale,A.M., ACS Catal. 3 (2013) 413.
[2] Brandenberger, S., Kröcher, O., Tissler, A. and Althoff, R., Al. Cat. Rev. - Sci. Eng. 50:4 (2008) 492.
[3] Gao,F., Walter,E.D., Karp,E.M., Luo,J., Tonkyn,R.G., Kwak,J.H., Szanyi,J. and Peden,C.H.F., J. Catal. 300 (2013) 20.
[4] Kwak, J.H., Lee,J.H, Burton,S.D., Lipton,A.S., Szanyi,J. and Peden,C.H.F, Angew. Chem. Int. Ed. 52:38 (2013) 9985

Appendix C

Article in preparation

Part of the calculations in this thesis are used during the preparation of the following manuscript:

"Examination of Cu coordination complexes formed in the presence of NO and NH3 within SSZ-13", Upakul Deka, Ines Lezcano-Gonzalez, David S. Wragg, Karen Hemelsoet, Andy Van Yperen-De Deyne, Tom Van Den Heede, Michel Waroquier, Veronique van Speybroeck, Bert M. Weckhuysen and Andrew M. Beale, 2014, in preparation

Chapter 7

References

1. National Pollutants Emission Volume. http://eng.me.go.kr/content.do?method=moveContent&menuCode=pol_cha_air_sta_emi_volume
2. Parvulescu, V. I.; Grange, P.; Delmon, B., Catalytic removal of NO. *Catalysis Today* **1998,** 46, (4), 233-316.
3. Beperking van de vervuilende emissies van lichte voertuigen. http://europa.eu/legislation_summaries/environment/air_pollution/l28186_nl.htm
4. Deka, U.; Lezcano-Gonzalez, I.; Weckhuysen, B. M.; Beale, A. M., Local Environment and Nature of Cu Active Sites in Zeolite-Based Catalysts for the Selective Catalytic Reduction of NOx. **2013**.
5. Nitrogen Oxides (NOx), Why and How They are Controlled - fnoxdoc.pdf. http://www.epa.gov/ttncatc1/dir1/fnoxdoc.pdf
6. Process overview and NOx reduction information. http://charmeck.org/mecklenburg/county/airquality/educationandoutreach/documents/noxreductionhandoutfinal.pdf (September 2000),
7. Deka, U.; Juhin, A.; Eilertsen, E. A.; Emerich, H.; Green, M. A.; Korhonen, S. T.; Weckhuysen, B. M.; Beale, A. M., Confirmation of Isolated Cu2+ Ions in SSZ-13 Zeolite as Active Sites in NH3-Selective Catalytic Reduction. *Journal of Physical Chemistry C* **2012,** 116, (7), 4809-4818.
8. DiMaggio, C. L.; Corp., D.; Fisher, G. B.; Corp., D.; Rahmoeller, K. M.; Corp., D.; Sellnau, M.; Corp., D., Dual SCR Aftertreatment for Lean NOx Reduction. *SAE Int. J. Fuels Lubr.* **2009,** 2(1), (2009-01-0277), 66-77.
9. Held, W.; AG, V.; König, A.; AG, V.; Richter, T.; AG, V.; Puppe, L.; AG, B., Catalytic NOx Reduction in Net Oxidizing Exhaust Gas. **1990**, (900496).
10. Smedler, G.; Division, J. M. C. S.; Ahlström, G.; Division, J. M. C. S.; Fredholm, S.; Division, J. M. C. S.; Frost, J.; Center, J. M. T.; Lööf, P.; Division, J. M. C. S.; Marsh, P.; Division, J. M. C. S.; Walker, A.; Center, J. M. T.; Winterborn, D.; Division, J. M. C. S., High Performance Diesel Catalysts for Europe Beyond 1996. **1995**, (950750).
11. Williamson, W. B.; Lunsford, J. H., Nitric-Oxide reduction with ammonia over Cu(II)Y zeolites *Journal of Physical Chemistry* **1976,** 80, (24), 2664-2671.
12. Brandenberger, S.; Kroecher, O.; Tissler, A.; Althoff, R., The State of the Art in Selective Catalytic Reduction of NOx by Ammonia Using Metal-Exchanged Zeolite Catalysts. *Catalysis Reviews-Science and Engineering* **2008,** 50, (4), 492-531.
13. Gao, F. H. K., Ja. Szanyi, Janos. H.F.Peden, Charles., Current Understanding of Cu-Exchanged Chabazite Molecular Sieves for Use as Commercial Diesel Engine DeNOx Catalysts - Springer. *Top Catal (2013) 56: 1441-1459* **2014**.
14. Lezcano-Gonzalez, I.; Deka, U.; Van Yperen-De Deyne, A.; Hemelsoet, K.; Waroquier, M.; Van Speybroeck, V.; Weckhuysen, B. M.; Beale, A. M., Determining the storage, availability and reactivity of NH3 within Cu-chabazite-based ammonia catalytic reduction systems. *Physical Chemistry Chemical Physics* **2014,** 16, 1639-1650.
15. Girard, J.; Co., F. M.; Snow, R.; Co., F. M.; Cavataio, G.; Co., F. M.; Lambert, C.; Co., F. M., The Influence of Ammonia to NOX Ratio on SCR Performance. **2007**, (2007-01-1581).

16. Kieger, S.; Delahay, G.; Coq, B.; Neveu, B., Selective catalytic reduction of nitric oxide by ammonia over Cu-FAU catalysts in oxygen-rich atmosphere. *Journal of Catalysis* **1999,** 183, (2), 267-280.
17. Schoonheydt, R. A., UV-VIS-NIR spectroscopy and microscopy of heterogeneous catalysts. *Chemical Society Reviews* **2010,** 39, (12), 5051-5066.
18. Giamello, E.; Murphy, D.; Magnacca, G.; Morterra, C.; Shioya, Y.; Nomura, T.; Anpo, M., The interaction of NO with copper ions in ZSM5 - An EPR and IR investigation. *Journal of Catalysis* **1992,** 136, (2), 510-520.
19. Deka, U.; Juhin, A.; Eilertsen, E. A.; Emerich, H.; Green, M. A.; Korhonen, S. T.; Weckhuysen, B. M.; Beale, A. M., Confirmation of Isolated Cu2+ Ions in SSZ-13 Zeolite as Active Sites in NH3-Selective Catalytic Reduction. **2012**.
20. Korhonen, S. T.; Fickel, D. W.; Lobo, R. F.; Weckhuysen, B. M.; Beale, A. M., Isolated Cu2+ ions: active sites for selective catalytic reduction of NO. *Chemical Communications* **2011,** 47, (2), 800-802.
21. Kispersky, V. F.; Kropf, A. J.; Ribeiro, F. H.; Miller, J. T., Low absorption vitreous carbon reactors for operando XAS: a case study on Cu/Zeolites for selective catalytic reduction of NOx by NH3. *Physical Chemistry Chemical Physics* **2012,** 14, (7), 2229-2238.
22. McEwen, J.-S. A., T. Schneider, W.F. Kispersky, V.F. Miller,J.T. Delgass,W.N. Ribeiro,F.H., Integrated operando X-ray absorption and DFT characterization of Cu–SSZ-13 exchange sites during the selective catalytic reduction of NOx with NH3. **2012,** 184, (1), 129–144.
23. Goeltl, F.; Hafner, J., Structure and properties of metal-exchanged zeolites studied using gradient-corrected and hybrid functionals. I. Structure and energetics. *Journal of Chemical Physics* **2012,** 136, (6), 064501.
24. Goeltl, F.; Hafner, J., Structure and properties of metal-exchanged zeolites studied using gradient-corrected and hybrid functionals. II. Electronic structure and photoluminescence spectra. *Journal of Chemical Physics* **2012,** 136, (6), 064502.
25. Goeltl, F.; Hafner, J., Structure and properties of metal-exchanged zeolites studied using gradient-corrected and hybrid functionals. III. Energetics and vibrational spectroscopy of adsorbates. *Journal of Chemical Physics* **2012,** 136, (6), 061503.
26. Brandenberger, S.; Kröcher, O.; Tissler, A.; Althoff, R., The State of the Art in Selective Catalytic Reduction of NOx by Ammonia Using Metal-Exchanged Zeolite Catalysts. *Catalysis Reviews, Vol. 50, No. 4, 2008: pp. 492–531* **2009**.
27. (ZrO2)0.85(REO1.5)0.15 (RE=Sc, Y) solid solutions prepared via three Pechini-type gel routes: 2—sintering and electrical properties. **2003,** 171, (Issues 1–2), 439–443.
28. G.Parr, R. Y., Weitao, *Density-Functional Theory of Atoms and Molecules*. 2014.
29. Engel, E. M. D., Reiner., *Density Functional Theory*. 2014.
30. Szabo, A. S. O., Neil, *Modern Quantum Chemistry*. 2014.
31. Hohenberg, P. K., W. Inhomogeneous Electron Gas - PhysRev.136.B864. http://journals.aps.org/pr/pdf/10.1103/PhysRev.136.B864
32. Kohn, W.; Sham, L. J., Self-Consistent Equations Including Exchange and Correlation Effects. *Physical Review* **1965,** 140, 1133-1138.
33. Shevlin, S. A. G., Z.X., Density functional theory simulations of complex hydride and carbon-based hydrogen storage materials. **2008**.
34. Perdew, J. P.; Ruzsinszky, A.; Tao, J.; Staroverov, V. N.; Scuseria, G. E.; Csonka, G. I., Prescription for the design and selection of density functional approximations: More constraint satisfaction with fewer fits. **2005**.
35. Haunschild, R.; Odashima, M. M.; Scuseria, G. E.; Perdew, J. P.; Capelle, K., Hyper-generalized-gradient functionals constructed from the Lieb-Oxford bound: Implementation via local hybrids and thermochemical assessment. *J. Chem. Phys.* **2012,** 136.
36. Becke, A. D., A new mixing of Hartree–Fock and local density-functional theories. **1993**.
37. Becke, A. D., Density-functional thermochemistry. III. The role of exact exchange. *J. Chem. Phys* **1993,** 98, (5648).

38. Lee, C. Y., Weitao. G. Parr, Robert., Development of the Colle-Salvetti correlation-energy formula into a functional of the electron density. *Phys. Rev. B 37, 785* **1988**.
39. P. Perdew, J. B., Kieron. Ernzerhof, Matthias., Generalized Gradient Approximation Made Simple. *Phys. Rev. Lett.* **1996,** 77, (3865).
40. Adamo, C.; Barone, V., Toward reliable density functional methods without adjustable parameters: The PBE0 model. *J. Chem. Phys.* **1999,** 110, (6158).
41. Perdew, J. P.; Burke, K.; Ernzerhof, M., Generalized gradient approximation made simple. *Physical Review Letters* **1996,** 77, (18), 3865-3868.
42. K.H.Madsen, G. Functional form of the generalized gradient approximation for exchange: the PBE functional. PhysRevB.75.195108. http://journals.aps.org/prb/pdf/10.1103/PhysRevB.75.195108
43. Grimme, S.; Antony, J.; Ehrlich, S.; Krieg, H., A consistent and accurate ab initio parametrization of density functional dispersion correction (DFT-D) for the 94 elements H-Pu. *Journal of Chemical Physics* **2010,** 132, (15).
44. Langreth, D. C.; Dion, M.; Rydberg, H.; Schröder, E.; Hyldgaard, P.; Lundqvist, B. I., Van der Waals density functional theory with applications. *International Journal of Quantum Chemistry* **2004,** 101, (5), 599-610.
45. Grimme, S., Accurate description of van der Waals complexes by density functional theory including empirical corrections. *J Comput Chem* **2004,** 25, (12), 1463-1473.
46. Density Functional Theory. http://www.iue.tuwien.ac.at/phd/goes/dissse14.html
47. CP2K: the gaussian plane wave (GPW) method - Basis sets and Kohn-Sham energy calculation - basis_sets.pdf. http://www.phenix.cnrs.fr/IMG/pdf/basis_sets.pdf
48. Lippert, G.; Hutter, J.; Parrinello, M., The Gaussian and augmented-plane-wave density functional method for ab initio molecular dynamics simulations. *Theoretical Chemistry Accounts* **1999,** 103, (2), 124-140.
49. Lippert, G.; Hutter, J.; Parrinello, M., A hybrid Gaussian and plane wave density functional scheme. *Molecular Physics* **1997,** 92, (3), 477-487.
50. VandeVondele, J.; Krack, M.; Mohamed, F.; Parrinello, M.; Chassaing, T.; Hutter, J., QUICKSTEP: Fast and accurate density functional calculations using a mixed Gaussian and plane waves approach. *Computer Physics Communications* **2005,** 167, (2), 103-128.
51. Schwerdtfeger, P.; Centre for Theoretical Chemistry and Physics (CTCP), T. N. Z. I. f. A. S. N., Massey University Auckland, Private Bag 102904, 0745 Auckland (New Zealand); Fachbereich Chemie, P. U. M., 35032 Marburg (Germany); Centre for Theoretical Chemistry and Physics (CTCP), T. N. Z. I. f. A. S. N., Massey University Auckland, Private Bag 102904, 0745 Auckland (New Zealand), The Pseudopotential Approximation in Electronic Structure Theory. *ChemPhysChem* **2014,** 12, (17), 3143-3155.
52. Krack, M., Pseudopotentials for H to Kr optimized for gradient-corrected exchange. *Theretical Chemistry Accounts* **2005,** 114, (1-3), 145-152.
53. Goedecker, S.; Teter, M.; Hutter, J., Separable dual-space Gaussian pseudopotentials. *Phys. Rev.* **1996,** B54, (1703).
54. Multiscale Molecular Modeling. http://www.mose.units.it/Lists/Multiscale%20Molecular%20Modeling/AllItems.aspx
55. Rappe, A. K. C., C.J. Colwell, K.S. Goddard III, W.A. Skiff, W.M. UFF, a full periodic table Force Field for molecular mechanics and molecular dynamics simulations. http://www.wag.caltech.edu/publications/sup/pdf/275.pdf
56. CP2K Open Source Molecular Dynamics. http://cp2k.org/
57. Hutter, J.; Switzerland, U. o. Z. P. C. I. W. Z.; Iannuzzi, M.; Switzerland, U. o. Z. P. C. I. W. Z.; Schiffmann, F.; ETH Zurich, W. P. S. N. S. Z. S.; VandeVondele, J.; ETH Zurich, W. P. S. N. S. Z. S., cp2k: atomistic simulations of condensed matter systems. *Wiley Interdisciplinary Reviews: Computational Molecular Science* **2014,** 4, (1), 15-25.
58. Versaevel, S. Studie van de microscopische structuur van koperhoudende zeolieten. Ghent University, 2012.

59. Frenkel, D. S., B., *Understanding Molecular Simulations, From Algorithms to Applications*. Academic Press: 2014.
60. Frenkel, A. I.; Rodriguez, J. A.; Chen, J. G., Synchrotron Techniques for In Situ Catalytic Studies: Capabilities, Challenges, and Opportunities. *Acs Catalysis* **2012,** 2, (11), 2269-2280.
61. Kwak, J. H.; Lee, J. H.; Burton, S. D.; Lipton, A. S.; Peden, C. H. F., A Common Intermediate for N2 Formation in Enzymes and Zeolites: Side-On Cu–Nitrosyl Complexes. *Angewandte Chemie International Edition* 52, (38), 9985-9989.
62. Deka, U. SelectiveCatalytic Reduction of NOx over Copper-based Microporous Catalysts. 2013.
63. Byrappa, K. S. K., B.B., Characterization of Zeolites by Infrared Spectroscopy. *Asian Journal of Chemistry* **2007,** 19, (6), 4933-4935.
64. Reed, A. E.; Weinstock, R. B.; Weinhold, F., Natural population analysis. *J. Chem. Phys* **1985,** 83, (735).

List of Tables

List of Figures